ADDIS ABABA UNIVERSITY
SCHOOL OF GRADUATE STUDIES
ADDIS ABABA INSTITUTE OF TECHNOLOGY
DEPARTMENT OF CIVIL ENGINEERING

M. Sc. Thesis on

WATER BALANCE OF UPPER AWASH BASIN BASED ON SATELLITE-DERIVED DATA (REMOTE SENSING)

By: Mussa Kurkura
Advisor: Dr. Ing. Yonas Michael

June 2011

WATER BALANCE OF UPPER AWASH BASIN BASED ON SATELLITE-DERIVED DATA (REMOTE SENSING)

Thesis submitted to School of Graduate Studies, Addis Ababa Institute of Technology, in partial fulfillment of the requirements for the Degree of Masters of Science in Civil Engineering (Hydraulics Engineering)

BY

MUSSA KURKURA

APPROVED BY BOARD OF EXAMINERS

	Name	Signature	Date
1.	Dr. Yonas Michael (Advisor)	_____	/____/____/_____/
2.	Dr. Dereje Hailu (Internal Examiner)	_____	/____/____/_____/
3.	Dr. Daniel F/Selassie (External Examiner)	_____	/____/____/_____/
4.	Ato Misgun Samuel (Chairman)	_____	/____/____/_____/
	Dr. Esayas G/Youhannes	_____	/____/____/_____/
	Chairman, Faculty Graduate Commission		
	Prof. Masresha Fetene	_____	/____/____/_____/
	Vice President for Research & Dean of the School of Graduate Studies		

Abstract

Understanding the temporal and spatial variation of key water balance components of the Upper Awash Basin will provide important information for the management of its water resources. Surface Energy Balance System (SEBS) model had been utilized to estimate the surface fluxes over the Upper Awash Basin using MODIS/Terra products, SPOT VGT4AFRICA products and SRTM-DEM in combination with ground-based meteorological data and derived surface biophysical parameters. Water balance components on monthly basis in the year 2008 were modeled in a grid cell environment at 0.01 degree (~1000m) spatial resolution using SEBS derived evapotranspiration and satellite-derived rainfall products of TRMM-3B43. Annual maps of rainfall, evapotranspiration and runoff were developed. Moreover, evapotranspiration and runoff as percent of rainfall maps were produced. The result showed that the annual rainfall, evapotranspiration and runoff from the Upper Awash Basin were 1049.60mm, 905.76mm and 143.84mm, respectively. The corresponding volumetric annual runoff to the Koka reservoir was 1545.99Mm^3. Areas where more than 80% of the rainfall is partitioned to evapotranspiration are shown to be in semi-arid regions. On the other hand, the highlands of the Upper Awash Basin fall below 80% of evapotranspiration as percent of annual rainfall. Further research is required for a thorough validation of the results and their integration with ecohydrologic models for better management of water and land resources in the basin ecosystems.

Acknowledgements

First and foremost, I wish to extend my sincere and deepest appreciation to my advisor, Dr. Ing. Yonas Michael, for his guidance, professional assistance and enthusiastic support without him this thesis will not come to end.

Very special thanks go to all staffs of Civil Engineering Department who contributed to the knowledge I acquired in Addis Ababa University. I would like to thank also MoWR and NMA for their help by providing Hydrological and Meteorological data to conduct this research, respectively.

My very special gratitude goes to Mr. Abeyou Wale, Lecturer at Bahirdar University, for he helped me in familiarizing ILWIS software. I would like to aknowledge as well my course mates for their being friendly and wonderful events we shared at Addis Ababa University.

I am also indebted to my brothers "Ditta Kurkura" and "Mohammed kurkura", for their all-round support. The last but not the least, my heartfelt appreciation goes to my lovely wife "Iman Jafer" and my honorable parents for their encouragement and continuous support during all circumstances, without them all these would have not been achievable. All others, relatives and friends, are greatly appreciated, who have directly or indirectly participated in this work.

Above all, I lack words to thank the Almighty Allah for he has given me endurance, health, and ability to successful completion of my thesis work.

Table of Contents

List of Figures

List of Tables

List of Acronyms

ABL	Atmospheric Boundary Layer
ASCII	American Standard Code of Information Interchange
ASL	Atmospheric Surface Layer
ASTER	Advanced Spaceborne Thermal Emission and Reflection Radiometer
BRDF	Bidirectional Reflectance Distribution Function
DEM	Digital Elevation Model
EDOS	EOS Data and Operations System
EOS	Earth Observing System
EROS	Earth Resources Observation and Science
EVI	Enhanced Vegetation Index
FAO	Food and Agricultural Organization
GEOS	Global Earth Observing System
GeoTIFF	Geographical Tag Image File Format
GES DISC	Gaddard Earth Sciences-Data and Information Services Center
GIS	Geographic Information Systems
GPCC	Global Precipitation Climatology Centre
GSFC	Goddard Space Flight Center
HDF	Hierarchical Data Format
HEG	HDF-EOS to GeoTIFF Conversion Tool
ILWIS	Integrated Land and Water Information System
IR	Infrared
JAXA	Japanese Aerospace Exploration Agency
LAI	Leaf Area Index
LP DAAC	Land Processes Distributed Active Archive Center
LST	Land Surface Temperature
LULC	Land Use/Cover
MODIS	Moderate Resolution Imaging Spectroradiometer
NASA	National Aeronautics and Space Administration
NBAR	Nadir BRDF-Adjusted Reflectance

NDVI	Normalized Difference Vegetation Index
NMA	National Meteorology Agency
PM	Passive Microwave
PR	Precipitation Radar
RMS	Root Mean Square
RS	Remote Sensing
SAVI	Soil Adjusted Vegetation Index
SEBAL	Surface Energy Balance Algorithm for Land
SEBS	Surface Energy Balance System
SPOT	Sensor Placement Optimization Tool
SRTM	Shuttle Radar Topography Mission
SSM/I	Special Sensor Microwave/Imager
SZA	Sun Zenith Angle
TCI	TRMM Combined Instrument
TMI	TRMM Microwave Imager
TRMM	Tropical Rainfall Measurement Mission
TSDIS	TRMM Science Data and Information System
TSEB	Two-Source Energy Balance
USGS	U.S. Geological Survey
VIRS	Visible and Infrared Scanner

1. Introduction

1.1 Background

The distribution of water resource on earth is quite wide-ranging where many locations have abundance while others have very little. Water exists on earth as solid (ice), liquid or gas (water vapour) in oceans, rivers, clouds and rain, all of which are in a frequent state of change (surface water evaporates, cloud water precipitates, rainfall infiltrates the ground, etc.). However, the total amount of the earth's water does not change (*Chow et al., 1988*). Water covers 70% of the earth's surface, but most water resources available for human consumption and the ecosystem are contained in lakes and rivers. The volume in those water bodies correspond to 0.27% of the global fresh water and only 0.008% of the earth water budget.

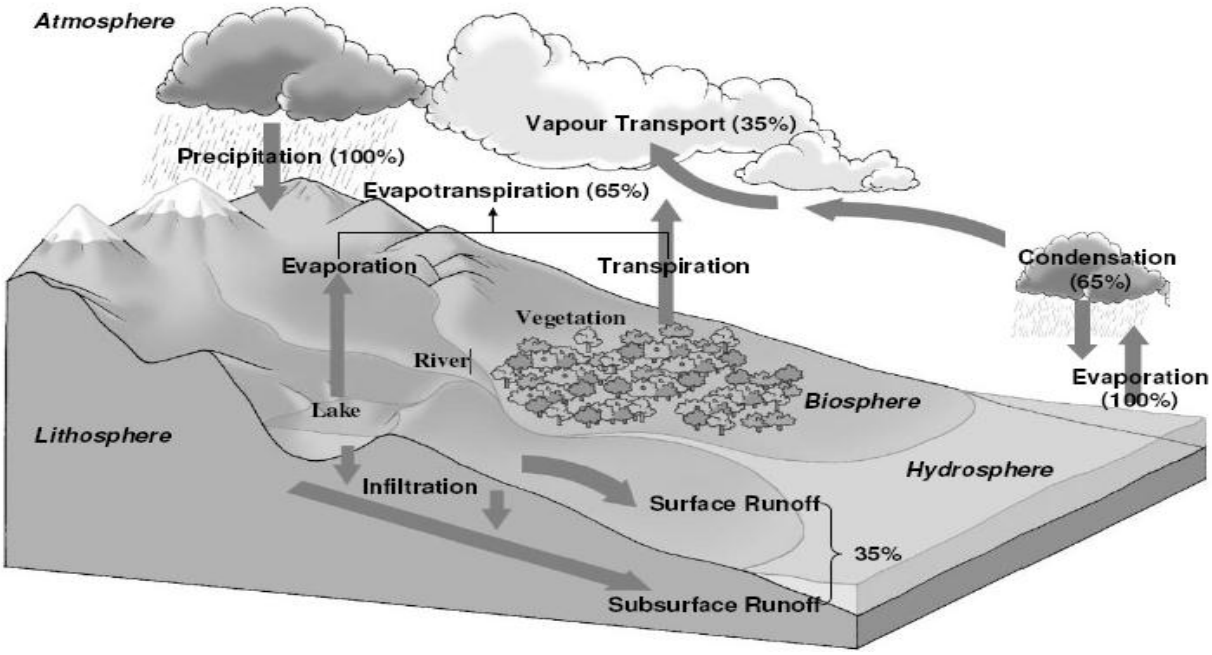

Figure 1-1 *Global water cycle*

Judicious management of precious land and water resources will be one of the biggest challenges of the 21st century. Both water and land resources are finite, but demand in various sectors is increasing. Irrigated agriculture, a major contributor to global food production, is one of biggest consumers of fresh water, accounting for about 70% of global diverted water resources (*Ahmed*

et al., 2006). Considering the rapidly growing water demand for industries and domestic use, it is essential to use irrigation water more efficiently. Most of the large irrigation systems are located in arid to semi-arid regions where rainfall is much less than evaporative demand and agriculture is only possible with surface or groundwater irrigation. As a result, evapotranspiration (ET) is one of the largest components in the overall water balance in these regions. Therefore, knowledge of actual evapotranspiration (ET_a) in irrigated river basins is essential for efficient management of scare water resources. Spatial Patterns of evapotranspiration explain whether the water is used as "intended" or not (*Ahmed et al., 2006*).

A physically based equation for potential evapotranspiration was derived by combining energy balance equation with the aerodynamic equation for vapour transfer *(Penman, 1956*). It was subsequently modified *Monteith (1973)* to include a canopy resistance for vapour diffusion out of stomata. Apart from above mentioned principles, there are many other methods that have been proposed for estimating ET_0. *Jensen (1990)* showed that the modified Penman-Monteith equation provides the best accurate estimate of evaporation from well-watered grass or alfalfa under varied climate conditions. However, these conventional techniques are based on the point measurements, are representative only of local scales and will fail for large scales because of the dynamic nature and regional variation of ET. On the other hands, Penman-Monteith equation provided only an estimation of the potential ET, which limits its use in actual evapotranspiration (ET_a) estimation.

Evaporation of water requires relatively large amounts of energy, either in the form of sensible heat or radiant energy. Therefore, the evapotranspiration process is governed by energy exchange at the vegetation surface and is limited by the amount of energy available. Because of this limitation, it is possible to predict the regional actual evapotranspiration by applying the principle of energy conservation. Recently, Remote Sensing (RS) techniques have developed rapidly. From satellite observation, people can obtain consistent and frequent spectral reflectance and emittance of radiation of the land surface in a basin scale, so it s possible to estimate the regional evapotranspiration rate by combining remotely sensing data with the solar radiation observation based on surface energy balance model. In the past decades, considerable effects

have been made to gaining experience and deriving appropriate models to counter this challenge *(Bastiaanssen et al., 1995; Su, 2002).*

1.2 Problem Statement

Due to the lack of basic understanding of the spatial and temporal variability of hydrological parameters, water resource management is becoming a major challenge in most countries. In this aspect, quantification of the components of hydrologic cycle is vital. ET is one of the most important hydrologic components in several respects; the difference between precipitation and evapotranspiration over the long term is the water available for direct use *(Dingman, 2002).*

Despite of its significance, ET is often treated as a lumped residual flux from the hydrologic budget, or estimated indirectly from local weather station data, which has a lack of uniformity in the quality and distribution of weather and flow observation points. In areas with heterogeneous vegetation cover like cropland, grassland, forests and other kind of plant species may coexist naturally within $1km^2$. Each vegetation species will have its own physiological nature.

The use of remote sensing is the recent development to resolve the challenge of the spatial distribution. Its capability of observing a number of physical characteristics of the earth's surface has been found useful for the parameterization of models for regional ET estimation using this technique *(Peters, 1995).*

Proper management to use the excess flow will be an enormous input for the dependable supply of water for various water resource projects in a basin. Models, therefore, will be a great tool both in predicting the amount of excess water leading to flooding as well as manage the shortage in case of drought.

The Awash basin is the most intensively utilized basin in Ethiopia. Extensive irrigation schemes have been functional for many years following the construction of the main structure, Koka dam in 1960. Nowadays, the reservoir is constantly filling up with sediment and has lost more than 30% of its water storage capacity *(Shimelis, 2004).* Moreover, different irrigation projects are being constructed (Fentale Irrigation Project and Welinchiti Irrigation Project) and

expansions of Wonji and Metehara sugar plantation are being accomplished. Due to this continuing reduction in capacity and high demand of the source, the water management of the reservoir is becoming very difficult.

Considering these all problem and challenges, this research is designed to analyze and map the spatial and temporal distribution of rainfall, actual evapotranspiration and water availability (runoff) for the Upper Awash Basin.

1.3 Objective of the Study

The objective of this study is to assess and evaluate the spatial and temporal variation of actual evapotranspiration and catchment water balance "precipitation minus evapotranspiration" in the Upper Awash Basin applying SEBS model by combined use of remote sensing, ground-based meteorological data and derived surface biophysical parameters.

1.4 Thesis Outline

Chapter 1 is the introduction part including background, problem statement and objectives of the research. Softwares used are also addressed in this chapter.

Literature review on concepts of evapotranspiration, methods of its estimation and application of remote sensing and GIS to natural resource management are presented in chapter 2. The chapter comprises general description of TRMM and MODIS satellites. Discussion of the SEBS algorithm in detail is included in the literature review chapter.

Chapter 3 gives description of the study area based on topography, climate and land cover information in addition to the description of materials used in this research.

The general methodology of this study is presented with chapter 4. In this chapter, preprocessing of images and ground-based data are given. Different methods assessed for surface biophysical and surface characteristics parameters estimation are also put in this chapter.

Chapter 5 discusses the results of major water balance components like rainfall, evapotranspiration and runoff temporally and spatially. In this chapter, comparison of SEBS derived evapotranspiration and different ET_0 approaches are discussed. Conclusion and recommendation are presented in the final chapter.

1.5 Software Employed

Softwares and tools that were used in this research are 1. Integrated Land and Water Information System (ILWIS); 2. Surface Energy Balance Systems (SEBS) model; 3. HDF-EOS to GeoTIFF (HEG) tool; 4. TSDIS Orbit Viewer; 5. Microsoft Offices.

2. Literature Review

2.1 Catchment Water Balance

Introduction

Catchment water balance allows to study the hydrologic process taking place in a catchment area and to determine the unknown and may be the difficult parameter based on the known ones. Like the reservoir water balance the catchment water balance is carried out based on water accounting principles in which water inflow to the catchment, leaving the catchment and change in storage (as ground water and as water in soil, ponds, micro dams and vegetation) for the period considered are taken in to account. By assuming the boundary of the surface water catchment coincides with that of the ground water, the net ground water flow was taken to be zero. The water inflow into the catchment area is, therefore, considered to be only from rainfall while the water leaving the catchment area includes runoff (R) and actual evapotranspiration (ET_a). The difference between them constitutes the change in both ground water and soil moisture storage (ΔS).

The advancement of satellite technology, the progressive reduction in the cost of images and the development of computer technology and associated software and models for processing have opened the opportunity to extract fundamental hydrological parameters such as actual evapotranspiration on pixel by pixel basis.

Catchment Water Balance Equation

Assuming that the boundary of the surface water catchment coincide with that of the ground water the catchment water balance is formulated as:

$$\Delta S = P - ETa - R \qquad 2.1$$

Where, ΔS is change in ground water and soil moisture storage for the time considered, P is precipitation, ET_a is actual evapotranspiration from the catchment and R is runoff.

The change in water storage on water balance depends on the period over which the water balance is computed. It can be significant when considered for a period of a day, a week or a

month; however, on annual basis, it is likely to be small in relation to the total water balance components and assumed to be zero. Equation of the catchment water balance on annual basis, therefore, is reduced to

$$R = P - ETa \qquad 2.2$$

2.2 Principle of Evapotranspiration Process

The combination of two separate processes whereby water is lost on the one hand from the soil surface by evaporation and on the other hand from the crop by transpiration is referred to as evapotranspiration *(Allen et al., 1998)*:

Evaporation

Evaporation is the process whereby liquid water is converted to water vapour (vaporization) and removed from the evaporating surface (vapour removal). Water evaporates from a variety of surfaces, such as lakes, rivers, pavements, soils and wet vegetation.

Energy is required to change the state of the molecules of water from liquid to vapour. Direct solar radiation and, to a lesser extent, the ambient temperature of the air provide this energy. The driving force to remove water vapour from the evaporating surface is the difference between the water vapour pressure at the evaporating surface and that of the surrounding atmosphere. As evaporation proceeds, the surrounding air becomes gradually saturated and the process will slow down and might stop if the wet air is not transferred to the atmosphere. The replacement of the saturated air with drier air depends greatly on wind speed. Hence, solar radiation, air temperature, air humidity and wind speed are climatological parameters to consider when assessing the evaporation process.

Where the evaporating surface is the soil surface, the degree of shading of the crop canopy and the amount of water available at the evaporating surface are other factors that affect the evaporation process. Frequent rains, irrigation and water transported upwards in a soil from a shallow water table wet the soil surface. Where the soil is able to supply water fast enough to satisfy the evaporation demand, the evaporation from the soil is determined only by the meteorological conditions. However, where the interval between rains and irrigation becomes

large and the ability of the soil to conduct moisture to pear the surface is small, the water content in the topsoil drops and the soil surface dries out. Under these circumstances, the limited availability of water exerts a controlling influence on soil evaporation. In the absence of any supply of water to the soil surface, evaporation decreases rapidly and may cease almost completely within a few days.

Transpiration

Transpiration consists of the vaporization of liquid water contained in plant tissues and the vapour removal to the atmosphere. Crops predominately lose their water through stomata. These are small openings on the plant leaf through which gases and water vapour pass. The water, together with some nutrients, is taken up by the roots and transported through the plant. The vaporization occurs within the leaf, namely in the intercellular spaces, and the vapour exchange with the atmosphere is controlled by the stomatal aperture. Nearly all water taken up is lost by transpiration and only a tiny fraction is used within the plant.

Transpiration, like direct evaporation, depends on the energy supply, vapour pressure gradient and wind. Hence, radiation, air temperature, air humidity and wind terms should be considered when assessing transpiration. The soil water content and the ability of the soil to conduct water to the roots also determine the transpiration rate, as do water logging and soil water salinity. Crop characteristics, environmental aspects and cultivation practices also influence the transpiration rate. Different kinds of plants may have different transpiration rates. Not only the type of crop, but also the crop development, environment and management should be considered when assessing transpiration.

Evapotranspiration

Evaporation and transpiration occur simultaneously and there is no easy way of distinguishing between the two processes. Apart from the water availability in the topsoil, the evaporation from a cropped soil is mainly determined by the fraction of the solar radiation reaching the soil surface. This fraction decreases over the growing period as the crop develops and the crop canopy shades more and more of the ground area. When the crop is small, water will predominately lost by soil evaporation, but once the crop is well developed and completely

covers the soil, transpiration becomes the main process. At sowing nearly 100% of ET comes from evaporation, while at full crop cover more than 90% of ET comes from transpiration.

2.3 Methods of Estimating Evapotranspiration

Direct measurement of evapotranspiration is more difficult and specific devices and accurate measurements of soil water balance in lysimeter are required. The methods are often expensive, demanding in terms of accuracy and can only be fully exploited by well-trained research personnel *(Allen et al., 1998)*. Owing to the difficulty of obtaining direct measurement of evapotranspiration , it is commonly estimated by indirect methods. *Gieske (2003)* listed some of the methods and models that have been currently applied for monitoring evapotranspiration on global, regional and local scales. He discussed the approaches these models used in estimating the actual and reference evapotranspiration, which they depend on the type of applications and available data. In general, the methods can be grouped as (i) direct measurement, (ii) modeling, and (iii) remote sensing.

2.3.1 Direct Measurement Techniques

Lysimeter

It is an artificially enclosed volume of soil for which the inflow and outflow of water can be measured. Commonly, changes in storage can be monitored by weighing. This technique is used to determine evaporation in a natural environment by accurately measuring the other water balance components; i.e., soil moisture storage and deep drainage. Lysimeter offer the only absolute way of precisely measuring water loss from soil and canopy surfaces. Due to its precise measurement, it can be used for comparison of actual evapotranspiration results obtained with satellite data.

Bowen Ratio Method

This method rearranges the energy balance equation in order to cancel out the aerodynamic transport terms. The Bowen ratio, β, is often written as *(Dingman, 2002)*:

$$\beta = \gamma \frac{T_2 - T_1}{e_2 - e_1} \qquad 2.3$$

Where, γ is the psychrometric constant, T_2 and T_1 are measured air temperatures at heights Z_1 and Z_2, e_2 and e_1 are the measured water vapour pressures at Z_1 and Z_2.

The implementation of this technique requires data loggers with humidity and temperature sensors *(Allen et al., 1998)*. Important advantage of the Bowen ratio method is the ability to measure actual evapotranspiration and the elimination of wind and turbulent transfer coefficients while the disadvantages are sophistication and fragility of sensors and data logging equipment and the numerical instability of *equation 2.3* during periods of β near -1. The need of adequate upwind fetch also place limits on the method.

Eddy Correlation Method

In this approach, fluctuations of the vertical wind (w') and the deviations (q') from the mean of absolute humidity (q) are measured directly with fast response sensors *(Brutsaert, 1982)*. The expression for evapotranspiration is accordingly given by:

$$ET = \frac{\overline{w'q'}}{\rho_w} \qquad 2.4$$

Where, the over bar indicates means over 1 to 5 minute intervals. The advantages of the eddy correlation method are the ability of direct sampling of the turbulent boundary layer and the determination of actual evapotranspiration. The disadvantages are the complexity of the instrumentation and the need adequate upwind fetch to establish an equilibrium transport within the boundary layer considered.

2.3.2 Water Balance and Hydrologic Modeling

Water Balance

The water balance method involves applying the water balance equation to the catchment area of interest over a time period ΔT and solving the equation for evapotranspiration as:

$$ET = P + Q_{in} + G_{in} - Q_{out} - G_{out} - \Delta S \qquad 2.5$$

Where, p is precipitation, Q_{in} is inflow of surface water, Q_{out} is outflow of surface water, G_{in} is ground water inflow, G_{out} is ground water outflow and ΔS is change for water stored over the period. The dimensions of these variables are [L^3] or if divided by drainage area, [L].

Even if this approach looks simple in concept, in practice it is difficult to measure exactly the true values of the components in *equation 2.5*. If reasonably accurate information on the balance components is available, the method can provide truthful estimation of evapotranspiration.

Hydrological models

Hydrological surface flow models, such as Source Water Assessment Program (SWAP), Semi-Distributed Land Use-Based Runoff Processes (SLURP), and Soil and Water Assessment Tool (SWAT), simulate the transformation of precipitation into stream flow taking into account that all the immediate process such as evapotranspiration, interception, infiltration, runoff and groundwater flow including all the artificial effects of dams, reservoirs, diversions and irrigation schemes. They are, therefore, able to estimate evaporation and transpiration at many points and at many times *(Kite and Droogers, 2000).*

2.3.3 Remote Sensing Techniques

Evaporation of water is like a commercial transition in which a wet surface sells water vapor to its environment in exchange for heat *(Gash and Shuttleworth, 2007)*. Therefore, water lost to the atmosphere through evaporation has the effect of cooling the earth's surface. Particularly, in arid and semi arid areas, recycling of moisture through ET appears to be responsible for more than 90% of the rainfall *(Savenije and Hubert, 1995)*. This means that knowledge of evapotranspiration is crucial for climatic studies, weather forecasts, ecological monitoring, hydrological surveys, and water resource management *(Bastiaanssen and Mekonnen, 2000)*.

RS provides a means of observing hydrological state variables over large areas *(Schmugge et al., 2002)*. Indeed, large-scale estimation of Actual evapotranspiration (ET_a) has many challenges and requires good estimation of surface biophysical parameters involved in the exchange energy between the land surface and atmosphere. In the past decades, large scale estimation of evapotranspiration was achieved using the two sources (soil and canopy) called Atmosphere-

Land Exchange Inverse (ALEXI) and model *(Anderson et al., 1997).* This model estimates surface fluxes of heat and water vapor on the 5-10km scale using primary satellite-derived input data, including surface radiometric temperature, down-welling short-wave and long-wave radiation, and vegetation indices. For particular applications, the coarser application of ALEXI output can be disaggregated to desired resolution by applying disaggregation algorithm called DisALEXI with additional model input, such as higher resolution thermal and shortwave imagery from satellite platforms like Advanced Spaceborne Thermal Emission and Reflection Radiometer (ASTER), Landsat or airborne *(Norman et al., 2003).*

Efforts have been undertaken by *Tang (2007)* as well to estimate land surface evapotranspiration from remote sensing data with special interest to achieve a near real-time crop water use estimation at the spatial scale ranging from a small basin to a region. In addition, *Mu et al. (2007)* developed a global remote sensing evapotranspiration algorithm based on *Cleugh et al (2007),* which considers both the surface energy partitioning process and environmental constraints on evapotranspiration. The result reveals that the spatial pattern of the Moderate Resolution Imaging Spectroradiometer (MODIS) ET agrees well with that of the MODIS global terrestrial gross and net primary production (MOD17), with the highest ET over tropical forests and the lowest ET values in dry areas with short growing seasons. They also concluded from the result that MODIS ET product can provide critical information on the regional and global water cycle and resulting environmental change.

Recently, *Minacapilli et al. (2009)* made a comparison between two different energy balance models (Surface Energy Balance Algorithm for Land, SEBAL; Two-Source Energy Balance, TSEB) in Mediterranean perennial crops. This research was done because the agricultural practice in the study area is converting from rain fed to irrigated crops. For this reason, the selection of the best energy balance model became an important issue for the region. Both are widely used models to estimate ET. SEBAL is a one-source model, where soil and vegetation are considered as the sole source (mostly appropriate in the case of uniform vegetation coverage) and TSEB a two-source model, where soil and vegetation components of the surface energy balance are treated separately. Actual evapotranspiration estimates by means of the two surface energy balance models were compared with the outputs of the agro-hydrological SWAP model,

which was applied in a spatially distributed way to simulate one-dimensional water flows in the soil-plant-atmosphere continuum. The results of this investigation appeared to prove better agreement between SWAP and TSEB for some fields of the study area. This agreement reveals that separate treatment of soil and vegetation components of land surface energy balances may provide good estimation of surface fluxes.

Regional scale water cycle estimates have been made by *Pan et al. (2008)* using multiple satellite remote sensing data (Tropical Rainfall Measurement Mission (TRMM), TRMM Microwave Imager (TMI) and MODIS with the support of previously developed assimilation techniques, such as the Ensemble Kalman Filter, the particle filter, the water balance constrainer, the copula error model and physically based models including the variable infiltration capacity, the Land Surface Microwave Emission Model (LSMEM) and the surface energy balance system (SEBS). They found that a land surface model driven by the bias corrected TRMM rainfall produces reasonable water cycle states and fluxes. The estimates are also moderately improved by assimilating TMI 10.67 GHz microwave brightness temperature measurements that provides information on the surface soil moisture state, while they mentioned that it remains challenging to improve the results by assimilating evapotranspiration estimated from satellite-based measurements. Nevertheless, they also successfully validated the evapotranspiration estimated using SEBS over the region. In addition, *Wenjing et al. (2006)* found in Hebei Plain, Northern China, a good agreement between ET_a estimated by SEBS and Lysimeter, but big differences were observed when SEBS estimated ET_a was compared to ET_a derived from empirical equation using a locally derived coefficient. Therefore, there are indications of the possibility of estimating ET_a over large area using those energy balance models, which gave good estimation of ET_a over relatively homogeneous land surface.

2.4 Principles of Remote sensing

2.4.1 Definition

Remote sensing can be defined as any process whereby information is gathered about an object, area or phenomenon without being in contact with it. Our eyes are an excellent example of a

remote sensing device. We are able to gather information about our surroundings by gauging the amount and nature of the reflectance of visible light energy from some external source (such as the sun or a light bulb) as it reflects off objects in our field of view.

Given this rather general definition, the term remote sensing has come to be associated more specifically with the gauging of interactions between earth surface materials and electromagnetic energy. However, any such attempt at a more specific definition becomes difficult, since it is not always the natural environment that is sensed (e.g., art conservation applications), the energy type is not always electromagnetic (e.g., sonar) and some procedures gauge natural energy emissions (e.g., thermal infrared) rather than interactions with energy from an independent source.

2.4.2 Fundamental Considerations

Energy Source

Sensors can be divided into two broad groups—passive and active. Passive sensors measure ambient levels of existing sources of energy, while active ones provide their own source of energy. The majority of remote sensing is done with passive sensors, for which the sun is the major energy source. The earliest example of this is photography. With airborne cameras we have long been able to measure and record the reflection of light off earth features. While aerial photography is still a major form of remote sensing, newer solid-state technologies have extended capabilities for viewing in the visible and near-infrared wavelengths to include longer wavelength solar radiation as well. However, not all passive sensors use energy from the sun. Thermal infrared and passive microwave sensors both measure natural earth energy emissions. Thus, the passive sensors are simply those that do not themselves supply the energy being detected.

By contrast, active sensors provide their own source of energy. The most familiar form of this is flash photography. However, in environmental and mapping applications, the best example is RADAR. RADAR systems emit energy in the microwave region of the electromagnetic

spectrum *(figure 2-1)*. The reflection of that energy by earth surface materials is then measured to produce an image of the area sensed.

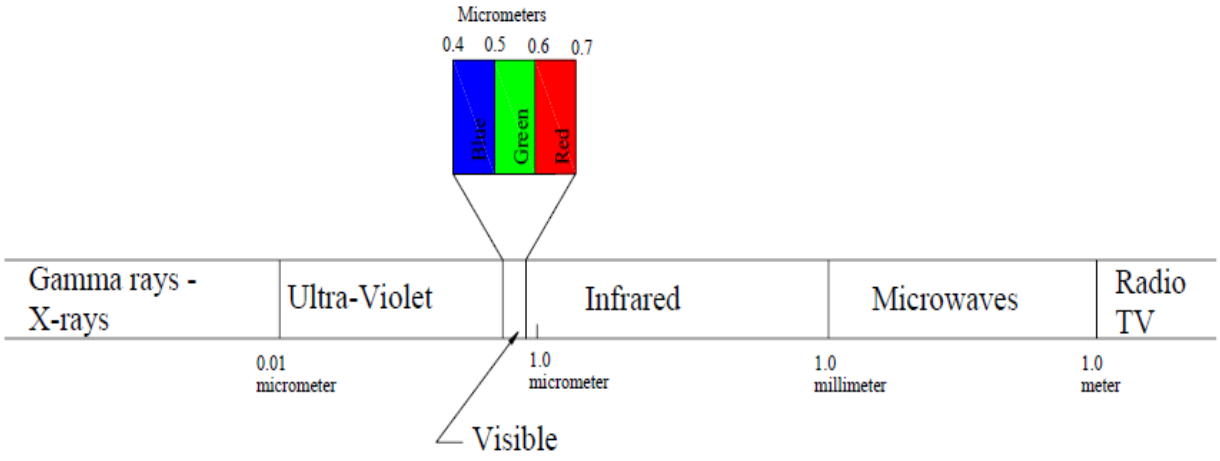

Figure 2-1 *The Electromagnetic Spectrum*

Wavelength

As indicated, most remote sensing devices make use of electromagnetic energy. However, the electromagnetic spectrum is very broad and not all wavelengths are equally effective for remote sensing purposes. Furthermore, not all have significant interactions with earth surface materials of interest to us. *Figure 2-1* illustrates the electromagnetic spectrum. The atmosphere itself causes significant absorption and/or scattering of the very shortest wavelengths. In addition, the glass lenses of many sensors also cause significant absorption of shorter wavelengths such as the ultraviolet (UV). As a result, the first significant window (i.e., a region in which energy can significantly pass through the atmosphere) opens up in the visible wavelengths. Even here, the blue wavelengths undergo substantial attenuation by atmospheric scattering, and are thus often left out in remotely sensed images. However, the green, red and near-infrared (IR) wavelengths all provide good opportunities for gauging earth surface interactions without significant interference by the atmosphere. In addition, these regions provide important clues to the nature of many earth surface materials. Chlorophyll, for example, is a very strong absorber of red visible wavelengths, while the near-infrared wavelengths provide important clues to the structures of plant leaves. As a result, the bulk of remotely sensed images used in GIS-related applications are taken in these regions.

Extending into the middle and thermal infrared regions, a variety of good windows can be found. The longer of the middle infrared wavelengths have proven to be useful in a number of geological applications. The thermal regions have proven to be very useful for monitoring not only the obvious cases of the spatial distribution of heat from industrial activity, but a broad set of applications ranging from fire monitoring to animal distribution studies to soil moisture conditions.

After the thermal IR, the next area of major significance in environmental remote sensing is in the microwave region. A number of important windows exist in this region and are of particular importance for the use of active radar imaging. The texture of earth surface materials causes significant interactions with several of the microwave wavelength regions. This can thus be used as a supplement to information gained in other wavelengths, and also offers the significant advantage of being usable at night (because as an active system it is independent of solar radiation) and in regions of persistent cloud cover (since radar wavelengths are not significantly affected by clouds).

Interaction Mechanisms

When electromagnetic energy strikes a material, three types of interaction can follow: reflection, absorption and/or transmission *(figure 2-2)*. The main concern is with the reflected portion since it is usually returns to the sensor system. Exactly how much is reflected will vary and will depend upon the nature of the material and where in the electromagnetic spectrum our measurement is being taken. As a result, if we look at the nature of this reflected component over range of wavelengths, we can characterize the result as a spectral response pattern.

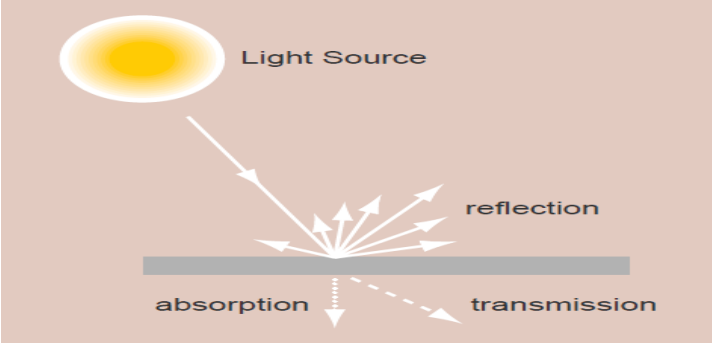

Figure 2-2 Interaction of electromagnetic energy and an object

Spectral Response Patterns

A spectral response pattern is sometimes called a signature. It is a description (often in the form of a graph) of the degree to which energy is reflected in different regions of the spectrum. Most humans are very familiar with spectral response patterns since they are equivalent to the human concept of color. For example, *figure 2-3* shows idealized spectral response patterns for several familiar colors in the visible portion of the electromagnetic spectrum, as well as for white and dark grey. The bright red reflectance pattern, for example, might be that produced by a piece of paper printed with a red ink. Here, the ink is designed to alter the white light that shines upon it and absorb the blue and green wavelengths. What is left, then, are the red wavelengths, which reflect off the surface of the paper back to the sensing system (the eye). The high return of red wavelengths indicates a bright red, whereas the low return of green wavelengths in the second example suggests that it will appear quite dark.

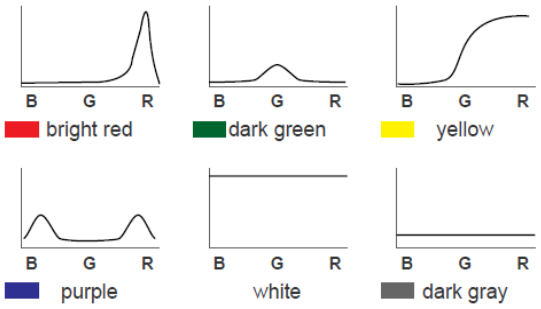

Figure 2-3 Spectral response patterns of familiar colors in the visible portion of the electromagnetic spectrum

The eye is able to sense spectral response patterns because it is truly a multi-spectral sensor (i.e., it senses in more than one place in the spectrum). Although the actual functioning of the eye is quite complex, it does in fact have three separate types of detectors that can usefully be thought of as responding to the red, green and blue wavelength regions. These are the additive primary

colors, and the eye responds to mixtures of these three to yield a sensation of other hues. For example, the color perceived by the third spectral response pattern in *figure 2-3* would be a yellow-the result of mixing a red and green. However, it is important to recognize that this is simply our phenomenological perception of a spectral response pattern. Consider, for example, the fourth curve. Here we have reflectance in both the blue and red regions of the visible spectrum. This is a bimodal distribution, and thus technically not a specific hue in the spectrum. However, we would perceive this to be a purple! Purple (a color between violet and red) does not exist in nature (i.e., as a hue-a distinctive dominant wavelength). It is very real in our perception, however. Purple is simply our perception of a bimodal pattern involving a non-adjacent pair of primary hues.

In the early days of remote sensing, it was believed (more correctly hoped) that each earth surface material would have a distinctive spectral response pattern that would allow it to be reliably detected by visual or digital means. However, as our common experience with color would suggest, in reality this is often not the case. For example, two species of trees may have quite a different coloration at one time of the year and quite a similar one at another.

Finding distinctive spectral response patterns is the key to most procedures for computer-assisted interpretation of remotely sensed imagery. This task is rarely trivial. Rather, the analyst must find the combination of spectral bands and the time of year at which distinctive patterns can be found for each of the information classes of interest.

The strong absorption by leaf pigments (particularly chlorophyll for purposes of photosynthesis) in the blue and red regions of the visible portion of the spectrum leads to the characteristic green appearance of healthy vegetation. However, while this signature is distinctively different from most non-vegetated surfaces, it is not very capable of distinguishing between species of vegetation—most will have a similar color of green at full maturation. In the near infrared, however, we find a much higher return from vegetated surfaces because of scattering within the fleshy mesophyllic layer of the leaves. Plant pigments do not absorb energy in this region, and thus the scattering, combined with the multiplying effect of a full canopy of leaves, leads to high reflectance in this region of the spectrum. However, the extent of this reflectance will depend

highly on the internal structure of leaves (e.g., broadleaf versus needle). As a result, significant differences between species can often be detected in this region. Similarly, moving into the middle infrared region we see a significant dip in the spectral response pattern that is associated with leaf moisture. This, again, is an area where significant differences can arise between mature species. Applications looking for optimal differentiation between species, therefore, will typically involve both the near and middle infrared regions and will use imagery taken well into the development cycle.

Multispectral Remote Sensing

In the visual interpretation of remotely sensed images, varieties of image characteristics are brought into consideration: color (or tone in the case of panchromatic images), texture, size, shape, pattern, context, and the like. However, with computer-assisted interpretation, it is most often color (i.e., the spectral response pattern) that is used. It is for this reason that a strong emphasis is placed on the use of multispectral sensors (sensors that, like the eye, look at more than one place in the spectrum and thus are able to gauge spectral response patterns), and the number and specific placement of these spectral bands.

It can be shown through analytical techniques such as Principal Components Analysis, that in many environments, the bands that carry the greatest amount of information about the natural environment are the near infrared and red wavelength bands. Water is strongly absorbed by infrared wavelengths and is thus highly distinctive in that region. In addition, plant species typically show their greatest differentiation here. The red area is also very important: because it is the primary region, in which chlorophyll absorbs energy for photosynthesis. Thus, it is this band, which can most readily distinguish between vegetated and non-vegetated surfaces.

Given this importance of the red and near infrared bands, it is not surprising that sensor systems designed for earth resource monitoring will invariably include these in any particular multispectral system. Other bands will depend upon the range of applications envisioned. Many include the green visible band since it can be used, along with the other two, to produce a traditional false color composite-a full color image derived from the green, red, and infrared bands (as opposed to the blue, green, and red bands of natural color images). In addition, the

combination of these three bands works well in the interpretation of the cultural landscape as well as natural and vegetated surfaces. However, it is increasingly common to include other bands that are more specifically targeted to the differentiation of surface materials. For example, LANDSAT TM Band 5 is placed between two water absorption bands and has thus proven very useful in determining soil and leaf moisture differences. Similarly, LANDSAT TM Band 7 targets the detection of hydrothermal alteration zones in bare rock surfaces. By contrast, the AVHRR system on the NOAA series satellites includes several thermal channels for the sensing of cloud temperature characteristics.

Hyperspectral Remote Sensing

In addition to traditional multispectral imagery, some new and experimental systems such as AVIRIS and MODIS are capable of capturing hyperspectral data. These systems cover a similar wavelength range to multispectral systems, but in much narrower bands. This dramatically increases the number of bands (and thus precision) available for image classification (typically tens and even hundreds of very narrow bands). Moreover, hyperspectral signature libraries have been created in lab conditions and contain hundreds of signatures for different types of land covers, including many minerals and other earth materials. Thus, it should be possible to match signatures to surface materials with great precision. However, environmental conditions and natural variations in materials (which make them different from standard library materials) make this difficult. In addition, classification procedures have not been developed for hyperspectral data to the degree they have been for multispectral imagery. Consequently, multispectral imagery still represents the major tool of remote sensing today.

2.4.3 Sensor/Platform Systems

Given recent developments in sensors, a variety of platforms are now available for the capture of remotely sensed data. Here we review some of the major sensor/platform combinations that are typically available to the GIS user community.

Aerial Photography

Aerial photography is the oldest and most widely used method of remote sensing. Cameras mounted in light aircraft flying between 200 and 15,000m capture a large quantity of detailed

information. Aerial photos provide an instant visual inventory of a portion of the earth's surface and can be used to create detailed maps. Aerial photographs commonly are taken by commercial aerial photography firms which own and operate specially modified aircraft equipped with large format (23cm x 23cm) mapping quality cameras. Aerial photos can also be taken using small format cameras (35mm and 70mm), hand-held or mounted in unmodified light aircraft.

Camera and platform configurations can be grouped in terms of oblique and vertical. Oblique aerial photography is taken at an angle to the ground. The resulting images give a view as if the observer is looking out an airplane window. These images are easier to interpret than vertical photographs, but it is difficult to locate and measure features on them for mapping purposes.

Vertical aerial photography is taken with the camera pointed straight down. The resulting images depict ground features in plan form and are easily compared with maps. Vertical aerial photos are always highly desirable, but are particularly useful for resource surveys in areas where no maps are available. Aerial photos depict features such as field patterns and vegetation that are often omitted on maps. Comparison of old and new aerial photos can also capture changes within an area over time.

Vertical aerial photos contain subtle displacements due to relief, tip and tilt of the aircraft and lens distortion. Vertical images may be taken with overlap, typically about 60 percent along the flight line and at least 20 percent between lines. Overlapping images can be viewed with a stereoscope to create a three-dimensional view, called a *stereo model*.

Large Format Photography

Commercial aerial survey firms use light single or twin-engine aircraft equipped with large-format mapping cameras. Large-format cameras, such as the Wild RC-10, use 23 cm x 23 cm film, which is available in rolls. Eastman Kodak, Inc., among others, manufactures several varieties of sheet film specifically intended for use in aerial photography. Negative film is used where prints are the desired product, while positive film is used where transparencies are desired. Print film allows detailed enlargements to be made, such as large wall-sized prints. In addition, print film is useful when multiple prints are to be distributed and used in the field.

Small Format Photography

Small-format cameras carried in chartered aircraft are an inexpensive alternative to large-format aerial photography. A 35mm or 70mm camera, light aircraft and pilot are required, along with some means to process the film. Because there are inexpensive commercial processing labs in most parts of the world, 35mm systems are especially convenient.

Oblique photographs can be taken with a hand-held camera in any light aircraft; vertical photographs require some form of special mount, pointed through a belly port or extended out a door or window. Small-format aerial photography has several drawbacks. Light unpressurized aircraft are typically limited to altitudes below 4000 m. As film size is small, sacrifices must be made in resolution or area covered per frame. Because of distortions in the camera system, small-format photography cannot be used if precise mapping is required. In addition, presentation- quality wall-size prints cannot be made from small negatives. Nonetheless, small-format photography can be very useful for reconnaissance surveys and can also be used as point samples.

Color Photography

Normal color photographs are produced from a composite of three film layers with intervening filters that act to isolate, in effect, red, green, and blue wavelengths separately to the different film layers. With color infrared film, these wavelengths are shifted to the longer wavelengths to produce a composite that has isolated reflectances from the green, red and near-infrared wavelength regions. However, because the human eye cannot see infrared, a false color composite is produced by making the green wavelengths appear blue, the red wavelengths appear green, and the infrared wavelengths appear red.

As an alternative to the use of color film, it is also possible to group several cameras on a single aircraft mount, each with black and white film and a filter designed to isolate a specific wavelength range. The advantage of this arrangement is that the bands are independently accessible and can be photographically enhanced. If a color composite is desired, it is possible to create it from the individual bands later. Clearly, photographs are not in a format that can

immediately be used in digital analysis. It is possible to scan photographs with a scanner and thereby create multispectral datasets either by scanning individual band images, or by scanning a color image and separating the bands. However, the geometry of aerial photographs (which have a central perspective projection and differential parallax) is such that they are difficult to use directly. More typically, they require processing by special photogrammetric software to rectify the images and remove differential parallax effects.

Aerial Videography

Light, portable, inexpensive video cameras and recorders can be carried in chartered aircraft. In addition, a number of smaller aerial mapping companies offer videography as an output option. By using several cameras simultaneously, each with a filter designed to isolate a specific wavelength range; it is possible to isolate multispectral image bands that can be used individually, or in combination in the form of a color composite. For use in digital analysis, special graphics hardware boards known as frame grabbers can be used to freeze any frame within a continuous video sequence and convert it to digital format, usually in one of the more popular exchange formats such as TIF. Like small-format photography, aerial videography cannot be used for detailed mapping, but provides a useful overview for reconnaissance surveys, and can be used in conjunction with ground point sampling.

2.5 Application of RS and GIS to Natural Resource Management

The success of planning for developmental activities depends on the quality and quantity of information available on both natural and socio-economic resources. It is, therefore, essential to devise the ways and means of organizing computerized information system. These systems must be capable of handling vast amount of data collected by modern techniques and produce up to date information. Remote Sensing technology has already demonstrated its capabilities to provide information on natural resources such as crop, land use, soils, forest etc on regular basis. Similarly, Geographic Information Systems (GIS) are the latest tools available to store, retrieve and analyze different types of data for management of natural resources. GIS facilitates systematic handling of data to generate information in a devised format. Thus, it plays an important role in evolving alternate scenarios for natural resources management.

RS data and GIS play a rapidly increasing role in the field of hydrology and water resources development. Although very few remotely sensed data can be directly applied in hydrology, such information is of great value since many hydrologically relevant data can be derived from remote sensing information. One of the greatest advantages of using RS data for hydrological modeling and monitoring is its ability to generate information in spatial and temporal domain, which is very crucial for successful model analysis, prediction and validation. However, the use of RS technology involves large amount of spatial data management and requires an efficient system to handle such data. The GIS technology provides suitable alternatives for efficient management of large and complex databases.

Image data have been used as a primary source of natural resources information in thematic mapping, which in turn is utilized in various hydrological studies *(Seth et al., 1996).* The remote sensing data provides synoptic view of a large area in the narrow and discrete bands of the electromagnetic spectrum at regular intervals. The space borne multispectral data enable generating timely, reliable and cost effective information on various natural resources, namely surface water, ground water, land use/cover, soil, forest cover and environmental hazards, namely water logging, salinity and alkalinity, soil erosion by water etc. For many hydrological purposes, remote sensing data alone are not sufficient and need to be merged with data from other sources. Hence, multitudes of spatially related (i.e. geographic) data concerning topography, rainfall, evaporation, vegetation, geomorphology, and soils have to be considered.

2.6 Rainfall Estimation from Satellite Observation

There is high demand for improved rainfall estimates from satellite systems throughout the entire range of scales in time and space, from global to local resolutions *(Kidd et al., 2003).* Applications requiring rainfall products cover a range of hydro-meteorological sciences, including water resources, flood forecasting and moisture budgets. A range of techniques has been developed to produce estimates of rainfall from satellite data. For example, GEOS precipitation index (GPI) uses the fraction of cloud colder than 235 K in the IR with a fixed rain rate. More complex algorithms have been developed with varying degrees of success, such as GEOS IR rainfall estimation technique (auto-estimator) and the GEOS Multispectral Rainfall Algorithm (GMSRA). A number of inter-comparison projects have taken place to assess the

validity of satellite estimates at different spatial and temporal scales *(Adler, 2000, Gomez, 2007)*. Results showed that the Passive Microwave (PM) estimates produced the best instantaneous results and the Infrared (IR) based estimates provided the best long-term estimates. *Adler et al. (1993)* noted that the combined use of the frequent observations of the IR with the accuracy of the instantaneous PM data would be advantageous. For this reason, recently combined PM and IR technique was developed by *Kidd et al. (2003)* that provide better spatial and temporal resolutions of rainfall estimate. It is believed that the Tropical Rainfall Measuring Mission (TRMM) satellite provides more accurate observational measures of spatiotemporal coverage and intensities of precipitation *(Irena, 2007; Gomez, 2007; Senay et al., 2009)*.

2.7 Tropical Rainfall Measuring Mission Satellite

In recent years, with the aid of satellite weather observing technologies, the power of viewing and understanding tropical rainfall systems has been improved. Hence, the National Aeronautics and Space Administration (NASA) of USA and the Japanese Aerospace Exploration Agency (JAXA) launched Tropical Rainfall Measuring Mission (TRMM) satellite on November 27, 1997 from the Tanegashima Space Center in Japan.

TRMM travels in a non-sun-synchronous 403 Km height orbit at 35 degree inclination angle to the Equator. The spacecraft takes about 91 minutes to complete one orbit around the earth. This orbit allows for as much coverage of the tropics and extraction of rainfall data over the 24-hour day (16 orbits) as possible. The revisit time for the TRMM satellite is around 15 hours *(NASA/GSFC, 2006)*.

The rainfall measuring instruments on the TRMM satellite include Precipitation Radar (PR), an electronically scanning radar operating at 13.8 GHz that measures the 3-D rainfall distribution; TRMM Microwave Imager (TMI), a nine-channel passive microwave radiometer that provides information on the integrated column precipitation content, cloud liquid water, cloud ice, rain intensity, and rainfall types; and Visible and Infrared Scanner (VIRS), a five-channel visible/infrared radiometer that provides high resolution observations on cloud coverage, cloud type, and cloud top temperatures *(GES DISC, 2006)*.

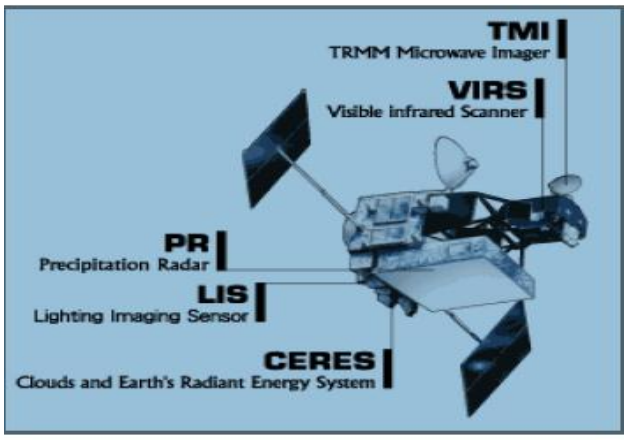

Figure 2-4 *TRMM satellite and instruments*

There are two other TRMM instruments: the Lighting Imaging Sensor (LIS) that observes the distribution and variability of lighting over Earth and the clouds, and Earth's Radiant Energy System (CERES) that measures emitted and reflected radiative energy from Earth's surface and the atmosphere and its constituents *(GES DISC, 2006).*

2.8 Moderate-Resolution Imaging Spectroradiometer

The Moderate-Resolution Imaging Spectroradiometer (MODIS) instrument operates on both the Terra (EOS AM) and Aqua (EOS PM) spacecraft. It has a viewing swath width of 2330 km and views the entire surface of the Earth every one to two days. Its detectors measure 36 spectral bands between 0.405 and 14.385 µm, and it acquires data at three spatial resolutions: 250m, 500m, and 1000m. Terra's orbit around the Earth is timed so that it passes from north to south across the Equator in the morning (10:30 local time), while Aqua passes from south to north over the Equator in the afternoon (13:30 local time).

Along with all the data from other instruments on board the Terra spacecraft and Aqua Spacecraft, MODIS data are transferred to ground stations in White Sands, New Mexico, via the Tracking and Data Relay Satellite System (TDRSS). The data are then sent to the Earth Observing System (EOS) Data and Operations System (EDOS) at the Goddard Space Flight Center (GSFC). The Level 1A, Level 1B, geo-location and cloud mask products and the Higher-level MODIS land and atmosphere products are produced by the MODIS Adaptive Processing System (MODAPS), and then are parceled out among three DAACs for distribution.

The many data products derived from MODIS observations describe features of the land, oceans and the atmosphere that can be used for studies of processes and trends on local to global scales

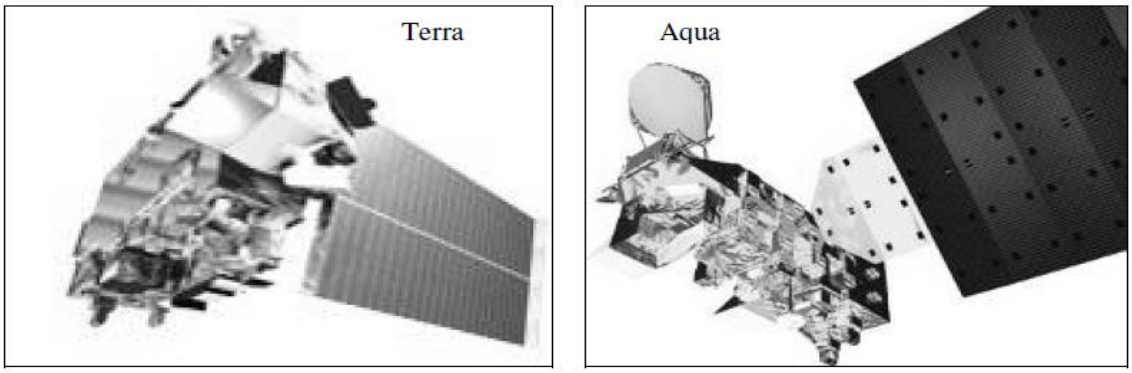

Figure 2-5 MODIS Terra (left) and Aqua (right) satellites

2.9 Integrated Land and Water Information System

Integrated Land and Water Information System (ILWIS) is a GIS that can handle both raster and vector data developed by Wim Koolhoven and Jelle Wind at the International Institute for Aerospace Survey and Earth Sciences, Enshede, the Netherlands (ITC).

ILWIS is a user-friendly and widely distributed GIS and Image Processing package. It is PC-based and designed for the Windows environments. Experts as well as beginners will easily find their way through the program. ILWIS provides a powerful tool for collection, storage, analysis, transformation and presentation of data. From the input data, information can be generated to model the spatial and temporal patterns and processes on the Earth's surface. It provides a set of documentation, dealing with the basics of GIS and Image Processing as well as its application in many fields, i.e. land evaluation, urban surveys, natural hazards and environmental management. The software is freely accessible through the institute web site: <*http://www.itc.nl/ilwis/*>.

2.10 Surface Energy Balance System

Evapotranspiration is not only an important component in the land surface energy balance, but also an important component in water cycle. Conventional models for ET estimation is based on the using of temperature and solar radiation, therefore, those methods can only to be used to estimate ET at certain location with point measurements, but cannot be easily used in large regional scale with a large degree of heterogeneity *(Su, 2002)*. Remote sensors are designed to measure energy in specific ranges of the electromagnetic spectrum, which mostly fall within atmospheric windows where atmosphere is almost transparent and atmospheric effect is minimal.

The evapotranspiration process of land surface is a consequence of energy change of fluxes between land surface and atmosphere, which can be expressed as the energy balance equation, and the values of the components in the energy balance equation can be determined with remote sensor, so evapotranspiration calculation based on the remote sensing methods comes in to truth.

The Surface Energy Balance System (SEBS) model was proposed by *Su (2002)* to estimate atmosphere turbulent fluxes and the evaporative fraction (the ratio of latent heat flux and the available energy) using satellite data and ancillary surface and meteorological information. SEBS is physically based and has the potential to be used across local, regional and continental scales with remotely sensed data and standard meteorological observations. SEBS consists of several separate modules to estimate the net radiation and soil heat flux, and to partition the available energy into sensible and latent heat flux, of which a detailed introduction is presented below.

2.10.1 Principle of Energy Balance Closure

Various forms of energy drive water transport through the hydrological cycle. Radiant energy, originating from the sun, provides the input energy for the cycle. Once matter absorbs this energy, it is converted into sensible heat that elevates the temperature of the air and the ground, and latent heat that causes evaporation, driving thereby the cycle against the pull of gravity. Further transport is generated by kinetic energy and pressure energy of the moving air masses. Translocation of vapor is accompanied by continuous interchanges among radiant, thermal, kinetic, and pressure energy. Large amounts of latent heat are released when water condenses in the clouds and falls as precipitation on the earth surface. It carries kinetic energy while flowing through watersheds. Vertical movement and percolation through the earth's crust finally causes changes in potential and pressure energies *(Langensiepen, 2008)*.

The first law of thermodynamics states that energy is neither created nor destroyed; only converted from one form into another. This effectively means that the input and output energies of a completely defined system must balance. Storage effects may temporarily disturb this equilibrium condition. The energy balance must thus be expressed in its most general form as:

$$Energy\ Input = Energy\ Output + Energy\ Storage \quad (2.6)$$

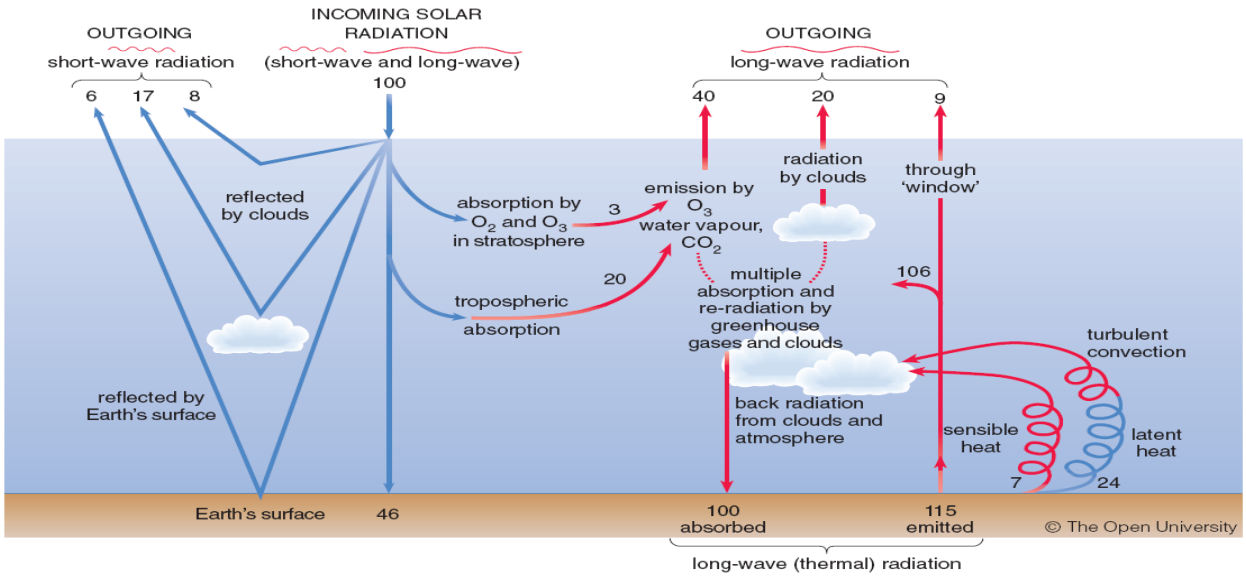

Figure 2-6 *Schematic illustration of the surface energy balance*

The water balance of the earth-atmosphere system can be treated analogically as the mass of water is conserved at all times. Evaporation is the connecting link between the system's water and energy balances. It is a surface process, which takes place at the lower boundary of the atmosphere and is an important component of the surface energy balance *(figure 2-6)*.

$$R_n = LE + H + G - A + S - L_p F_p \qquad 2.7$$

Where, R_n is flux of net all wave-radiation, L is latent heat, E is evaporation rate, H is flux of sensible heat, G is heat flux at the lower boundary of the surface, S is heat storage and A is the energy advected to the surface when the ground properties have horizontal discontinuities. The energy balance is sometimes parameterized for a volume of surface material (for example water body, soil, or canopy volume). As the solar energy input undergoes diurnal and annual fluctuations, heat storage may become an important component of the balance when it is applied at time intervals shorter than the fluctuation period. When the layer includes vegetation, biochemical energy storage due to photosynthesis can also be considered. L_p is then the thermal conversion factor of carbon dioxide, and F_p is the flux of carbon dioxide. The partitioning of R_n into the remaining terms of the surface energy balance determines the rate of surface evaporation and depends on the availability of surface water.

SEBS model was based on the conservation of energy principle. All the energy involved in the soil-vegetation-atmosphere interface comes from solar radiation, and then expressed as several forms, which can be given as energy balance equation:

$$R_n = G + H + \lambda E \quad 2.8$$

Where, R_n is net radiation G is soil heat flux, H is sensible heat flux and λE is the latent heat flux, which can be expressed as height of water, i.e., evapotranspiration. All units in this equation are expressed in (Wm^{-2}), and all fluxes are defined positive if directed downwards. Note that the energy required for photosynthesis and heat stored in the vegetation was neglected in this equation.

2.10.2 Net Radiation

Net radiation (R_n) is the amount of radiation left after all out going radiations are subtracted from all incoming radiations; it is the sum of incoming and outgoing short and long wave radiation at the surface, which constitutes a key driver for heating the atmosphere and the ground. It is formulated as:

$$R_n = R_{swd} - R_{swu} + R_{lwd} - R_{lwu} \quad 2.9$$

Where, $R_{swd}, R_{swu}, R_{lwd}\ and\ R_{lwu}$ stand for the incoming short wave radiation, outgoing short wave radiation, incoming long wave radiation and outgoing long wave radiation, respectively.

Due to the truth that some terms required in this equation are always missing, so this equation can also be expressed as:

$$R_n = (1 - \alpha) * R_{swd} + \varepsilon * R_{lwd} - \varepsilon * \sigma * T_0^4 \quad 2.10$$

Where, α is surface albedo, ε is emissivity of the surface, σ is the Stefan-Boltzmann constant, equals to $5.6697*10^{-8}$ $Wm^{-2}K^{-4}$ and T_0 is surface radiative temperature measured by a remote sensor. α, ε and T_0 can be derived from remote sensing data from the visible to the thermal infrared spectral range, and some empirical methods are developed to retrieve those parameters from remotely sensed data, which will be discussed in chapter four.

Instantaneous incoming short wave radiation $(\boldsymbol{R_{swd}})$

Normally, incoming short wave radiation can be estimated by multiplying terrestrial short wave radiation with a transmission coefficient, which descript the transmit ability of short wave through the atmosphere (Iqbal, 1983):

$$R_{swd} = \tau \cdot K_{\downarrow}^{exo} \qquad 2.11$$

Where, τ is optical thickness (atmospheric transmissivity coefficient), $K_{\downarrow}^{exo}$ is terrestrial short wave radiation (Wm^{-2}).

The terrestrial short wave radiation is a function of the solar zenith angle at certain latitude and time and the distance between sun and earth. The maximum instantaneous short wave radiation outside the atmosphere, measured at an average sun-earth distance and perpendicular to the solar rays is equal to 1367 Wm^{-2}, which is the solar constant. Instantaneous terrestrial short wave radiation is given by:

$$K_{\downarrow}^{exo} = SC \cdot E_0(sin\delta sin\emptyset + cos\delta cos\emptyset cos\omega) = SC \cdot E_0 Cos\theta \qquad 2.12$$

Where, SC is solar constant (1367 Wm^{-2}), E_0 is eccentricity correction factor, θ is solar zenith angle, δ is solar declination, $\emptyset$ is latitude of the target area and ω is hour angle.

Eccentricity correction factor explains the variances of earth-sun distance throughout the year due to the circle orbit that earth around the sun. It is given by

$$E_0 = 1.000110 + 0.034221\, cos(da) + 0.001280\, sin(da) + 0.000719\, cos(2da) + 0.000077 si\, n(2da) \qquad 2.13$$

Where, the day angle (*da)* is defined as:

$$da = (d_n - 1) * \frac{2\pi}{365} \qquad 2.14$$

Where, d_n is day number of the year, which ranging from 1 on January 1st to 365 on December 31. Note that on leap years, the number of days in the year is 366. Therefore, the accuracy of *equation 2.13* varies slightly; another simple equation can be used:

$$E_0 = 1 + 0.033Cos\left[\frac{2\pi d_n}{365}\right] \quad 2.15$$

Hour angle is calculated based on the local solar time (LAT):

$$\omega = 15(LAT - 12)\frac{\pi}{180} \quad 2.16$$

When the Universal Time or (GMT) is given, LAT can be calculated as follows.

$$LAT = UTC + 4\frac{L_c}{60} + \frac{E_t}{60} \quad 2.17$$

Where, L_c is longitude at the point of interest, and E_t is the so-called equation of time, which descript the fluctuation of local time due the earth rotates around its axis when it moves in an elliptical orbit around the sun. It is given by

$$E_{\mathrm{t}} = 0.000075 + 0.001868\,cos(da) - 0.032077\,sin(da) - 0.014615\,cos(2da) - 0.04089sin(2da) \quad 2.18$$

Solar declination δ is the angle between the elliptic plane and the earth's equatorial plane, which describe the position of the sun during different seasons. It can be calculated as:

$$\delta = 0.006918 + 0.399912\,cos(da) - 0.070257\,sin(da) - 0.006758\,cos(2da) + 0.000907sin(2da) - 0.002697cos(3da) + 0.00148sin(3da) \quad 2.19$$

The much simpler equation for solar declination is given by

$$\delta = 0.409Sin\left[\frac{2\pi}{365}d_n - 1.39\right] \quad 2.20$$

Atmospheric transmissivity coefficient τ can be derived from measurements at the weather station. If no measurement is found, a simple relation development by Tasumi et al. (2000) can be used, which is expressed as

$$\tau = 0.75 + 2 * 10^{-5} * h \quad 2.21$$

Where, *h* is elevation in meters above mean sea level.

Instantaneous incoming long wave radiation $(\boldsymbol{R_{lwd}})$

The incoming long wave radiation is emitted by atmosphere when it has a certain temperature, so it depends on the temperature of the atmosphere and transmittance process in the atmosphere. It can be calculated according to Planck law:

$$R_{lwd} = \sigma \cdot \varepsilon_a \cdot (T_a + 273)^4 \qquad 2.22$$

Where, T_a is atmosphere temperature in Celsius at reference height, σ is Stefan-Boltzmann constant, ε_a is the emissivity of the atmosphere, and a few practical approaches can be selected to drive this parameter. In SEBS, the Swinbank formula is used:

$$\varepsilon_a = 9.2 * 10^{-6}(T_a + 273.15)^2 \qquad 2.23$$

Instantaneous outgoing short wave radiation $(\boldsymbol{R_{swu}})$

Part of the incoming short wave radiation will go back to atmosphere from surface due to the surface reflectance between certain ranges of wave lengths. The ratio of incident solar radiation to reflected solar radiation is called albedo and the instantaneous outgoing short wave radiation multiply the incoming short wave radiation with surface albedo:

$$R_{swu} = R_{swd} * \alpha \qquad 2.24$$

Where, α is surface broadband albedo that can be estimated from single bands reflectance recorded in satellite-based sensors.

Instantaneous outgoing long wave radiation $(\boldsymbol{R_{lwu}})$

The outgoing long wave radiation is directly calculated from Stefan-Boltzmann's law:

$$R_{lwu} = \varepsilon_0 \sigma T_0^4 \qquad 2.25$$

Where, ε_0 is surface broadband emissivity, σ is Stefan-Boltzmann constant and T_0 is surface temperature. All can be derived from remote sensing data from the visible to the thermal infrared spectral range.

Daily incoming global radiation $(K_{24}^{\downarrow})$

Daily incoming global radiation is a function of geometric and atmospheric factors and it can be estimated by

$$K_{24}^{\downarrow} = 11.5741 \cdot \left[\left(a_s + b_s \cdot \frac{n}{N}\right) K_{24}^{\downarrow exo}\right] \quad 2.26$$

Where, $K_{24}^{\downarrow exo}$ is daily terrestrial solar radiation ($MJm^{-2}day^{-1}$), $\frac{n}{N}$ is sunshine fraction (-), a_s and b_s are constants to be evaluated at ground stations, default values for them are 0.25 and 0.5, respectively.

The daily terrestrial solar radiation at the point of consideration is defined as:

$$K_{24}^{\downarrow exo} = \frac{24}{\pi} \cdot SC' \cdot E_0 \cdot sin\emptyset \cdot sin\delta \cdot (\omega_s - tan\omega_s) \quad 2.27$$

Where, SC' is the solar constant, equals to $1367*0.0036 MJm^{-2}hour^{-1}$ and w_s is sunshine hour angle given by

$$cos\omega_s = -tan\emptyset tan\delta \quad 2.28$$

For the sunshine fraction $\frac{n}{N}$, n is the amount of hours that the sun was actually shining for a certain day and location. It can be obtained from meteorological observation. N is the total hours of sunshine for a perfect clear day, which is given by

$$N = \frac{360}{15\pi}\omega_s \quad 2.29$$

Daily net long wave radiation (L_{24})

Daily long wave radiation is the energy exchange between the earth's surface and atmosphere in form of radiation at longer wavelengths. Appropriate instruments in stations can measure it. If the station does not have any net long wave radiometer, the mean daily air temperature can be used to retrieve this term through combination with air emissivity as given below.

$$L_{24} = -f \cdot \varepsilon \cdot \sigma \cdot (T_{a-mean} + 273)^4 \quad 2.30$$

Where, σ is the Stefan-Boltzmann constant (5.6697x 10^{-8}Wm^{-2}K^{-4}), ε is emissivity between the atmosphere and the ground and T_{a-mean} is mean daily air temperature at screen level (^{0}C).

2.10.3 Soil Heat Flux

The soil heat flux (G) is the rate of heat storage in a soil because of temperature gradient between soil surface and the underlying topmost soil layers. The temperature gradient varies with the fractional vegetation cover and the leaf area index, as light interception form and shadow formation on the bare soil determine radiative heating of the bare soil surface. It is determined as an unfixed percentage of the total available energy, which is given by

$$G_0 = R_n * [\Gamma_c + (1 - f_c) * (\Gamma_s - \Gamma_c)] \quad 2.31$$

Where, Γ_c and Γ_s are empirical coefficient. These values have been determined using exponential observations, but depend also on the soil and vegetation type. For most bare soil conditions a Γ_s value of 0.315 is valid *(Kustas et al., 1989)*, and for vegetation often Γ_c is assumed to be 0.05 *(Choudhury and Monteith, 1988)*. An interpolation is then performed between these limiting cases using the fractional canopy coverage, f_c , which can be determined from remote sensing data.

2.10.4 Sensible Heat Flux

Sensible heat flux (H) is the rate at which energy loss from soil through convection and diffusion process because of temperature difference between the surface and lower most overlaying atmosphere. To determine the sensible heat flux, similarity theory is applied. The relationships for the mean wind and temperature profiles are written in integral form as:

$$u = \frac{u^*}{k}\left[ln\left(\frac{z - d_0}{z_{0m}}\right) - \Psi_m\left(\frac{z - d_0}{L}\right) + \Psi_m\left(\frac{z_{0m}}{L}\right)\right] \quad 2.32$$

$$\theta_0 - \theta_a = \frac{H}{ku^*\rho C_p}\left[ln\left(\frac{z - d_0}{z_{0h}}\right) - \Psi_h\left(\frac{z - d_0}{L}\right) + \Psi_h\left(\frac{z_{0h}}{L}\right)\right] \quad 2.33$$

Where, ρ is density of air (Kgm^{-3}), C_p is dry air heat capacity (-), k is the Von Karman constant (=0.41), z is height at which the meteorological observations are made (m), u^* is friction velocity ($u^* = (\tau_0/\rho)^{1/2}$, ms^{-1}) , $\theta_0$and θ_a are potential air temperature (K) at height z_{0h} and at height z,

d_0 is zero plane displacement height (m), z_{0h} and z_{0m} are surface roughness heights for heat and momentum transfer (m), Ψ_h and Ψ_m are stability correction functions for heat and momentum transfer, respectively. L is Obukhov stability length (m) given by,

$$L = -\frac{\rho C_p u_*^3 \theta_v}{kgH} \quad 2.34$$

Where, g is the acceleration due to gravity (ms^{-2}) and θ_v is the potential virtual temperature near the surface (K).

The actual sensible heat flux (H) is determined by using the friction velocity (u^*) and stability length (L) obtained from iterative procedure.

The generation of the sensible heat flux in SEBS model is driving by the difference between the aerodynamic temperature (T_{aero}) or θ_0 and the air temperature *(T_a)* or θ_a. The difference between these two temperatures is corrected for stability in the Atmospheric Boundary Layer (ABL) and Atmospheric Surface Layer (ASL) to obtain the sensible heat flux. Detailed discussion for Similarity Stability Correction Functions can be found in *Su and Jacobs (2001).*

2.10.5 Latent Heat of Vaporization

Latent heat of vaporization, λ, express the energy required to change a unit mass of water from liquid to water vapour in a constant pressure and temperature process. It can be calculated by the equation below:

$$\lambda = 2.501 - (2.361 * 10^{-3}) * T \quad 2.35$$

Where, λ is latent heat of vaporization ($MJKg^{-1}$) and T is the air temperature (^0C).

The value of latent heat varies only slightly over normal temperature ranges (Harrison, 1963). A single value may be taken (for T=20^0C): $\lambda = 2.45 MJKg^{-1}$.

2.10.6 Evaporative Fraction

Subsequent to determination of the latent heat flux as a residual term of the energy balance on instantaneous base, the evaporative fraction (L), which represents the proportion of energy used for evapotranspiration relative to the total energy available for evapotranspiration process is calculated. The surface energy balance computation with the SEBS algorithm is based on the determination of the relative evaporation fraction:

$$\Lambda_r = 1 - \frac{H - H_{wet}}{H_{dry} - H_{wet}} \quad 2.36$$

Where, Λ_r is the relative evaporation fraction (-), H_{wet} is the wet-limit of sensible heat flux (Wm^{-2}) and H_{dry} is the dry-limit of sensible heat flux (Wm^{-2}).

The values for H_{dry} are simply determined by assuming the latent heat flux become negligible. Energy balance is then represented by:

$$H_{dry} = R_n - G_0 \quad 2.37$$

The sensible heat flux at the wet limit is given as follow.

$$H_{wet} = \left\{ \frac{(R_n - G_0) - \frac{\rho C_p}{r_{ah\_wet}} * \frac{e_s - e}{\gamma}}{1 + \frac{\Delta}{\gamma}} \right\} \quad 2.38$$

The aerodynamic resistance (r_{ah_wet}) for wet surface conditions can be derived with:

$$r_{ah_{wet}} = \frac{1}{ku^*}\left[ln\left(\frac{z - d_0}{z_{0h}}\right) - \Psi_h\left(\frac{z - d_0}{L_{wet}}\right) + \Psi_h\left(\frac{z_{0h}}{L_{wet}}\right)\right] \quad 2.39$$

The stability length suitable for wet conditions (L_{wet}) is estimated as:

$$L_{wet} = -\frac{\rho u_*^3}{0.61kg(R_n - G_0)/\lambda} \quad 2.40$$

2.10.7 Turbulent Heat Fluxes and Actual Evaporation

The actual sensible and latent heat fluxes are expressed as:

$$H = (1 - \Lambda)(R_n - G) \quad 2.41$$

$$\lambda E = \Lambda(R_n - G) \quad 2.42$$

When the evaporative fraction is known, daily evaporation can be determined as:

$$E_{daily} = 8.64 * 10^7 * \bigwedge_0^{24} * \frac{\bar{R}_n - \bar{G}_0}{\lambda \rho_w} \quad 2.43$$

Where, E_{daily} is actual evaporation on daily basis (mmd^{-1}); $\bigwedge_0^{24}$ is daily average evaporative fraction, which can be approximated by the SEBS estimate since the evaporative fraction is conservative *(Shuttleworth et al., 1989)*. $\bar{R}_n$ and $\bar{G}_0$ are the daily net radiation flux and soil heat flux, λ is the latent heat of vaporization (JKg^{-1}), ρ_w is the density of water (Kgm^{-3}).

Since the daily soil heat flux is close to zero because of the downward flux in day time and the upward flux at night approximately balance each other, the daily evaporation only depends on the net radiation flux given by:

$$\bar{R}_n = (1 - \alpha)K_{24}^{\downarrow} + \varepsilon L_{24} \quad 2.44$$

Where, $K_{24}^{\downarrow}$ is daily incoming global radiation and L_{24} is daily net long wave radiation. The daily average albedo, α, and emissivity, ε, can be approximated easily with the same values as used previously in the energy balance equation.

By summing up the corresponding daily evaporation for a certain period, the actual evaporation for that period (i.e. a week, a month or a year) can be determined. However, errors will occur due to cloud effects. Such effects can be further removed by using the time series processing or by data assimilation procedures.

3. Study Area and Materials

3.1 Description of the Study Area

3.1.1 Location and Coverage of Awash River Basin

The Awash River Basin is the fourth largest catchments in Ethiopia by area (covers 116,000Km^2), but only the seventh interms of water resources, (mean annual runoff). It is located in the center-east of Ethiopia borderedto the north by the Dankil River Basin, to the west by the Abbay River Basin, to the west-south by the Omo-Gibe and Rift Valley Lakes River Basins, to the south-east by the Wabe-Shebele River Basin and to the east by the Republic of Djibouti, the Somali Democratic Republic and the Aysha Dray Basin *(Halcrow, 2006)*. The basin lies between longitude 7^{0}52'12''N and 12^{0}08'24''N, and latitude 37^{0}56'24''E and 43^{0}17'24''E.

TheAwash river rises to the west of Addis Ababa at an elevation of about 3,000m in the central Ethiopia high lands, flowing eastwards through the Becho Plains before entering the Koka Reservoir, a dual-purpose dam for flood control and hydropower generation. It then flows in a north easterly direction through the northern extension of Rift Valley to eventually discharge in to Lake Abe near the Djibouti boarder at an altitude of 250m. The length of the river is about 1,200Km. Due to its strategic location, good road communications and availability of land and water resources, it is the most developed river basin in Ethiopia with respect to irrigation *(Halcrow, 2006)*.

The Awash Basin master plan study *(Halcrow, 1989)* classifies the basin in to Uplands, the Valleys and the Plains, in terms of location, altitude, climate, topography, agricultural development and administrative boundaries as. The Uplands encompasses the area of the basin above 1,500m. The Uplands are further divided in to the Upper Basin or the Koka Catchment upstream of Koka Dam (1,500m – 3,000m), the Eastern Catchment (>1,500m) and the Western Catchment (1,500m – 2,700m) based on location. The Valleys consist of the Upper (1,000m – 1,500m) and Middle Valley (500m – 1,000m) areas and the Plain (250m – 500m) demarcates the Lower Awash.

3.1.2 Topography and Drainage Network of the UAB

The Upper Awash Basin, which corrosponds to the Koka Catchment, covers about 10,748 km^2, contributes a significant proportion of the flow in the river. It is located approximately $8^0$12'59.39''N to $9^0$18'00.64''N, latitude and $37^0$56'41.73''E to $39^0$16'53.09''E, longitude. Land elevation of the sub basin ranges from 3,000m on the plateau, where the Awash River rises, to 1,500m at the break of the Rift Valley. Soil erosion and land degradation are the most important problems in the Upper Awash Basin *(Halcrow, 2006)*.

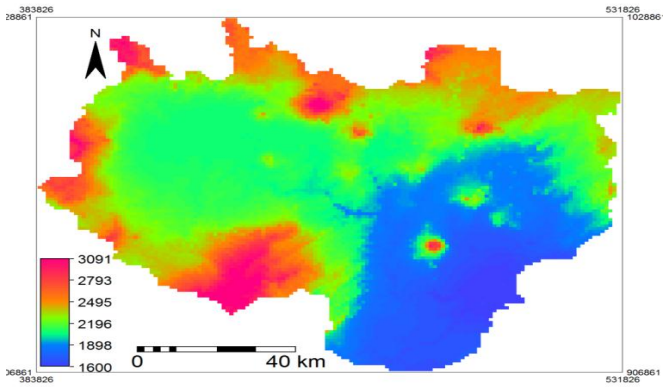

Figure 3-1 *DEM of the Upper Awash Basin (Projection: UTM zone 37N, Datum: WGS1984, Ellipsoid: WGS84)*

The major rivers that flow to the sub-basin are River Awash and River Modjo. The other major tributaries of Awash River upstream of Lake Koka are Akaki, Holeta, Berga and Legedadi Rivers. The sub basin is also divided in to five watersheds (*Paulos, 1998*) as shown in *table 3-1*.

Table 3-1 *Watersheds of Upper Awash Basin and their coverage*

Watersheds	Drainage area (km^2)	Perimeter (km)	Stations found within the watersheds
Watershed 1 (W_1)	4530.378	412.352	Ginchi, Berga, Awash Belo, Teji and Melaka Kunture
Watershed 2 (W_2)	474.106	108.853	Holeta
Watershed 3 (W_3)	1608.802	219.062	Little Akaki, Akaki
Watershed 4 (W_4)	2176.574	216.994	Hombole
Watershed 5 (W_5)	1901.694	235.382	Modjo

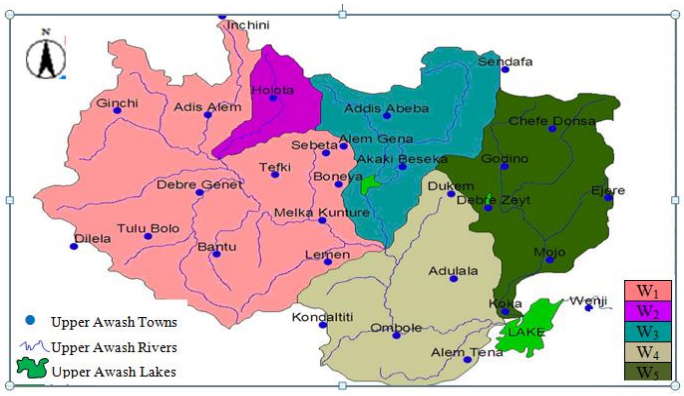

Figure 3-2 Watersheds of Upper Awash Basin

3.1.3 Climate

Rainfall

The mean annual rainfall of the area calculated using the daily long-term rainfall record of six stations (1999-2008) namely Addis Ababa, Debre Zeit, Shola Gebeya, Chefe Donsa, Ejere and Sendafa obtained from National Meteorology Agency (NMA) amounts to 981mm. As shown in figure 3.3, the annual rainfall has consistency in nature with slight degree of variation. The wettest year in the record period is 2003 with rainfall of 1123mm; the amount recorded in the driest year (2002) is only 21% and 30% lower than the mean annual rainfall and the wettest year rainfall, respectively. The wet period in a year lies between June and September and the dry period between October and February. The remaining months (March through May) have moderate rainfall. The wet period contributes 79% of the mean annual rainfall. December is the driest month in a year contributing only 9mm of rainfall.

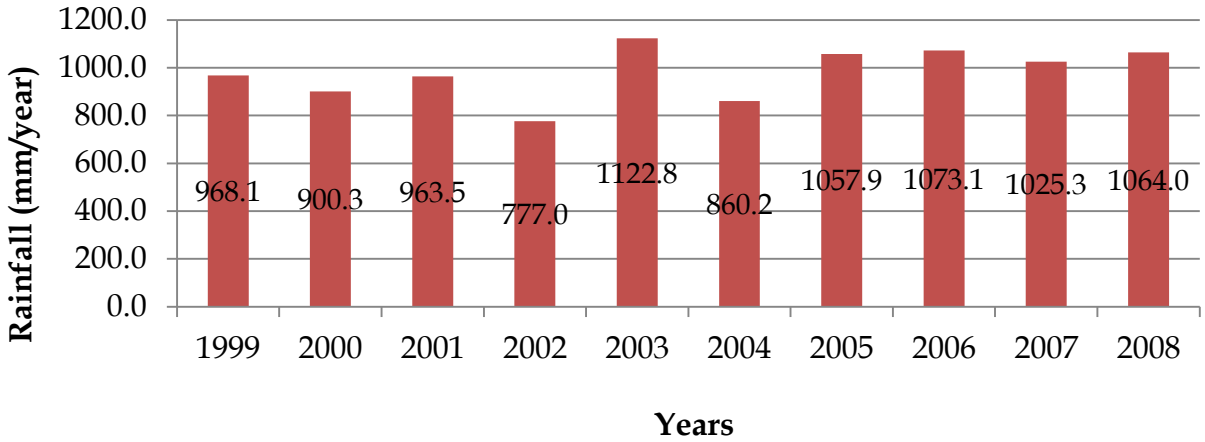

Figure 3-3 Distribution of annual rainfall (1999-2008)

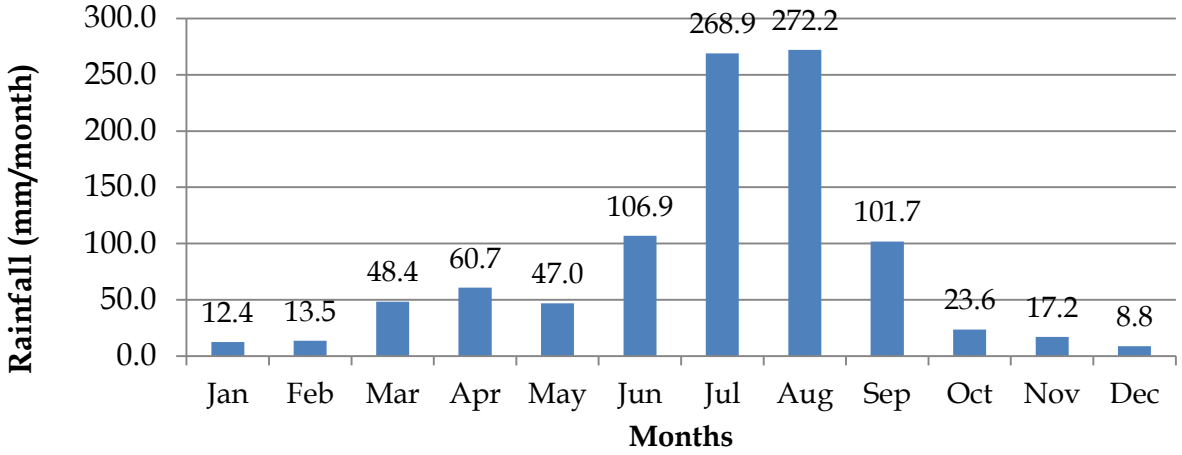

Figure 3-4 Distribution of mean monthly rainfall (1999-2008)

Temperature

Figure 3.5 shows the mean monthly temperature calculated using the long-term daily record at four stations namely Addis Ababa, Debre Zeit, Shola Gebeya and Chefe Donsa. Accordingly, the hottest month is May with mean daily temperature of 18.8^{0}C and the coldest months are November and December with mean daily temperature of 14.9^{0}C.

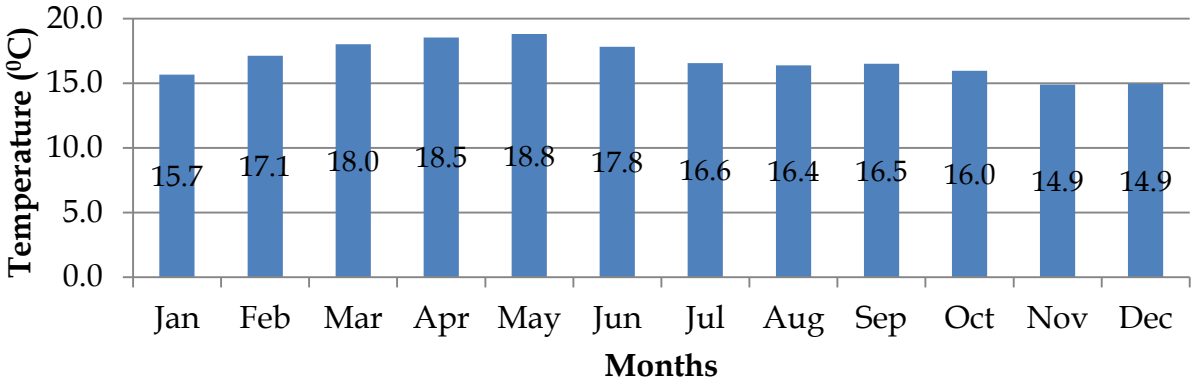

Figure 3-5 Distribution of mean monthly temperature (1999 - 2008)

3.1.4 Land Use/Cover

The land use/cover (LULC) of Upper Awash Basin consists mainly of cultivated agricultural land, grass land and shrub land, which cover 93.2% of the total area; about 3.6% is covered by savanna and the remaining 3.2% comes from the other land cover types as shown in *table 3-2*.

Figure 3-6 represents the MODIS product raster map of different land use/cover in the study area that was developed within the temporal coverage of 2001 and 2004.

Table 3-2 *MODIS land use/cover product classification*

Value	Description	Coverage [Km^2]	Value	Description	Coverage [Km^2]
0	Water body	15	5	Broadleaf forest land	71
1	Grasses/Cereal crops land	4504	6	Needle leaf forest land	80
2	Shrubs land	3325	7	Non-vegetated land	67
3	Broadleaf crops land	2206	8	Urban area	109
4	Savanna land	383	254	Unclassified area	---

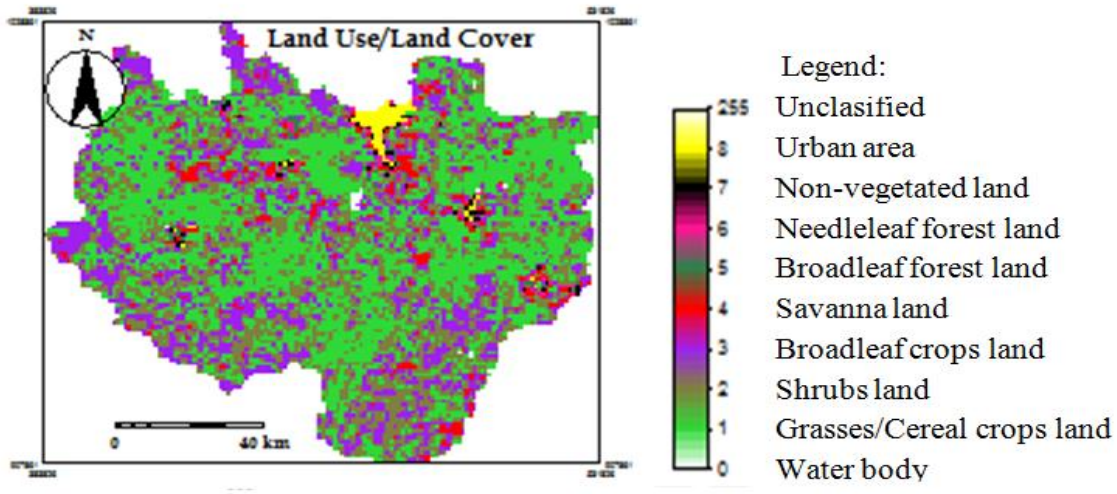

Figure 3-6 *MODIS land use/cover product*

3.2 Materials

In this research, both satellite-derived and ground-based data were collected for estimation of evapotranspiration using SEBS model. Apart from that, the satellite- derived rainfall data were collected for water balance analysis. Both remote sensing and ground-based data collected for this research cover the study period from March to September 2008. Except rainfall data, all data described in this chapter were collected for a day representing respective month for a total of seven days during the study period. The selection of days in each month was based on the daily

rainfall occurrence and clear sky over the study area. The monthly rainfall product was collected for the whole study period.

3.2.1 Meteorological and Hydrological Data

Addis Ababa (Bole) and Nazareth stations meteorological data of the study area and study period (2008), namely daily precipitation, daily minimum and maximum air temperature, three hours relative humidity, three hours wind speed and daily sunshine hours data, were collected from the National Meteorological Agency (NMA) Head Office and Nazareth Branch Office, respectively. The flow records of the Hombole station, the nearby station to the outlet of the Upper Awash Basin, for 2008 was collected from Ministry of Water Resource (MoWR).

3.2.2 Digital Elevation Model

90m resolution Digital Elevation Model (DEM) was freely downloaded from Shuttle Radar Topography Mission (SRTM), *figure 3-1*, through the URL *<srtm.csi.cgiar.org/selection/inputcoord.asp>*. SRTM is an international project spreadsheet by the National Geospatial-Intelligence Agency (NGA), NASA, the Italian Apace Agency (ASI) and the German Aerospace Center (GLR). It provides three resolution outputs: 1Km and 90m resolution DEMs for the world and 30m resolution DEM for the U.S.

3.2.3 MODIS Land Surface Products and Acquirement

3.2.3.1 MODIS Land Surface Products

Surface Reflectance Products

- *MODIS/Terra Surface Reflectance Daily L2G Global 1 km and 500 m SIN Grid Day (MOD09GA)*

The MODIS Surface Reflectance products provide an estimate of the surface spectral reflectance, as it would be measured at ground level in the absence of atmospheric scattering or absorption. Low-level data are corrected for atmospheric gases and aerosols, yielding a level-2 basis for several higher-order gridded level-2 (L2G) and level-3 products.

MOD09GA provides Bands 1-7 in a daily gridded L2G product in the Sinusoidal projection, including 500-meter reflectance values and 1-kilometer observation and geolocation statistics.

500-m Science Data Sets provided for this product include reflectance for bands 1-7, a quality rating, observation coverage, observation number, and 250-m scan information. 1-kilometer Science Data Sets provided include number of observations, quality state, sensor angles, solar angles, geolocation flags, and orbit pointers.

Land Surface Temperature/Emissivity products

- *MODIS/Terra Land Surface Temperature/Emissivity 8-Day L3 Global 1 km SIN Grid Day (MOD11A2 Day)*

The level-3 MODIS global Land Surface Temperature (LST) and Emissivity 8-day data are composed from the daily 1-kilometer LST product (MOD11A1) and stored on a 1-km Sinusoidal grid as the average values of clear-sky LSTs during an 8-day period.

MOD11A2 is comprised of daytime and nighttime LSTs, quality assessment, observation times, view angles, bits of clear sky days and nights, and emissivities estimated in Bands 31 and 32 from land cover types.

Land Cover Type Products

MODIS/Terra Land Cover Type Yearly L3 Global 1km SIN Grid (MOD12Q1)

The V004 MODIS Land Cover Dynamics (MOD12Q2) product (informally called the MODIS Global Vegetation Phenology product) provides estimates of the timing of vegetation phenology at global scales. Additionally, it also provides information related to the range and summation of the Enhanced Vegetation Index (EVI) computed from MODIS surface reflectance data at each pixel. It identifies the vegetation growth, maturity, and senescence that mark seasonal cycles. MOD12Q2 is produced twice a year with 24 months of input data (i.e., the 12 months of interest data bracketed by six month's data on either side). The version 004 MOD12Q2 products range from 2001 through 2004.

MOD12Q2 primarily uses MODIS EVI, which is computed from the MODIS Nadir Bidirectional Reflectance Distribution Function (BRDF)-Adjusted Reflectance (NBAR) product instead of the MOD09 surface reflectance product. It uses NBAR values computed from a 16-

day period at 1 km spatial resolution. Huete et al. (2002) provide the formula used to derive the EVI from the NBAR data.

3.2.3.2 Acquirement of MODIS Products

MODIS data and products are available at no charge and distributed by the Land Processes Distributed Active Archive Center (LP DAAC), located at the U.S. Geological Survey (USGS) Earth Resources Observation and Science (EROS) Center through the URL *<http://lpdaac.usgs.gov/lpdaac/get_data/data_pool>*.

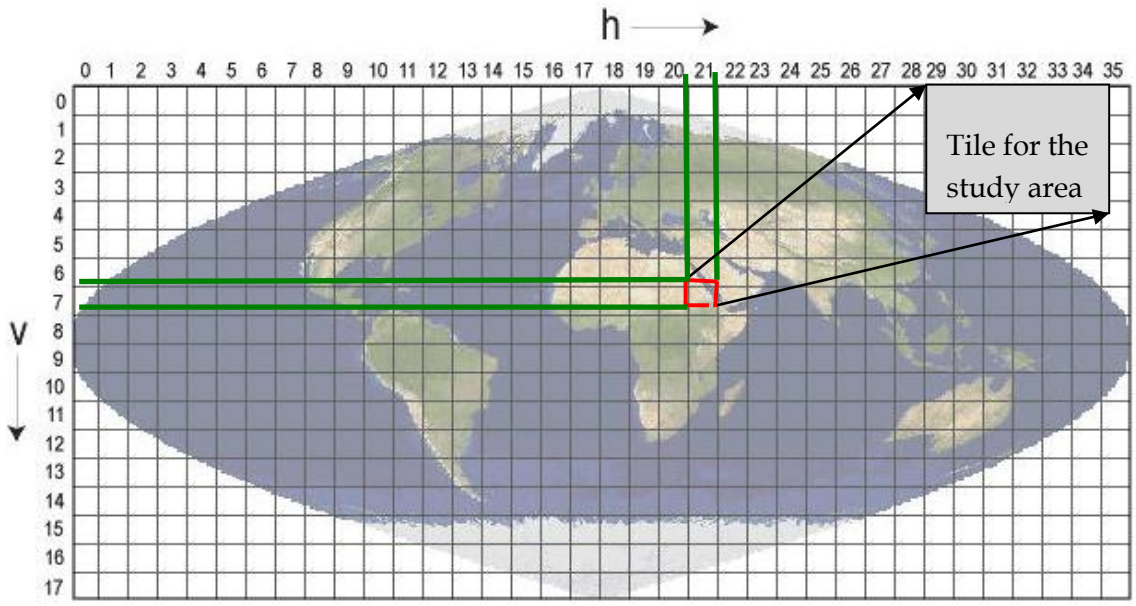

Figure 3-7 *MODIS satellite tile coverage and tile location for the study area*

MODIS Level 2G, Level 3, and Level 4 products are defined on a global 250 m, 500 m, or 1 km sinusoidal grid (the particular spatial resolution is product dependent). Because these grids are unmanageably large in their entirety (43200X21600 pixels at 1 km, and 172800X86400 pixels at 250 m); they are divided into a fixed tiles approximately 10^0X10^0 in size. Each tile is assigned a horizontal (H) and vertical (V) coordinate, ranging from 0 to 35 and 0 to 17, respectively. The tile in the upper left (i.e. northernmost and westernmost) corner is numbered (0, 0).

3.2.4 SPOT VGT4AFRICA Products

Normalized Difference Vegetation Index (NDVI) images for the study period were freely downloaded from websites of the VGT4AFRICA. The VGT4AFRICA project distributes VEGETATION data (all advanced products derived from the VEGETATION instrument on board from the Sensor Placement Optimization Tool (SPOT) satellites and high level derived products) to all African countries through EUMETCast telecommunication system.

All products from the product portfolio are made available in near real time to the end-users at 10-daily intervals and 1-kilometer spatial resolution with Hierarchical Data Format (HDF) and at no cost. Products are computed from atmospherically corrected bi-directional surface reflectance that have been masked for water, clouds, heavy aerosols, and cloud shadows.

3.2.5 3B43-TRMM Product

The purpose of 3B43 algorithm, TRMM and Other Data Sources, is to produce the best-estimate precipitation rate (mm/hr) and Root-Mean-Square (RMS) precipitation-error estimates from TRMM and other data sources.

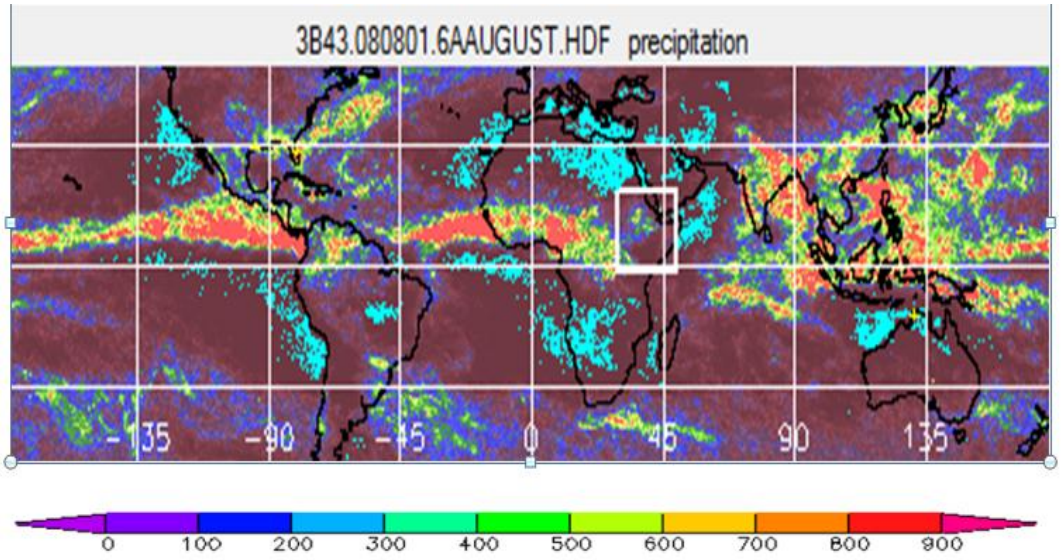

Figure 3-8 *Monthly TRMM 3B43 map for August 2008*

The algorithm combines four independent precipitation fields: (1) the monthly average unclipped TRMM Microwave Imager (TMI) estimate (intermediate product from Algorithm 3B42), (2) the

monthly average Special Sensor Microwave/Imager (SSM/I) estimate (TRMM product 3A46), (3) the pentad-average adjusted merged-infrared (IR) estimate (TRMM product 3B42), and (4) the monthly accumulated Climate Assessment and Monitoring System (CAMS) or Global Precipitation Climatology Centre (GPCC) rain gauge analysis (TRMM product 3A45). All input data have a calendar month temporal resolution except the adjusted merged-IR data, which have a daily resolution. To obtain the requisite calendar month average of adjusted merged-IR data, the 3B43 algorithm averages the adjusted merged-IR daily data that span the calendar month of interest. Also, the monthly average unclipped TMI data, prior to their combination with the SSM/I, adjusted merged-IR, and rain gauge data, are converted (calibrated) to TRMM Combined Instrument (TCI) data, using the TMI/TCI calibration parameters (from TRMM product 3B31). After the preprocessing is complete, the four independent precipitation fields are merged together to form the best-estimate precipitation rate and RMS precipitation-error estimates. These gridded estimates have a calendar month temporal resolution and a 0.25 degree by 0.25 degree spatial resolution. Spatial coverage extends from 50 degrees south to 50 degrees north latitude. The data are stored in the HDF format, which includes both core and product specific metadata *(Huffman et al., 2004)*. These products are freely accessed through the website: *< http://daac.gsfc.nasa.gov>*.

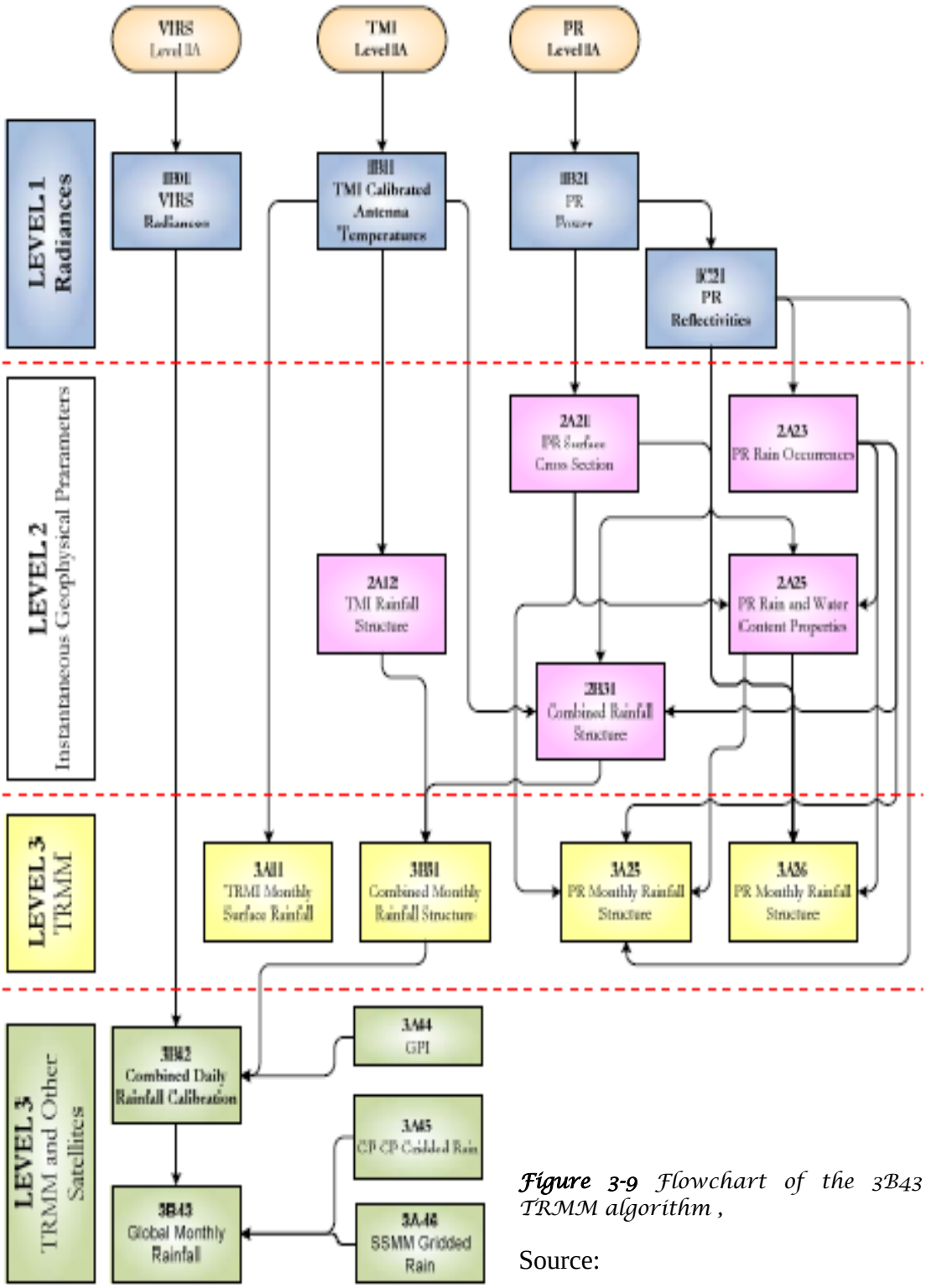

Figure 3-9 *Flowchart of the 3B43 TRMM algorithm ,*

Source:

<http://trmm.gsfc.nasa.gov>

4. Methodology

4.1 General

In this research, the surface energy balance system (SEBS) model for the estimation of atmospheric turbulent fluxes was used. The model is based on the energy involved in the soil-vegetation-atmosphere interface, which can be given as energy balance equation *(equation 2.8)*. In order to retrieve regional turbulent heat flux (evapotranspiration), SEBS needs three sets of data as input.

The former data set includes land surface albedo, emissivity, land surface temperature [LST], fraction of vegetation cover [FVC], leaf area index [LAI], canopy height, normalized difference vegetation index [NDVI], digital elevation model [DEM], and Sun Zenith Angle (SZA). Those inputs can be either extracted or derived from remote sensing data. For example, MODIS products (like MOD09 for land surface albedo extraction, MOD11 for LST and emissivity extraction and MOD12 for land cover type extraction), SRTM for DEM extraction, VGT4AFRICA products for NDVI extraction, National Oceanic and Atmospheric Administration (NOAA) for SZA calculation; the FVC and LAI can be derived from NDVI products.

The second data set is meteorological data that consists of specific humidity, atmospheric pressure at surface and reference height, air temperature, relative humidity, sunshine hours and wind speed at a reference height. Some of this data set can be collected from National Meteorological Agency [NMA] and the others are derived from the collected ones.

The final data set includes downward solar radiation and downward long wave radiation that should either be measured or modeled.

The other major imput component for water balance equation is rainfall. This rainfall point data [3B43] are accessed from TRMM and then processed to raster maps applying spatial

interpolation technique. Finally, estimation of water availability/run off was conducted using simple water balance equation *(equation 2.2)*.

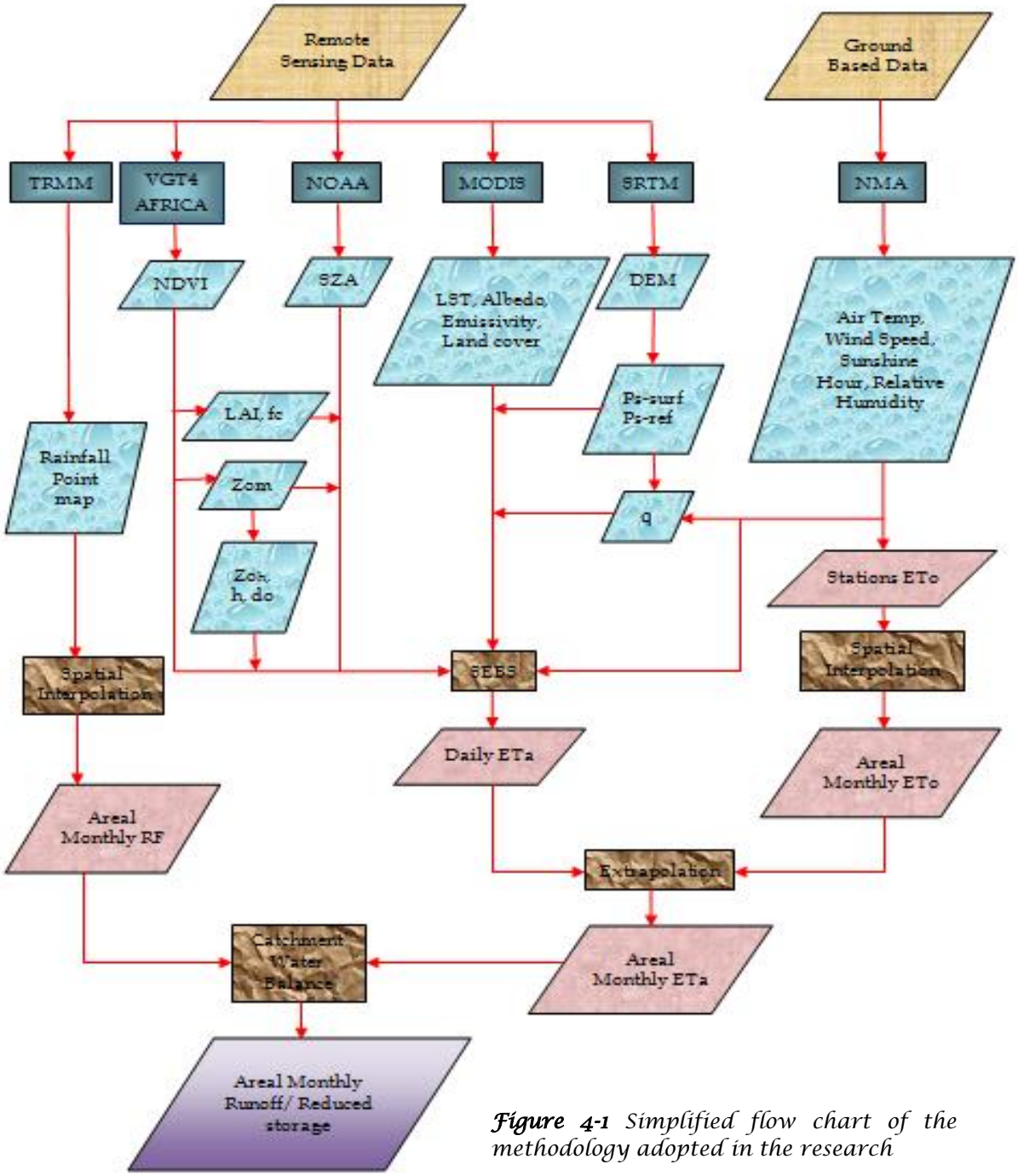

Figure 4-1 *Simplified flow chart of the methodology adopted in the research*

Simple flow chart in *figure 4-1* outlines the general work flow of the paper that was followed during data preparation and analysis of the results. furthermore, the detailed descriptions of the procedures followed in deteminig each parameters are given in the following sub topics with calculation procedures and formulations.

4.2 Satellite Images Processing

4.2.1 MODIS Product Processing

Images re-projection

MODIS imagery, however, is in a new map projection called the Integrated Sinusoidal (ISIN) projection, Hierarchical Data Format (HDF), which is not supported by most existing software packages. So before those images can be used by other software packages like ENVI, ILWIS and ERDAS, re-projection to GeoTIFF (Geographical Tag Image File Format) should be pre-processed.

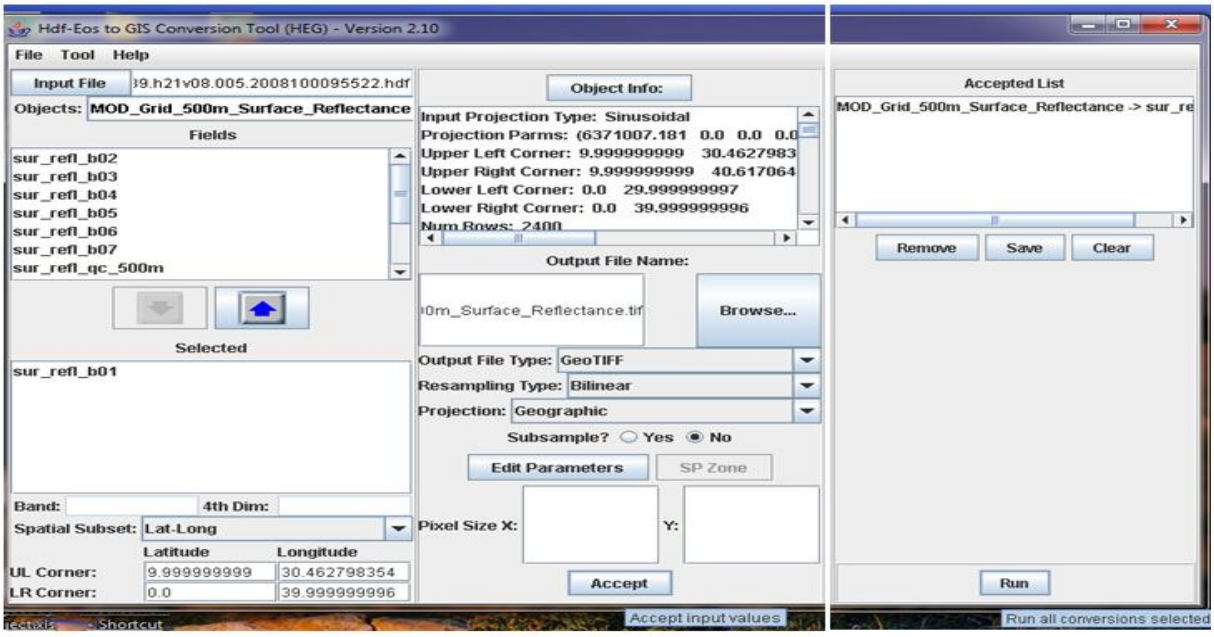

Figure 4-2 *HegWINv2.10_FullCyg tool conversion interface*

All MODIS images re-projection processes were done by the help of HDF-EOS to GeoTIFF Conversion Tool (HEG) and imported to ILWIS as GeoTIFF format for further pre-processing. The re-projection parameters used were Output files Type - GeoTIFF, Spatial subset - Latitude/Longitude, Output projection type - Geographic, Resampling type - Bilinear and Output

pixel size -1000m as shown in *figure 4-2*. The tool can be freely downloaded from the web site: *< http://newsroom.gsfc.nasa.gov/sdptoolkit/ HEG/HEGDownload.html>*.

Image Resampling and Masking

All images downloaded from their respective web sites were different horizontal resolutions and coverage. The resample operation resamples a raster map from the map's current georeference to another target georeference. The coordinate of each output pixel is used to calculate a new value from close-by pixel values in the input map. Resampling process is used to combine raster maps obtained from various sources (different projections, pixel size), to combine satellite imagery of different dates or resolutions and to combine satellite images or scanned photographs with existing rasterized vector data. Final outputs of the ILWIS software were masked to the Upper Awash Basin shape leaving the other pixels undefined.

Interpolation

While computing the evaporative fraction, output of SEBS model, some undefined pixels must happen. These undefined values were filled by interpolation process using Kriging method. The method provides more reliable results than almost any other method, in particular because in this method, the standard error can be stated though the method is restricted to interpolate to a distance of 40 times the pixel size. General description and steps of the interpolation technique is found in ILWIS software user guide web site: *<http://www.itc.nl/ilwis/userguide>*.

4.2.2 3B43 Rainfall Data Processing

The data for TRMM were downloaded as ASCII output with utilization of any RS software was converted as a point map. The interpolation of the point net was done by moving average method using ILWIS software; the method assigns to pixels weighted averaged point values. This method was used because TRMM data are grided 0.25 by 0.25 degrees, and it has short-range variation. It conform a very good established net.

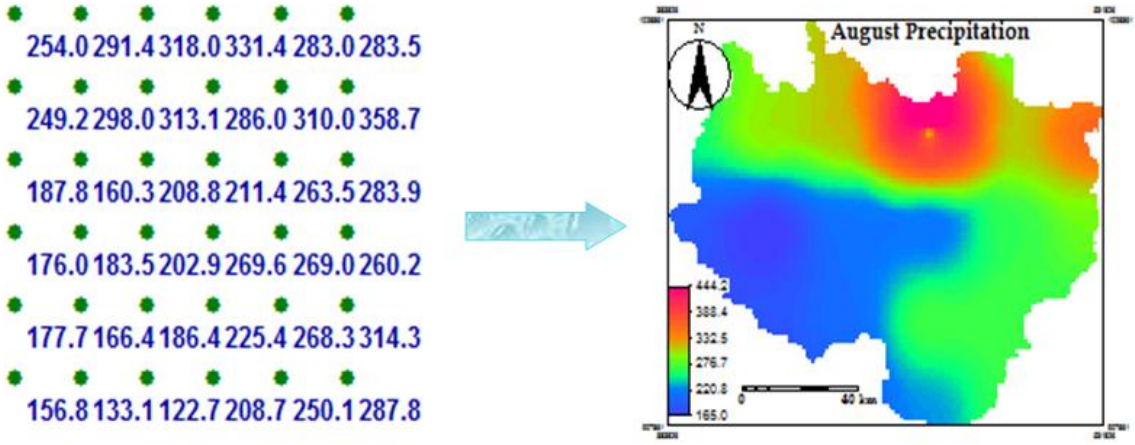

Figure 4-3 Example of moving average interpolation for the TRMM retrievals (left: point map; right: raster map)

The uniform distribution of the TRMM data is ideal for the application of standard interpolation techniques. The inverse distance function was selected as the data was very accurately measured point values and local variation, within a pixel, is small. This function ensures that the computed output values equal the input point values. Detail information on the method can be found in ILWIS software user guide. General description and steps of the interpolation technique is found in ILWIS software user guide web site: <*http://www.itc.nl/ilwis/userguide*>.

4.2.3 Tool for Visualizing TRMM Data

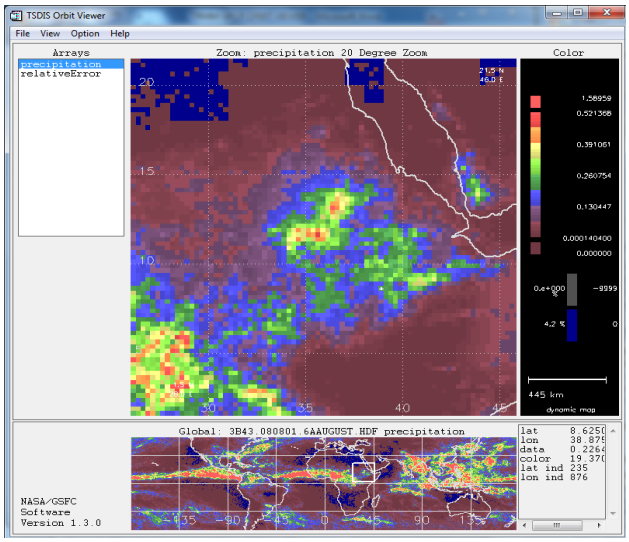

Figure 4-4 TSDIS Orbit Viewer, with 3B43 V6-August 2008, accumulated rainfall (mm)

TRMM Science Data and Information System (TSDIS) Orbit Viewer is the tool for examining, viewing and verifying HDF files; can be freely downloaded from <*ftp://disc2.nascom.nasa.gov/software/trmm_software/Orbit_Viewer/*>. It is a menu-driven graphical interface for dynamically generating images from TRMM HDF files. The viewer can display, at the full instrument resolution of TRMM satellite data products *(GES DISC, 2006).*

4.3 Meteorological Data Processing

According to frequency of observation, elements of these meteorological stations can be divided into two groups: daily base and hourly base. Hourly base include relative humidity and wind speed at 2m height, which are observed every three hours, i.e., at the time of 06:00, 09:00, 15:00 and 18:00 o'clock in a day, and daily based items include sunshine hours and temperature. Appendix A give meteorological data collected from NMA at Addis Ababa-Bole and Nazareth meteorological stations. These point data were further analyzed and converted to raster maps using ILWIS algorithm.

1. Atmospheric pressure

Atmospheric pressure at surface and reference height is other parameter required by SEBS algorithm to estimate land surface turbulent heat flux. It depends on not only on the local elevations but also the local atmospheric conditions. However, to a small and smoothly area, the average value is sufficient in the calculation procedures. In this study, the average values were adopted due to the relatively smooth conditions in the study area and little difference of air pressure between different places. A simplification of the ideal gas law, assuming 20^0C for a standard atmosphere, can be employed to calculate atmospheric pressure, P_s:

$$P_s = 101300\left(\frac{293 - 0.0065z}{293}\right)^{5.26} \qquad 4.1$$

Where, *z* is elevation of calculation height (m).

Atmospheric pressure and pressure at reference height (2m) raster map of the study area were developed with ILWIS software using Upper Awash Basin DEM and DEM plus 2m in terms of z in *equation 4.1*, respectively.

2. Specific Humidity

Specific humidity (q) is the mass of water vapour present in a unit mass of air. Where temperature is high and rainfall is excessive, the specific humidity of the air reaches high proportion. Accurate information is required to determine the surface virtual temperature in

SEBS algorithm. It can be estimated based on the actual water vapour pressure and surface pressure data:

$$q = \frac{5}{8} * \frac{e_a}{P_s} \quad 4.2$$

Where, P_s is surface pressure and e_a is actual water vapour pressure, given by:

$$e_a = \frac{RH * e_s}{100} \quad 4.3$$

Where, RH is relative humidity (%) and e_s is saturation air pressure, given by:

$$e_s(T) = 0.6108 \exp\left(\frac{17.27 * T}{T + 237.3}\right) \quad 4.4$$

Where, $e_s(T)$ is saturation air pressure at the air temperature T (KPa) and T is air temperature (^{0}C). The specific humidity raster map of the study area for each image acquisition dates were developed using surface atmospheric pressure raster map.

3. Wind Speed

Wind speeds measured at different heights above the soil surface are different. Surface friction tends to slow down wind passing over it. Wind speed is slowest at the surface and increases with height. For this reason, anemometers are placed at a chosen standard height, i.e., 10 m in meteorology (in this study Adama station) and 2 or 3 m in agrometeorology (in this study Addis Ababa Bole station). For the calculation of evapotranspiration, wind speed measured at 2 m above the surface is required. To adjust wind speed data obtained from instruments placed at elevations other than the standard height of 2m, a logarithmic wind speed profile may be used for measurements above a short-grassed surface:

$$U_2 = U_z \frac{4.87}{\ln(67.8z - 5.42)} \quad 4.5$$

Where, u_2 is wind speed at 2 m above ground surface (ms^{-1}), u_z is measured wind speed at z m above ground surface (ms^{-1}) and z is height of measurement above ground surface (m).

4.4 Evapotranspiration Estimation

1. *Daily Actual Evapotranspiration (ET_{a_day})*

The daily actual evapotranspiration (mmd^{-1}) is calculated using *equation 2.43* taking latent heat of vaporization as $2.45*10^6$ $JKg^{-1}$and density of water as 1000 Kgm^{-3}. Where, R_{n_day} is daily net radiation in wm^{-2} and $\mathbf{\Lambda}$ is evaporative fraction derived from SEBS model. Both are outputs of SEBS algorithm. The daily net radiation is the difference between the incoming net shortwave radiation (R_{ns}) and the outgoing net longwave radiation (L_{24}). *Equation 4.9* gives a formula for L_{24} based on Stefan-Boltzman law.

$$R_{n\_day} = R_{ns} - L_{24} \quad 4.6$$

The net solar or shortwave radiation resulting from the balance between incoming ($K^{\downarrow}_{day}$) and reflected solar radiation given by:

$$R_{ns} = (1 - \alpha)K^{\downarrow}_{day} \quad 4.7$$

Where, α is albedo or canopy reflection coefficient, which is 0.23 for the hypothetical grass *(Allen et al., 1998)* and $K^{\downarrow}_{day}$ is daily incoming solar radiation.

2. *Reference Evapotranspiration*(ET_0)

Reference evapotranspiration is defined as "the rate of transpiration from hypothetical reference crop with assumed crop height of 0.12m, a fixed surface resistance of $70sm^{-1}$ and an albedo of 0.23; the reference surface closely resembles an extensive surface of green, well-watered grass of uniform height, actively growing and completely shading the ground" *(Allen et al., 1998).*

Daily evapotranspiration used later for the determination of daily relative evapotranspiration has been calculated on pixel by pixel basis for the catchment area using *Priestly-Taylor (1972)* equation with a=1.26 as applied by *Bastiaanssen and Mekonnen (2000)*:

$$(ET_{0\_day} = 1.26 \times [(1 - 0.23) \times K^{\downarrow}_{day} + L_{24}] \quad 4.8$$

Where, $K^{\downarrow}_{day}$ is incoming daily shortwave radiation, determined using *equation 2.26* and $L_{24}$is daily net long wave radiation determined based on Stefan-Boltzman law:

$$L_{24} = \sigma \left[\frac{T_{max,K}^4 + T_{min,K}^4}{2}\right] \left(0.34 - 0.14\sqrt{e_a}\right) \left[1.35\frac{K_{day}^{\downarrow}}{R_{so}} - 0.35\right] \quad 4.9$$

Where, L_{24} is net outgoing longwave radiation ($MJm^{-2}day^{-1}$), σ is Stefan-Boltzmann constant ($4.903*10^{-9}MJK^{-4}m^{-2}day^{-1}$), $T_{max,\,K}$ is maximum absolute temperature during the 24-hour period ($K = °C + 273.16$), $T_{min,\,K}$ is minimum absolute temperature during the 24-hour period [$K = °C + 273.16$], e_a is actual vapour pressure (kPa) that can be calculated using *equation 4.3*, $\frac{K_{day}^{\downarrow}}{R_{so}}$ is relative shortwave radiation (limited to ≤ 1.0), $K_{day}^{\downarrow}$ is calculated daily incoming solar radiation ($MJm^{-2}day^{-1}$) and R_{so} is calculated (equation 4.11) clear-sky radiation ($MJm^{-2}day^{-1}$).

An average of the maximum air temperature to the fourth power and the minimum air temperature to the fourth power is commonly used in the Stefan-Boltzmann equation for 24-hour time series. The term $\left(0.34 - 0.14\sqrt{e_a}\right)$ expresses the correction for air humidity, and will be smaller if the humidity increases. The effect of cloudiness is expressed by $\left[1.35\frac{K_{day}^{\downarrow}}{R_{so}} - 0.35\right]$. The term becomes smaller if the cloudiness increases and hence $K_{day}^{\downarrow}$ decreases. The smaller the correction terms, the smaller the net outgoing flux of longwave radiation. Note that the $\frac{K_{day}^{\downarrow}}{R_{so}}$ term in *equation 4.9* must be limited so that $\frac{K_{day}^{\downarrow}}{R_{so}} \leq 1.0$. The calculation of the clear-sky radiation, R_{so} when n = N, is required for computing net longwave radiation. For near sea level or when calibrated values for a_s *and* b_s are available:

$$R_{so} = (a_s + b_s)K_{24}^{\downarrow exo} \quad 4.10$$

Where, $(a_s + b_s)$ is fraction of extraterrestrial radiation reaching the earth on clear-sky days (n = N). When calibrated values for a_s *and* b_s are not available:

$$R_{so} = (0.75 + 2 * 10^{-5}z)K_{24}^{\downarrow exo} \quad 4.11$$

Where, z is station elevation above sea level (m) and $K_{24}^{\downarrow exo}$ is calculated *(equation 2.27)* daily terrestrial solar radiation ($MJm^{-2}day^{-1}$).

Daily reference evapotranspiration later aggregated to monthly reference evapotranspiration were calculated from daily weather data using FAO Penman-Monteith equation *(Allen et al., 1998).*

$$ET_0 = \frac{0.408\Delta(R_n - G) + \gamma \frac{900}{T+273} u_2 (e_s - e_a)}{\Delta + \gamma(1 + 0.34u_2)} \qquad 4.12$$

Where, ET_0 is reference crop evapotranspiration (mmday^{-1}), R_n is net radiation at the crop surface (MJm^{-2}day^{-1}), G is soil heat flux density (MJm^{-2}day^{-1}), T is mean daily temperature at 2m height (^{0}C), u_2 is wind speed at 2m height (msec^{-1}), e_s is saturation vapour pressure (KPa), e_a is actual vapour pressure (KPa), $e_s - e_a$ is saturation vapour pressure deficit (KPa), Δ is slope of vapour pressure curve (KPa^{0}C^{-1}) and γ is psychrometric constant (KPa^{0}C^{-1}). The computation of all parameters put in *equation 4.12* followed the method and procedure given in FAO (Food and Agricultural Organization) Irrigation and Drainage Paper 56 and computed with spreadsheet developed for the study.

Daily and monthly ET_0 were computed by the FAO Penman–Monteith formula *(equation 4.12)* based on routine weather data (temperature, sunshine hours, wind speed, relative humidity) at point stations. Areal monthly reference evapotranspiration over the study area was then determined from points reference evapotranspiration using nearest neighbour interpolation (Thiessen polygon) method. Daily and monthly ET_0 estimation by Hargreaves and Tornthwaite empirical equations were done to compare with other methods stated above.

3. Monthly actual evapotranspiration (ET_{a_mon})

Monthly actual evapotranspiration is determined based on the assumption that the daily relative evapotranspiration a date an image acquired remains the same for the whole period of a month in which an image is acquired *(Tasumi et al., 2000).*

$$ET_{a\_mon} = \frac{ET_{a\_day}}{ET_{0\_day}} \times ET_{0\_mon} \qquad 4.13$$

Where, ET_{a_day} is daily actual evapotranspiration, ET_{0_day} and ET_{0_mon} are daily and monthly reference evapotranspiration, respectively. The first term on the right hand side represents

relative evapotranspiration on daily basis. Daily and monthly ET_0 were computed by the FAO Penman–Monteith formula *(Allen et al., 1998)* based on routine weather data (temperature, sunshine hours, wind speed, relative humidity) at point stations.

4.5 Surface Biophysical Properties Estimation

Computation of various biophysical parameters is among the most important processes in ET_a calculation by using remote sensing data. A few experimental and mathematical approaches have been developed for the past few decades. The availability and accuracy of those methods should be taken in account carefully when utilize them in a new area. Some of the approaches for different surface biophysical parameters (NDVI, LAI, fractional vegetation cover, and vegetation height) estimation are summarized below.

4.5.1 Normalized Difference Vegetation Index

The Normalized Difference Vegetation Index (NDVI) is a simple numerical indicator that can be used to analyze remote sensing measurements, typically but not necessarily from a space platform, and assess whether the target being observed contains live green vegetation or not.

Negative values of NDVI (values approaching -1) correspond to water. Values close to zero (-0.1 to 0.1) generally correspond to unproductive areas of rock, sand, or snow. Low positive values represent shrub and grassland (approximately 0.2 to 0.4), while high values indicate temperate and tropical rainforests (values approaching 1). A default value of 0.001 had been used instead of negative values for the convenience of calculations. It can be freely downloaded from a web site *<http://earthobservatory.nasa.gov/Features/MeasuringVegetation/>*.

NDVI can be calculated from individual reflectance measurements (the difference in reflectance divided by the sum of the two reflectance bands, near infrared and red bands) as follows:

$$NDVI = \frac{\rho_{nir} - \rho_{red}}{\rho_{nir} + \rho_{red}} \qquad 4.14$$

Where, ρ_{nir} and ρ_{red} are atmospherically corrected ground reflectance in the near infrared (band 4) and red (band 3) bands, respectively.

In this research, NDVI products of SPOT VGT4AFRICA at 1000m spatial resolution were used except for the date 25 June 2008, for which *equation 4.14* was used.

4.5.2 Leaf Area Index

Leaf Area Index (LAI) is the ratio of total upper leaf surface of vegetation divided by the surface area of the land on which the vegetation grows. LAI is a dimensionless value, typically ranging from 0 for bare ground to 6 for a dense forest.

1. Leaf Area Index determined from SAVI

Choudhury et al. (1994) simulated relationships between Soil Adjusted Vegetation Index (SAVI) and LAI for different crops stated as below.

$$LAI = -\frac{1}{C_3} \cdot ln\left(\frac{C_1 - SAVI}{C_2}\right) \quad 4.15$$

Where, SAVI is the SAVI value of the current pixel (SAVI map). The constant C_1, C_2 and C_3 should be determined based on study area, C_1 always take the maximum value of the SAVI map, if no information about vegetation available, default values, which adopt the average of many experiences developed by several authors *(table 4.1)* can be used:C_1=0.69, C_2=0.59 and C_3=0.91. SAVI resembles the NDVI with some added terms to adjust for different brightness of background soil. It is given by equation as below.

$$SAVI = \frac{(1 + L)(\rho_{nir} - \rho_{red})}{\rho_{nir} + \rho_{red} + L} \quad 4.16$$

Where, L is a soil-adjusted factor, which range from 0 for very high vegetation cover to 1 for very low vegetation cover, and it can be calculated by equation:

$$L = 1 - 2 \cdot a \cdot NDVI \cdot (\rho_{nir} - \gamma \cdot \rho_{red}) \quad 4.17$$

Where, coefficient a equals 1.6, and γ is coefficient of soil line. Based on a simplified radiative transfer model, *Huete et al. (1999)* has shown that a value L=0.5 permits the best adjustment, i.e. to minimize the secondary backscattering effect of canopy-transmitted soil background reflected radiation.

Table 4-1 Empirical constants for Leaf Area Index determination for different crops in the world

Crops	Country	C_1	C_2	C_3	R^2	Max. LAI
Cotton	USA	0.82	0.78	0.60	0.98	3.5
Maize	Italy	1.27	1.10	1.20	0.79	3.3
Maize	USA	0.68	0.50	0.55	0.90	6.0
Soybean	USA	0.72	0.61	0.65	0.70	6.0
Wheat	Italy	0.73	0.67	0.97	0.94	5.0
Fruit trees	Italy	1.34	2.70	2.40	0.39	2.6
Winter Vegetables	Niger	1.31	2.75	2.20	0.54	4.2
Bush and grassland	Niger	0.14	0.30	-	0.95	1.2
Grassland	Niger	0.13	0.35	-	0.98	1.3
Millet	Niger	0.13	0.47	-	0.83	0.8
Degraded bush	Niger	0.11	0.28	-	0.96	1.0
All crops		0.69	0.59	0.91	-	6.0

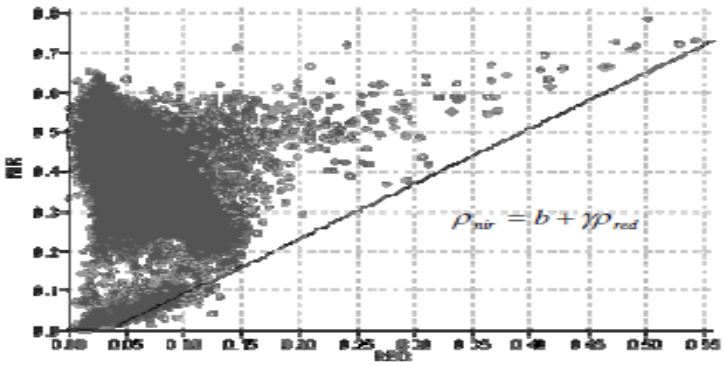

Figure 4-5 Definition and determination of the soil line combining the near infrared and red reflectance bands

2. Leaf Area Index determined from NDVI

Su and Jacobs (2001) simulated relationships between NDVI and LAI as follow.

$$LAI = \left(NDVI \cdot [\frac{1 - NDVI}{1 + NDVI}]\right)^{1/2} \quad 4.18$$

Due to the limited ground truth data about the land cover in the study area, some uncertainty must happened when applying method 1 to retrieve LAI. Though, method 2 is restricted to low vegetation area, this limitation is neglected and applied in this study as none of equation clearly exist for estimation of LAI in forest environments.

4.5.3 Fractional Vegetation Cover

Fractional Vegetation Cover is an important parameter to separate non-vegetated, partially vegetated and densely vegetated land surfaces. This parameter is employed in SEBS model to drive surface temperature, LAI and ground heat flux. Several methods have been developed for estimation of fractional vegetation cover:

1. ***Fractional Vegetation Cover estimation by*** *Choudhury et al. (1994):*

$$f_c = 1 - \left(\frac{NDVI_{max} - NDVI}{NDVI_{max} - NDVI_{min}}\right)^p \qquad 4.19$$

Where, p represents the ratio of the leaf angle distribution and taken as a constant, 0.625; $NDVI_{max}$ is the NDVI value of the full vegetation cover, and $NDVI_{min}$ is the NDVI value of the bare soil.

2. ***Fractional Vegetation Cover estimation by*** *Valor and Caselles (1996):*

By considering a mixed pixel with a vegetation cover *f* and soil proportion *(1-f)* and inverting the NDVI expression, *Valor and Caselles (1996)* have developed a new algorithm to retrieve fractional vegetation cover:

$$f = \frac{(1 - K_g)}{(1 - K_g) - K(1 - K_v)} \qquad 4.20$$

Where,

$$K_g = \frac{NDVI}{NDVI_g}, \qquad K_v = \frac{NDVI}{NDVI_v}, \qquad K = \frac{r_{2v} - r_{1v}}{r_{2g} - r_{1g}}$$

Where, r_2 is the reflectance measured in the near infrared and r_1 is the reflectance corresponding to the red wave bands, subscript v and g refers to observed vegetation top and ground, respectively.

The ground truth information of bare land and dense canopy is highly required in all methods stated above. Due to the shortage of these data about land cover over the study area, some uncertainty must happen when determining the values of these parameters. Therefore, in order to decrease the uncertainty, method 1 (method that requires minimum parameters) is used in this study.

4.5.4 Vegetation Height

Having limited knowledge about the vegetation structure in the study area, vegetation height can be estimated by inverting the equation that calculates the z_{0m} based on the vegetation height *(Richard and Luis, 1998)*:

$$h = \frac{z_{0m}}{0.136} \qquad 4.21$$

Where, z_{0m} is the aerodynamic roughness height, which will be discussed in section 5.7.3 below.

4.6 Surface Characteristics Parameters Estimation

4.6.1 Surface Albedo

Surface albedo of typical materials in visible light ranges from 0.9 for fresh snow, to about 0.04 for charcoal, one of the darkest substances. Deeply shadowed cavities can achieve an effective albedo approaching the zero of a blackbody. When seen from a distance, the ocean surface has a low albedo, as do most forests, while desert areas have some of the highest albedo among landforms. Most land areas are in an albedo range of 0.1 to 0.4. The average albedo of the Earth is about 0.3 *(Goode et al., 2001).* Albedo can be measured easily by using special instrument, but it is only limited to a small scale with point values. Remote sensing is the only practical means for mapping land surface albedo globally.

Based on extensive radiative transfer simulations, *Liang (2001)* proposed a series of formulas to convert single band albedo that were recorded in different narrow bands sensors to broad bands albedo:

$$\alpha_{short} = 0.16\alpha_1 + 0.29\alpha_2 + 0.243\alpha_3 + 0.116\alpha_4 + 0.112\alpha_5 + 0.081\alpha_7 - 0.0015 \quad 4.22$$

Where, α_{short} is simulated total shortwave albedo, α_i *(i = 1~7)* is the narrow bands albedo of MODIS shortwave bands.

4.6.2 Land Surface Emissivity

1. Land Surface Emissivity from land use map:

Empirical relationships using the vegetation cover method developed by *Valor and Caselles (1996)* together with the land use map used to derive surface emissivity (ε_0):

$$\varepsilon_0 = \varepsilon_c f_c + \varepsilon_s(1 - f_c) + 4(d\varepsilon)f_c(1 - f_c) \quad 4.23$$

Where, ε_c is the emissivity of full vegetation cover, ε_s is emissivity of bare soil, f_c is fractional vegetation cover, and $d\varepsilon$ is vegetation structure parameter. According to Valor and Caselles (1996), ε_c, ε_s and $d\varepsilon$ are taken as 0.985, 0.960 and 0.015, respectively.

2. Land Surface Emissivity using vegetation cover method:

Empirical formula developed by *Sobrino et al. (2003; 2001)* relates land surface emissivity with NDVI threshold, proportion of vegetation, and red band surface reflectance *(table 4.2)*.

Table 4-2 *Relationship between land surface emissivity with NDVI threshold, proportion of vegetation, and red band surface reflectance*

Pixel type	Mixed pixel (0.2=<NDVI<=0.5	Pixels covered by vegetation (NDVI>0.5)	Bare soil pixels (NDVI<0.5)	Water body (albedo<0.035)
Algorithm	ε = 0.971+0.018P_v	ε = 0.990+de	ε = 0.9832-0.058ρ_{red}	ε = 0.995

Where, P_v is proportion of vegetation, given by $\frac{(NDVI-0.2)^2}{0.09}$, *de* is the emissivity difference of MODIS Band 31 and 32, equal to 0.005 for pixels covered by vegetation, and ρ_{red} is land surface reflectance of red band (band 3).

3. Land Surface Emissivity from NDVI:

Van de Griend and Owe (1993) developed experimental relationship between land surface emissivity and NDVI:

$$\varepsilon = 1.0094 + 0.047 \ln(NDVI) \quad 4.24$$

This equation is restricted to NDVI values ranging from 0.16~0.74. It is not valid for water bodies with low NDVI and high emissivity ($\varepsilon = 0.99\ to\ 1.0$).

Though, the above methods could help in determining land surface emissivity, the average of band 31 and band 32 of MODIS land surface temperature/emissivity products were used for each dates in SEBS model.

4.6.3 Aerodynamic Roughness Height for Momentum Transport

Aerodynamic roughness height for momentum transport (z_{0m}) is a very important parameter in surface energy balance model, which influence significantly the turbulent characteristics near the surface where the heat fluxes originate. There are number of approaches to retrieve this parameter:

1. Estimation of z_{0m} from NDVI:

A simple relationship that was used to derive the roughness length for momentum transfer developed by *Su and Jacobs (2001)* is given as,

$$z_{0m} = 0.005 + 0.5 \cdot \left(\frac{NDVI}{NDVI_{max}}\right)^{2.5} \quad 4.25$$

Bastiaanssen (1995) also found a relationship between z_{0m} and *NDVI* using field measurement data:

$$z_{0m} = \exp(c_1 + c_2 \cdot NDVI) \quad 4.26$$

Where, c_1 and c_2 are constants depending on local field conditions.

2. Estimation of z_{0m} from vegetation height:

$$z_{0m} = 0.136 \cdot h \quad 4.27$$

3. Estimation of z_{0m} from leaf area index:

Raupach (1994) states that aerodynamic roughness height is inflected by vegetation height, displacement length, friction velocity, and wind speed, etc. and is presented as,

$$z_{0m} = \frac{(h-d)}{e^{\left[\frac{ku_h}{u_*} - \Psi_h\right]}} \quad 4.28$$

Where, *h* is the vegetation height, *d* is the displacement height, *k* Von Korman's constant taken as 0.41 as default value, u_* is friction velocity, Ψ_h is a vegetation influence and u_h is wind speed at the top of canopy. The vegetation influence function and the ratio $\frac{u_*}{u_h}$ are given by,

$$\Psi_h = \ln(c_w) - 1 + c_w^{-1} \quad 4.29$$

$$\frac{u_*}{u_h} = \left(c_s + c_r \cdot \frac{LAI}{2}\right)^{0.5} \quad 4.30$$

Note that when the values of $\frac{u_*}{u_h}$ calculated is greater than 0.3, take 0.3 as the default value. Constant c_r is taken as 0.35, and c_s is given by,

$$c_s = \frac{k^2}{\left[ln\left(\frac{h-d}{z_0}\right) + \Psi_h\right]^2} \quad 4.31$$

Where, constant z_0 is default value taken as 0.01.

4. Estimation of z_{0m} from land use classifications:

By studying its relationship with different land use cover, *Jensen (1990)* summarized for aerodynamic roughness height values for different land use/cover *(table 4-3).*

To apply second method, detailed information about the vegetation height required first, this limits its use in large area with heterogeneous land cover. The third approach seems to be the most accurate method but due to the surface topographic and canopy structure and variation of wind speed and direction, it is only limited again to local area. Estimation of z_{0m} from LAI, fourth approach, depends on the displacement height and the LAI information, which are unavailable for this study. The last method provides a convenient way to estimate z_{0m} on the assumption that the detailed land use information is available; however, due to seasonal diversity of the different vegetation heights, especially the heights of crops in agricultural land use area, some error must be practiced when applying the same z_{0m} values to certain crops for temporal analysis of regional ET_a distribution. Therefore, z_{0m} estimation developed by *Su and Jacobs (2001)*, method 1, considered to be suitable for this study.

Table 4-3 *Summary of z_{om} values for different land use/cover*

No.	Land use	z_{0m} (m)	No.	Land use	z_{0m} (m)
1	Grass	0.0340	13	Other open spaces in natural areas	0.0408
2	Maize	0.4966	14	Bare soil in natural areas	0.0012
3	Potatoes	0.0639	15	Fresh water	0.0002
4	Beets	0.0639	16	Salt water	0.0002
5	Cereals	0.4966	17	Continuous urban area	1.1052
6	Other crops	0.0639	18	Built-up area in urban area	0.5488
7	Greenhouses	0.4066	19	Deciduous forest in urban area	1.2214
8	Orchards	0.6065	20	Coniferous forest in urban area	1.2214
9	Bulbs	0.0639	21	Built-up area with dense forest	1.2214
10	Deciduous forest	1.2214	22	Grass in built-up area	0.0334
11	Coniferous forest	1.2214	23	Bare soil in built-up area	0.0012
12	Heather	0.0408	24	Main roads and railways	0.0035
			25	Buildings in natural areas	0.5488

4.6.4 Surface Roughness Length for Heat Transport

The scalar roughness height for heat transfer, z_{0h}, is derived from,

$$z_{0h} = \frac{z_{0\mathrm{m}}}{\exp(k\mathrm{B}^{-1})} \qquad 4.32$$

Where, B^{-1} is the inverse Stanton number, a dimensionless heat transfer coefficient. To estimate the kB^{-1} value (called excess resistance for heat transfer, used to compare $z_{0\mathrm{m}}$ and $z_{0\mathrm{h}}$ values), the following model proposed by *Su et al. (2001)* can be used,

$$k\mathrm{B}^{-1} = \frac{kC_d}{4C_t\frac{u_*}{u(h)}(1-e^{\frac{-n_{ec}}{2}})}f_c^2 + 2f_cf_s\frac{k.\frac{u_*}{u(h)}.\frac{z_{0m}}{h}}{C_t^*} + kB_s^{-1}f_s^2 \qquad 4.33$$

Where, f_c is the fractional canopy coverage and f_s is its compliment. C_t is the heat transfer coefficient of the leaf. For most canopies and environmental conditions, C_t is bounded as $0.005 \leq sC_t \leq 0.075N$ (N is number of sides of a leaf to participate in heat exchange). The heat transfer coefficient of the soil is given by $C_t^* = P_r^{-2/3}R_{e*}^{-1/2}$ where, P_r is the Prandtl number, the roughness Reynolds number $R_{e*} = h_s u_*/v$, where, h_s is the roughness height of the soil. The kinematic viscosity of the air is given by $v = 1.327 * 10^{-5}(P_0/P)(T_a/T_{a0})^{1.81}$ *(Massman, 1999b),* with P and T_a the ambient pressure and temperature, and $P_0 = 101.3\ kPa$ and $T_{a0} = 273.15K$. n_{ec} is the within canopy wind speed profile extinction, given by $n_{ec} = \mathrm{c_d}.\mathrm{LAI}/[2\mathrm{u}_*^2/\mathrm{u(h)}^2]$

Physically and geometrically, the first term of right hand side of *equation 4.33* follows the full canopy only model of *Choudhury and Monteith (1988),* the third term is that of *Brutsaert (1982)* for a bare soil surface, while the second term describes the interaction between vegetation and bare soil surface. A quadratic weighting based on the fractional canopy coverage is used to accommodate any situation between the full vegetation and bare soil conditions. For bare soil surface kB_s^{-1} is calculated according to *Brutsaert (1982)*:

$$kB_s^{-1} = 2.46(Re_*)^{1/4} - \ln(7.4) \qquad 4.34$$

Baastiaanssen (2005) had found a constant value of 2.3 for kB^{-1} in estimation of sensible heat flux for a cotton plant. Though, *equation 4.33* is best to estimate KB^{-1}, the parameters involved in the equation were difficult. So, the constant value stated by *Baastiaanssen (2005)* was used in this study.

4.6.5 Displacement Height

Displacement height (d_0), same as zero-plane displacement, a height scale in turbulent flow over tall roughness elements associated with the average level of action of momentum transfer between the flow and the roughness elements. It is the height that the surface level is normally displaced to a level just below the vegetation canopy due to tall vegetation canopy, where the wind speed is zero. It can be estimated either from leaf area index (LAI) or from aerodynamic roughness height (z_{0m}):

1. ***Displacement height determined from LAI:***

Verhoef and McNaughton (1997) made the following empirical equation to estimate displacement height:

$$d_0 = h\left[1 - \frac{1 - e^{-\sqrt{c_1 LAI}}}{\sqrt{c_1 LAI}}\right] \qquad 4.35$$

Where, h is vegetation height, taken 1 m as default values; if no information is available, constant c_1 is taken as 20.6. Note that, when LAI equal to 0, d_0 is filtered to adopt 0 value.

2. ***Displacement height estimated from z_{0m}***

Displacement height can be derived from the relationship with aerodynamic roughness height (z_{0m}):

$$d_0 = c \cdot z_{0m} \qquad 4.36$$

Where, c is constant based on the local conditions. For a grass reference, it can be taken as 5.42 *(Richard and Luis, 1998)*.

Due to the absence of detail information in the diferent vegetation height, temporally and spatially, its relationship with z_{0m} was used in this study.

5. Results and Discussion

This chapter is designed to analyze the findings and discuss the results of reference and actual evapotranspiration, rainfall and water availability of the study area. The spatio-temporal variability of ET_a found using SEBS has been analyzed. A simple water balance estimation called catchment water balance (precipitation minus evapotranspiration) for the year 2008 was conducted. Surface reflectance (among different land surface variables) and NDVI (among different vegetation variables) were also selected and discussed their spatial and temporal distribution. In analysis, median values were chosen to reduce the influence of some extreme values from the relatively short time-series dataset, where it is believed that there are extremes.

5.1 Spatio-Temporal Distribution of Surface Reflectance

Surface reflectance (surface albedo) is one of the important parameters required for the surface energy balance modeling that can be used to model how many incoming solar radiation were dissipated again in to the atmosphere by surface reflection. It depends not only on the surface soil type and mineral that solar radiation hitting but also on the land cover types of given time that reflectance happened. Since the land cover type over the entire area is relatively coherent at a certain time, the surface reflectance at that time could be considered homogenous. However, due to the large size of the study area, spatial difference between crop types and spatial unstable soil moisture, the surface reflectance over the area shows wide range spatially and temporally.

Table 5-1 *Statistical summaries of surface albedo over the study area for cloud free days*

	Mar. 29	Apr. 06	May 24	Jun. 25	Jul. 03	Aug. 12	Sep. 05
Minimum	0.059	0.044	0.051	0.020	0.057	0.062	0.050
Maximum	0.478	0.656	0.582	0.460	0.743	0.789	0.740
Median	0.197	0.182	0.160	0.130	0.146	0.160	0.170

Table above shows the lowest surface albedo (0.13) occurred in the month of June due to cropland is the dominant land use, type of soil (black cotton) and time for land preparation to plant cereals over the study area. *Figure 5-1* presents the histograms of the surface albedo having one peak value, which indicates the homogeneity of land cover over the study area.

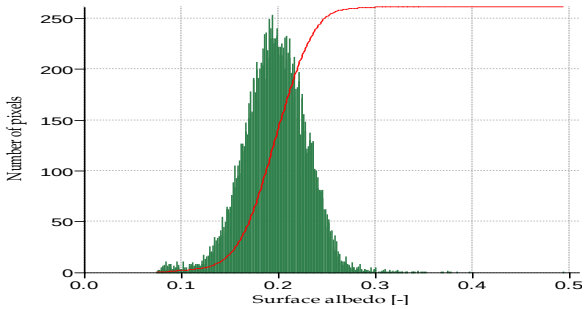

(a) March 29, 2008

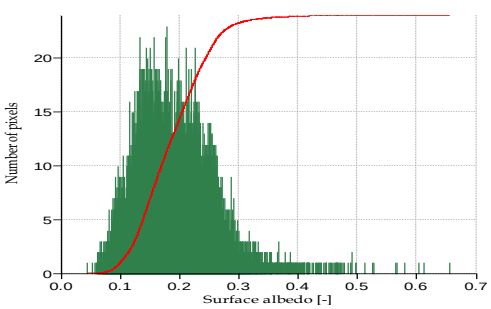

(b) April 06, 2008

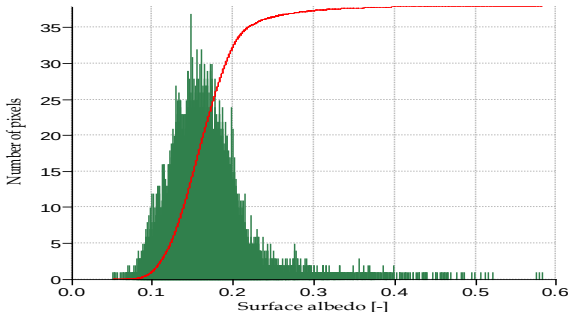

(c) May 24, 2008

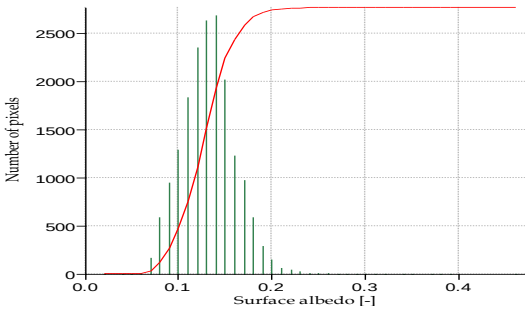

(d) June 25, 2008

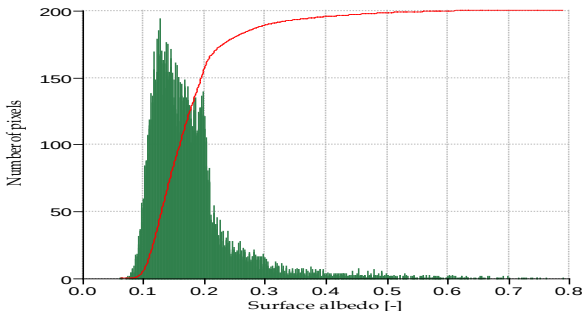

(e) July 03, 2008

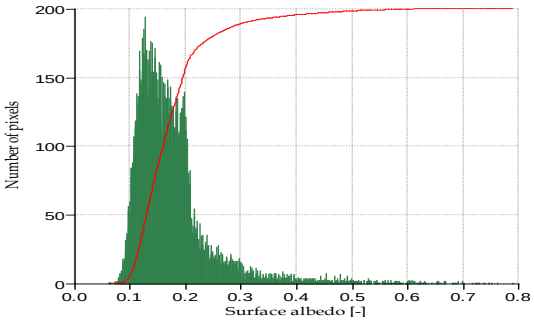

(f) August 12, 2008

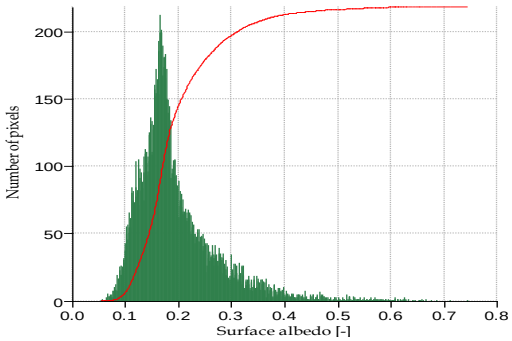

(g) September 05, 2008

Figure 5-1 *Histograms of surface albedo over the study area*

5.2 Spatio- Temporal Distribution of Vegetation Variables

5.2.1 Temporal Distribution of Normalized Difference Vegetation Index

Normalized Difference Vegetation Index (NDVI) is the most widely used vegetation index to monitor the spatial and temporal comparisons of vegetation conditions, which is derived from red and near infrared reflectance. Vegetation indices are used for global monitoring of vegetation conditions and are used in products displaying land cover and land cover changes. These data may be used as input for modeling global biogeochemical and hydrologic processes and global and regional climate. These data also may be used for characterizing land surface biophysical properties and processes, including primary production and land cover conversion.

The statistical summary of the NDVI values of the study area for cloud free days during March to August 2008 is presented in *table 5-2*. From this table of summary and *figure 5-2* it is clear that there are three different categories. The former is the low value category during March to May 2008 having an average NDVI value of 0.21. The second category is the month of May 2008 having NDVI value little more than the first category (0.27). The last category ranges between the month of July and September 2008 with average NDVI value of 0.50, which is almost twice the second category. Therefore, this indicates that the vegetation condition of the study area varies temporally: the first category is the dry (or less rain) season and the second and third categories are the wet (cropping) season whereas the month of June is the transition period where the land became covered with different crops. In general, the major land of the study area is covered with cereal crops like teff and wheat.

Table 5-2 *Statistical summaries of time series NDVI for cloud free days*

	Mar. 29	Apr. 06	May 24	Jun. 25	Jul. 03	Aug. 12	Sep. 05
Minimum	0.001	0.001	0.003	0.002	0.003	0.001	0.004
Maximum	0.616	0.589	0.624	0.650	0.832	0.810	0.813
Median	0.214	0.199	0.228	0.270	0.415	0.540	0.541

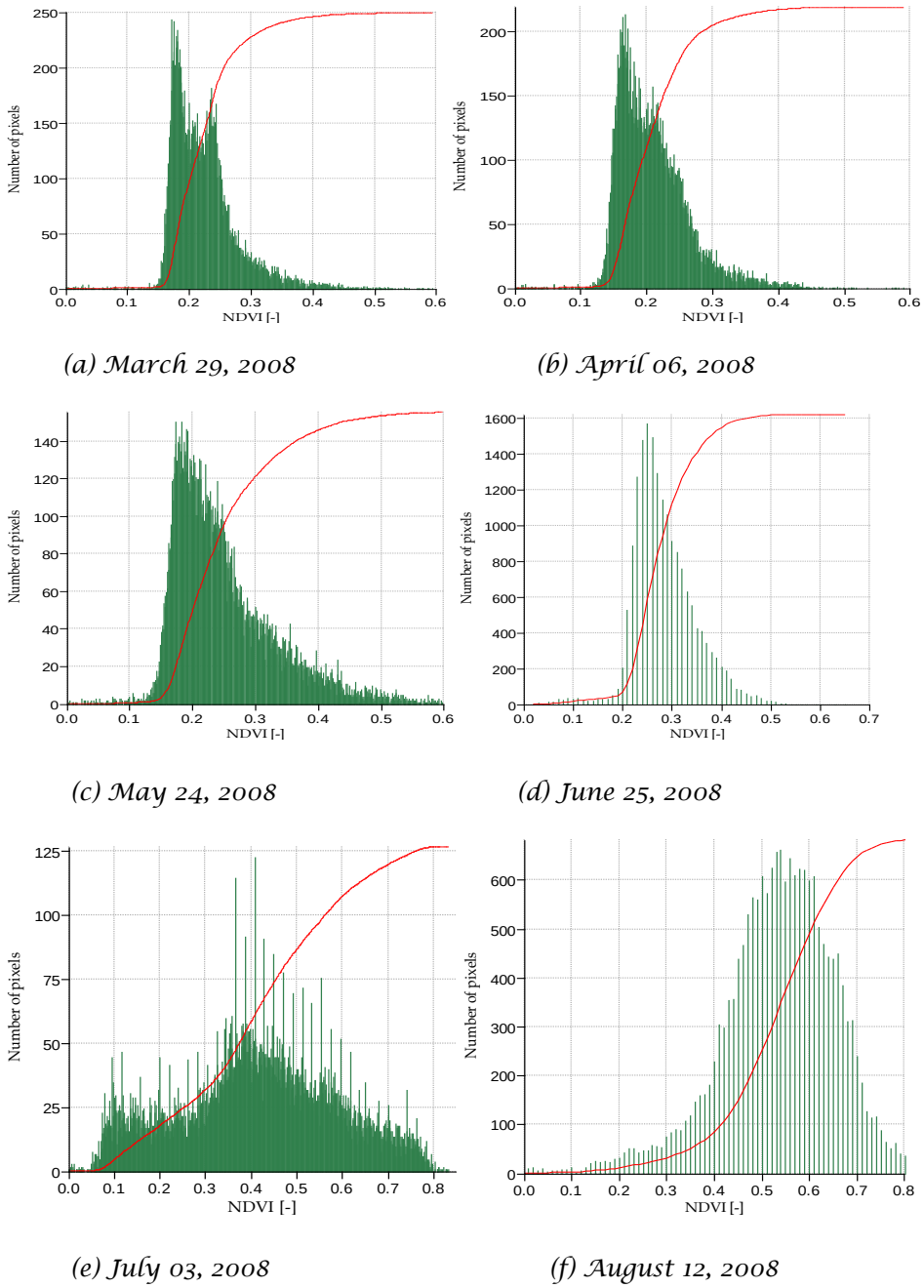

(a) March 29, 2008 (b) April 06, 2008

(c) May 24, 2008 (d) June 25, 2008

(e) July 03, 2008 (f) August 12, 2008

Figure 5-2 *Histograms of NDVI over the study area*

5.2.2 Spatial Distribution of Normalized Difference Vegetation index

A raster map of NDVI for the date 12th of August 2008 *(figure 5-3)* is preferred for the spatial comparison of vegetation condition over the study area as it is an intermediate instance between planting and harvesting time for all crop types (dominant land cover).

Table 5-3 *Statistical summaries of spatial NDVI for the date 12th of August 2008*

Value	Description	Coverage [Km^2]	Average NDVI [-]
0	Water body	38	0.507
1	Grasses/Cereal crops land	4447	0.516
2	Shrubs land	3323	0.527
3	Broadleaf crops land	2174	0.544
4	Savanna land	383	0.505
5	Broadleaf forest land	71	0.511
6	Needle leaf forest land	80	0.503
7	Non-vegetated land	67	0.47
8	Urban area	109	0.438

The lower and higher NDVI values occurred in the urban area and broadleaf crops land cover with 0.438 and 0.544, respectively.

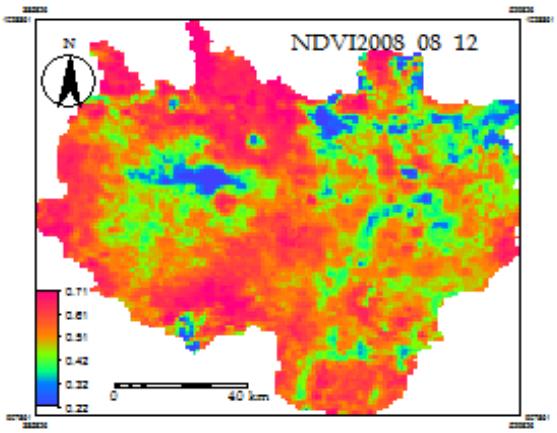

Figure 5-3 *NDVI raster map for the date of August 12, 2008*

5.3 Spatio-Temporal Distribution of Evapotranspiration

Actual daily evapotranspiration (ET_a) were calculated using Surface Energy Balance Systems (SEBS) model using satellite-derived data in combination with some meteorological data and derived surface biophysical parameters. Penman-Monteith method of estimating reference evapotranspiration had also been carried out in daily and monthly bases for deriving actual monthly evapotranspiration. The daily and monthly reference evapotranspiration derived from Penman-Monteith approach were presented in appendix A; Hargreaves method is also conducted for purpose of comparison and applied instead of Penman-Monteith ET_0 where data were missed.

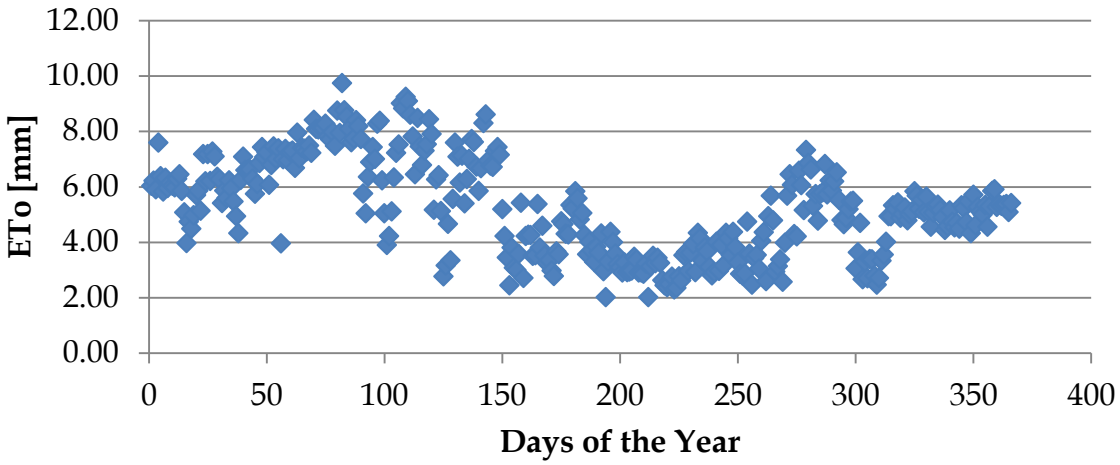

Figure 5-4 Penman-Monteith daily reference evapotranspiration in 2008 at Addis Ababa station

Reasonable ET_a values were observed over most land cover since the selected dates for estimation of ET_a are either dry or moderately wet, before or after rainy days. This indicates that SEBS can be used in most land cover to estimate the daily ET_a with acceptable error. Similarly, different studies *(Su, 2001; Su and Jacobs, 2001; Wenjing et al., 2006; Wendimagegn, 2006; Tadesse, 2010)* have proven that SEBS can give good estimation of ET_a over different land covers (cotton field, shrub land, wheat and other crops). The statistical summary of the SEBS derived daily ET_a values of the study area for cloud free days during March to September 2008 is presented in *table 5-4*.

Table 5-4 Summaries of average ET_a values over different land cover types

LULC (2008)	29/03	06/04	24/05	25/06	03/07	12/08	05/09	Average
Water body	4.34	4.64	1.15	3.18	3.48	1.35	3.14	3.04
Grasses/Cereal crops land	3.83	4.78	1.20	2.94	3.18	1.88	2.66	2.92
Shrubs land	3.78	4.82	1.18	2.92	3.15	1.80	2.70	2.91
Broadleaf crops land	3.60	4.74	1.18	2.95	3.20	1.81	2.54	2.86
Savanna land	3.27	4.50	1.21	3.10	3.33	2.15	2.83	2.91
Broadleaf forest land	3.13	4.64	1.27	3.18	3.31	2.39	2.93	2.98
Needle leaf forest land	3.26	5.28	1.23	3.46	3.49	2.69	2.67	3.15
Non-vegetated land	3.19	5.32	1.26	3.63	3.47	2.68	2.88	3.20
Urban area	3.92	6.32	1.30	5.08	3.57	3.18	3.02	3.77
Weighted Average	3.74	4.80	1.19	2.97	3.19	1.88	2.66	2.92

Among the cloud free days selected, April 6th had the highest value of daily evapotranspiration over the study area. On the contrary, the lowest daily evapotranspiration resulted from May 24th. Generally, as shown in *table 5-4*, lower and higher actual daily evapotranspiration occurred on May 24th and April 6th with values 1.19mmday^{-1} and 4.80mmday^{-1}, respectively over the Upper Awash Basin.

More to the point, considering the average evapotranspiration during the study area, urban areas contribute relatively high evapotranspiration resulting 3.77mmday^{-1}; on the other hand, broadleaf crops land has comparatively low contribution to evapotranspiration resulting 2.86mmday^{-1}. If a single value for actual daily ET_a needed to be mentioned over the study area, the weighted average is taken as 2.92mmday^{-1}, same as ET_a value for the dominant land cover, grass/cereal crops land. The SEBS algorithm based actual daily evapotranspiration maps for the selected cloud free days are shown in *figure 5-5*.

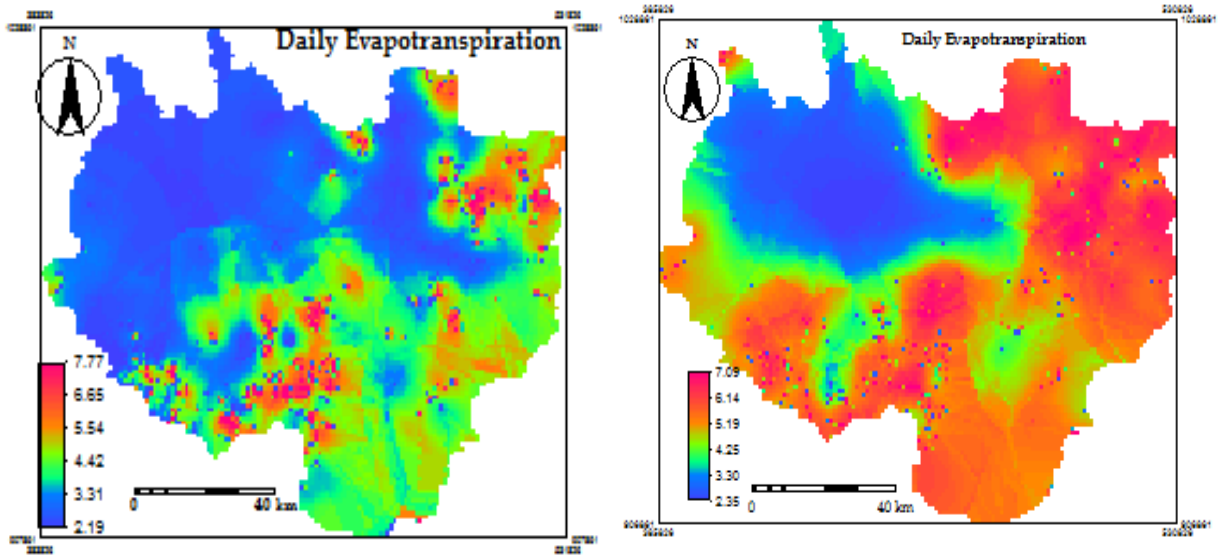

(a) March 29, 2008

(b) April 06, 2008

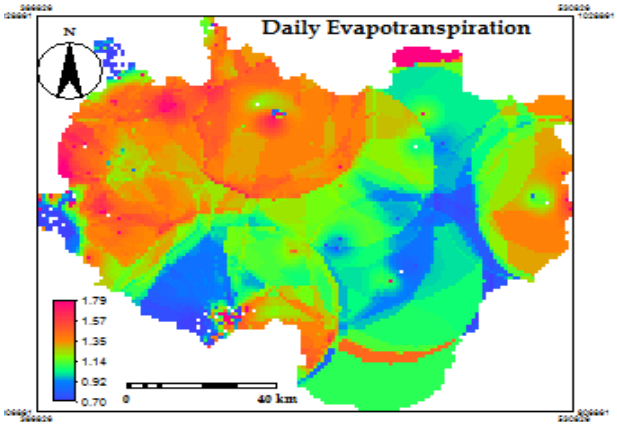

(c) May 24, 2008

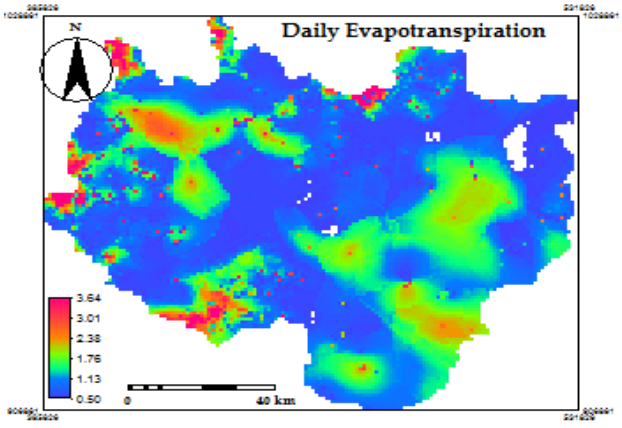

(d) June 25, 2008

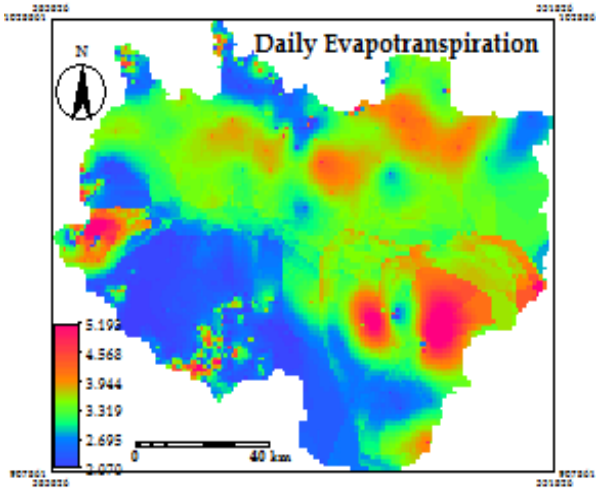

(e) July 03, 2008

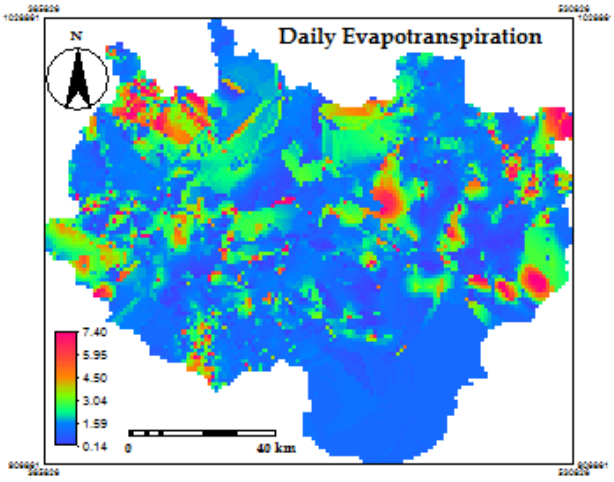

(f) August 12, 2008

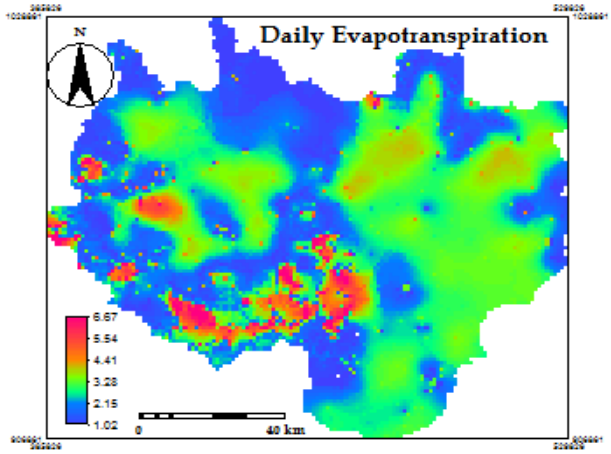

(g) September 05, 2008

Figure 5-5 SEBS derived daily ET_a maps

5.4 Water Balance Components

The spatial pattern of rainfall distribution, ET_a estimated from instantaneous data with SEBS model and ET_0 estimated by Penman-Monteith equation over the Upper Awash Basin during the study period are discussed in detail as below. The water availability (runoff or reduced storage) from the study area was also discussed.

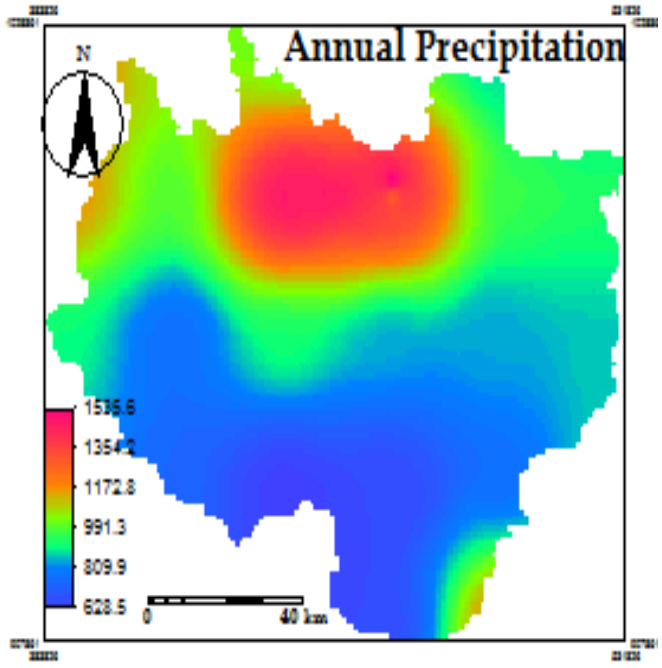

Figure 5-6 Annual satellite-derived rainfall map

Figure 6-6 shows the spatial distribution of satellite-derived annual rainfall in 2008. The average annual rainfall over the study area was identified to be 1049.6mm. High rainfall values in excess of 1200mm are shown to occur in much of Addis Ababa City and its surrounding to an average radius of 25-30Km. Relatively low rainfall totals (less than 850mm) are generally seen in the lower part of the study area. In general, the spatial pattern of rainfall follows the elevation of Upper Awash Basin. *Figure 6-7* presents the monthly spatial rainfall distribution in the study area.

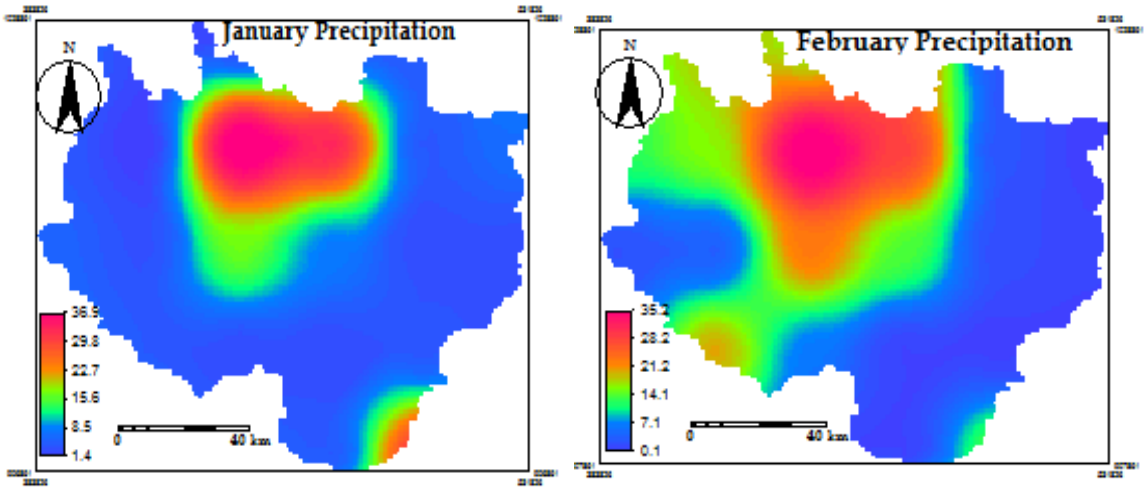

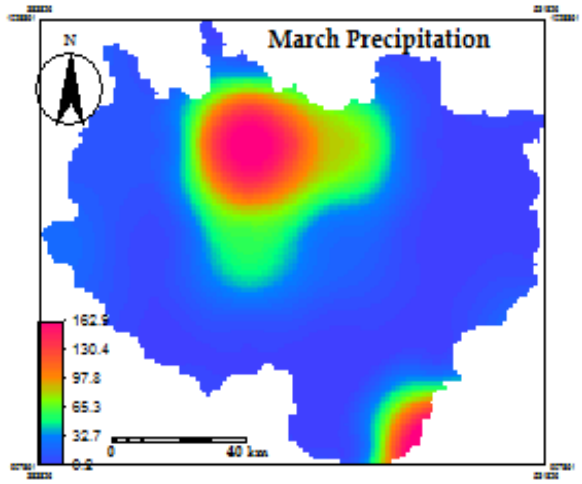
March Precipitation
N
162.9
130.4
97.8
65.3
32.7
0
40 km

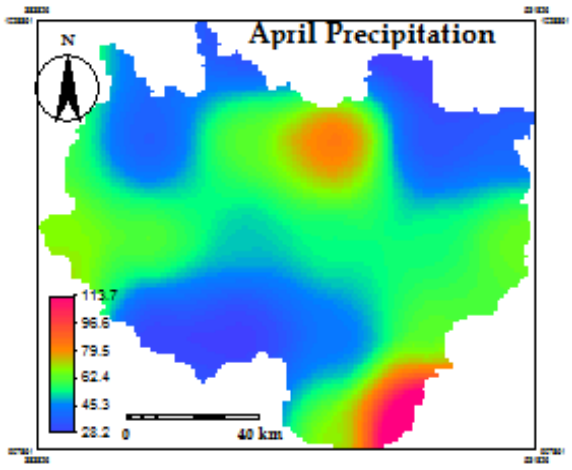
April Precipitation
N
113.7
96.6
79.5
62.4
45.3
28.2
0
40 km

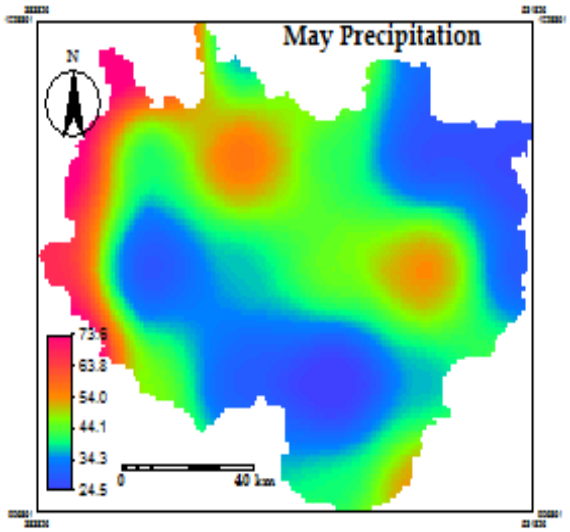
May Precipitation
N
73.6
63.8
54.0
44.1
34.3
24.5
0
40 km

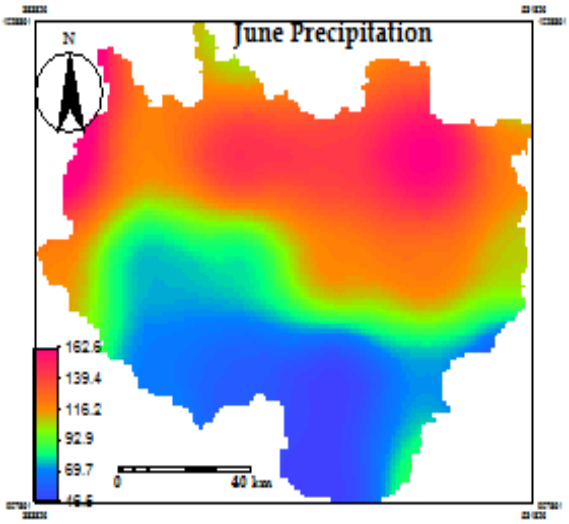
June Precipitation
N
162.6
139.4
116.2
92.9
69.7
0
40 km

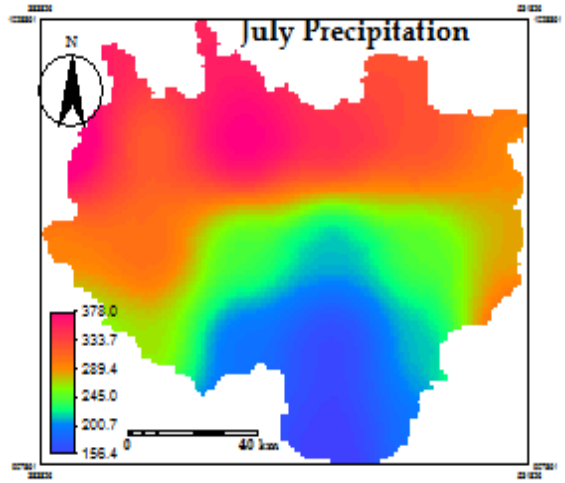
July Precipitation
N
378.0
333.7
289.4
245.0
200.7
156.4
0
40 km

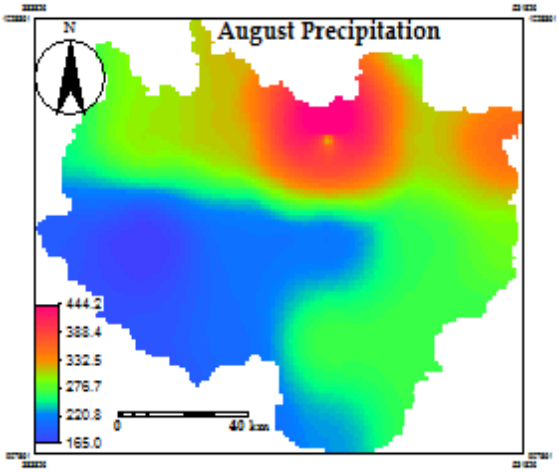
August Precipitation
N
444.2
388.4
332.5
276.7
220.8
165.0
0
40 km

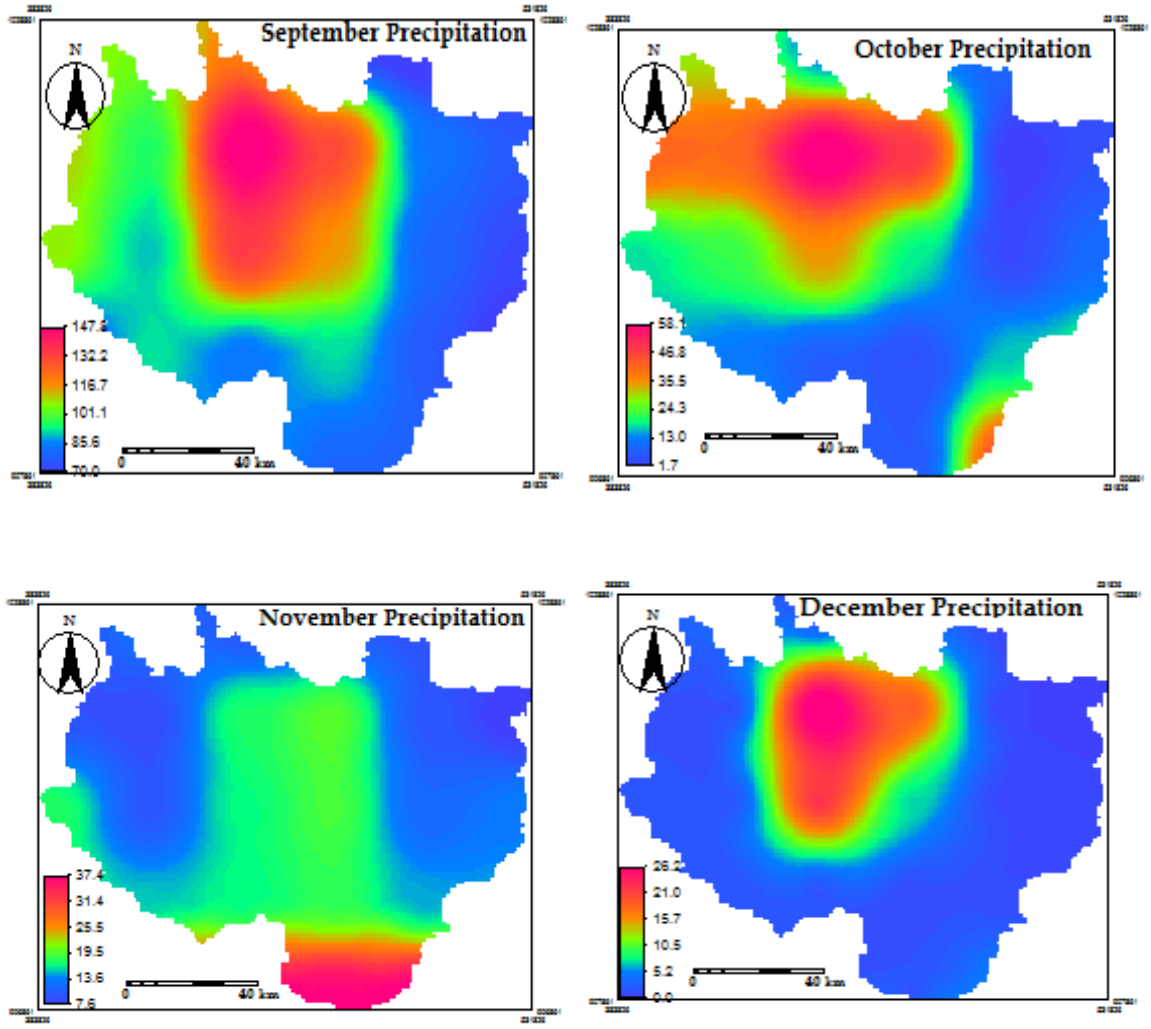

Figure 5-7 *Monthly rainfall maps of the Upper Awash Basin*

From the histograms of monthly rainfall maps, it was simply recognized that the maximum and minimum rainfall occurred in July (270mm) and December (14.4mm), respectively. The wet season (June to September) made a contribution of 71% of the annual rainfall in the Upper Awash Basin.

The average annual ET_a estimate was 905.76mm. Annual ET_a, perceived from SEBS model output, shows that relatively high values (more than 850mm) were happened on some areas of North-East and South-West parts of the study area including Addis Ababa City. On the contrary, major areas of the North-West parts of the Upper Awash Basin release 560-800mm of ET_a to the atmosphere.

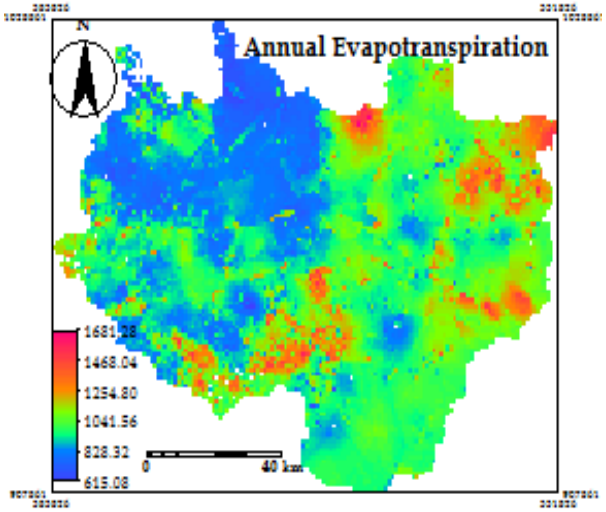

Figure 5--8 *Annual ETa map over the study area*

Areas with annual ET_a greater than 400mm can be considered well vegetated, while areas with less than 200mm ET_a would require a substantial irrigation to produce enough vegetation biomass to support a substantial animal community and human settlement *(Senay et al., 2009). FAO (1986)* reported that even a drought resistant crop such as sorghum has a seasonal water requirement of 450-650mm. Therefore, the area is capable of raising different crop types, as the average annual ET_a estimate was almost twice the range reported by *FAO (1986),* and categorized under well-vegetated area. The monthly ET_a estimate maps were presented in *figure 5-9.*

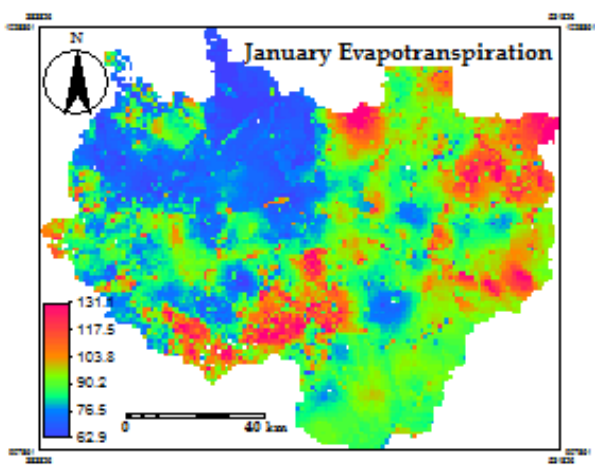

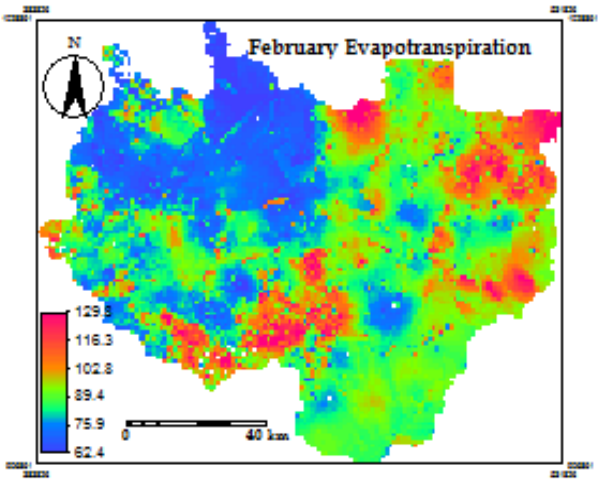

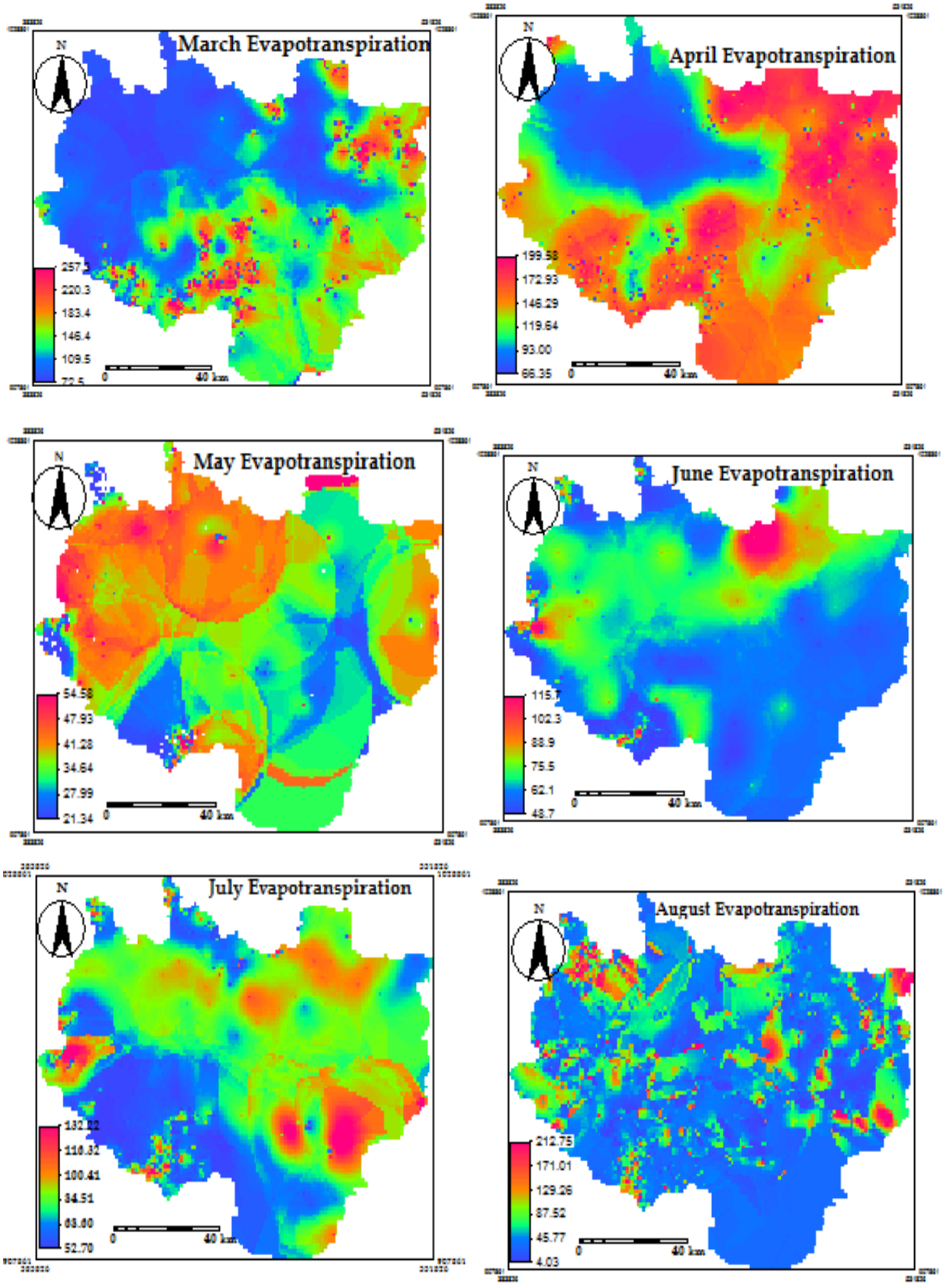
March Evapotranspiration
N
257.1
220.3
183.4
146.4
109.5
72.5
0
40 km
April Evapotranspiration
N
199.58
172.93
146.29
119.64
93.00
66.35
0
40 km
May Evapotranspiration
N
54.58
47.93
41.28
34.64
27.99
21.34
0
40 km
June Evapotranspiration
N
115.7
102.3
88.9
75.5
62.1
48.7
0
40 km
July Evapotranspiration
N
132.22
116.32
100.41
84.51
68.60
52.70
0
40 km
August Evapotranspiration
N
212.75
171.01
129.26
87.52
45.77
4.03
0
40 km

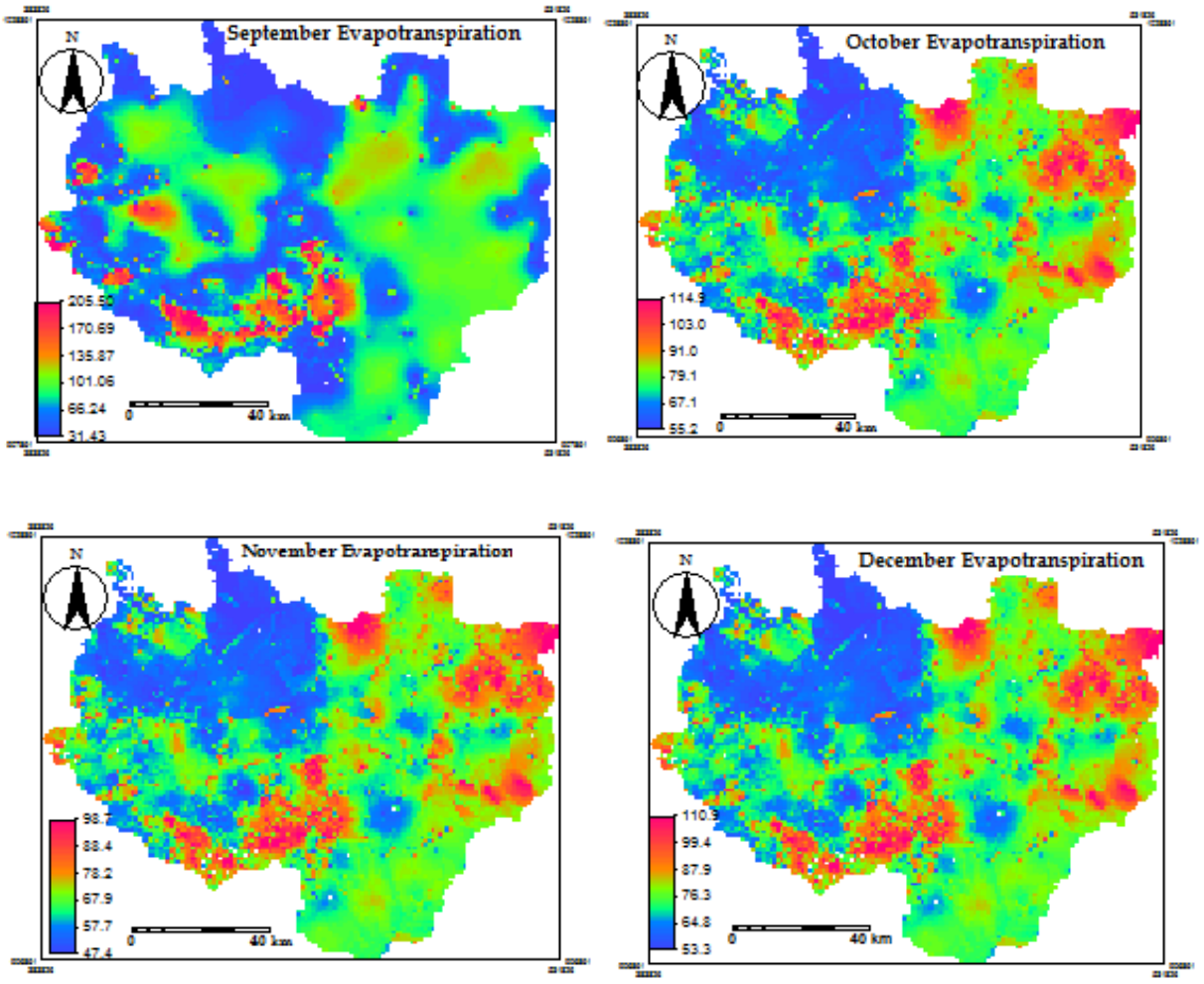

Figure 5-9 Monthly ETa maps in the Upper Awash Basin

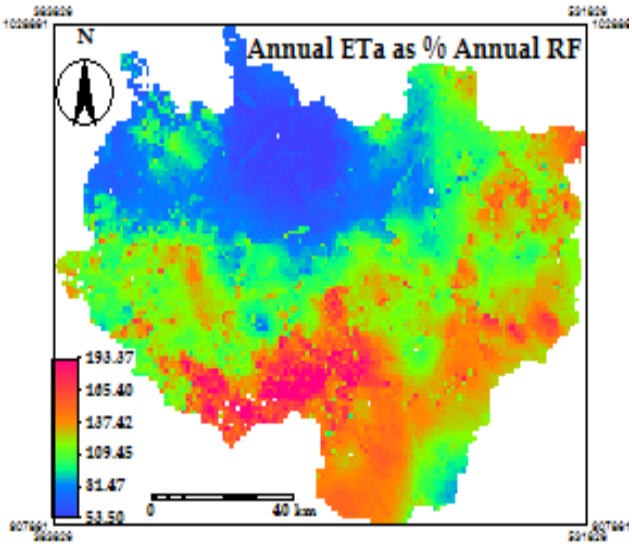

The annual ET_a distribution can be used to assess the integrated response of the landscape from the nature of its rainfall distribution and ability of the land cover to use the rainfall. In this study, we hypothesize that degraded landscape will exhibit disproportionately lower ET_a amounts despite good rainfall distribution.

Figure 5-10 Annual ET_a estimate as percent annual rainfall

Figure 5-10 shows the ratio between annual ET_a and annual rainfall totals. We used global water balance studies that show 63% of terrestrial rainfall is lost to ET_a *(Peixoto and Kettani, 1973)* as a reference to create two broad classes for the Upper Awash Basin region. Areas where more than 80% of the rainfall is partitioned to ET_a are shown to be in semi-arid regions, most agricultural lands of the Upper awash Basin. On the other hand, the highlands of the Upper Awash Basin fall below 80% of ET_a as percent of annual rainfall.

Generally, the balance between rainfall and ET_a is considered runoff, although some other losses, particularly interception-evaporation, still account for some of the balance. *Figure 5-11 (a)* and *(b)* show the estimated annual runoff on a pixel-by-pixel basis and runoff as a percent of the rainfall. The annual runoff produced from the study area in 2008 was estimated to be 143.84mm depth or volumetric value of 1545.992Mm^3; this is in agreement with that of the estimate from ground based flow record at Hombole station, the nearby station to the outlet of the Upper Awash Basin, (=1575.024Mm^3), the difference can be attributed to the likely uncertainties involved in the process while deriving the water balance components.

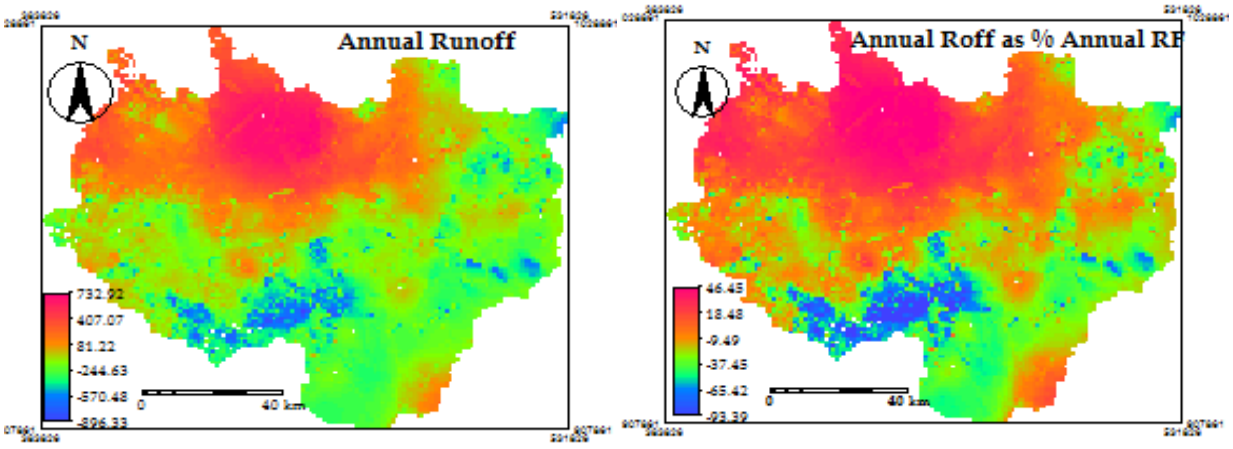

(a) (b)

Figure 5-11 *(a) Annual runoff estimate map (b) annual runoff as a percent of annual rainfall map*

Negative values in the runoff/reduced storage column appeared in months when actual evapotranspiration exceeds the rainfall. The source of water to meet the difference comes from water stored in soil moisture, ground water and vegetation from rainfall in the previous months and the water pumped to irrigated farmlands from the rivers, mainly Awash and Modjo.

Major lower parts of the study area and areas on the reach of both Modjo and Awash rivers had been cultivated and irrigated throughout the year; it was subjected to relatively high evapotranspiration even in dry season. This made the availability of water below zero in months between October and April, though SEBS overestimates evapotranspiration in dry season *(Wenjing et al., 2006; Tadesse, 2010).*

Table 5-5 *Upper Awash Basin annual water balance components*

Month	Rainfall [mm]	ET_a [mm]	Runoff/Reduced Storage [mm]	Runoff/Reduced Storage [Mm^3]
January	20.90	88.00	-67.10	-721.19
February	18.40	87.10	-68.70	-738.39
March	77.80	119.50	-41.70	-448.19
April	69.30	143.34	-74.04	-795.78
May	52.50	36.28	16.22	174.33
June	107.60	63.00	44.60	479.36
July	270.00	46.89	223.11	2397.99
August	256.40	41.69	214.71	2307.70
September	108.30	62.26	46.04	494.84
October	30.90	77.10	-46.20	-496.56
November	23.10	66.20	-43.10	-463.24
December	14.40	74.40	-60.00	-644.88
Total	1049.6	905.76	143.84	1545.99

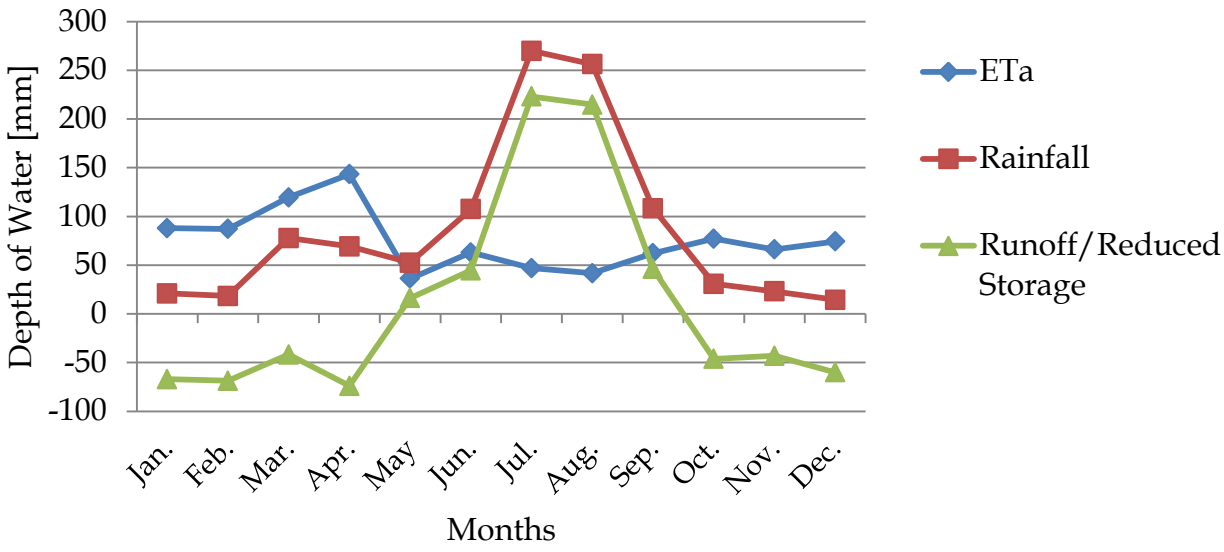

Figure 5-12 *Upper Awash Basin water balance components*

Figure 5-12 shows that the average monthly rainfall depth and runoff/ reduced storage depth had the same pattern, despite the consequences of the evapotranspiration, with the same time to peak in July with values 270mm and 223.11mm, respectively.

5.5 Water Balance Components per Land Use/Cover Units

The monthly actual evapotranspiration was crossed with land use/cover map of the catchment area to get actual evapotranspiration from each land use/cover units. The process is done only for a month of August 2008. The detail of monthly actual evapotranspiration per land use/cover units is given in *table 5-6*. The histogram of monthly and daily actual evapotranspiration in August is given in *figure 5-13* to see the difference between mean and median values. The volume of runoff and the volume of runoff per unit area are calculated for simplicity of runoff comparisons from different land use/covers. The rate of runoff also helps to visualize the impact change in land use on runoff.

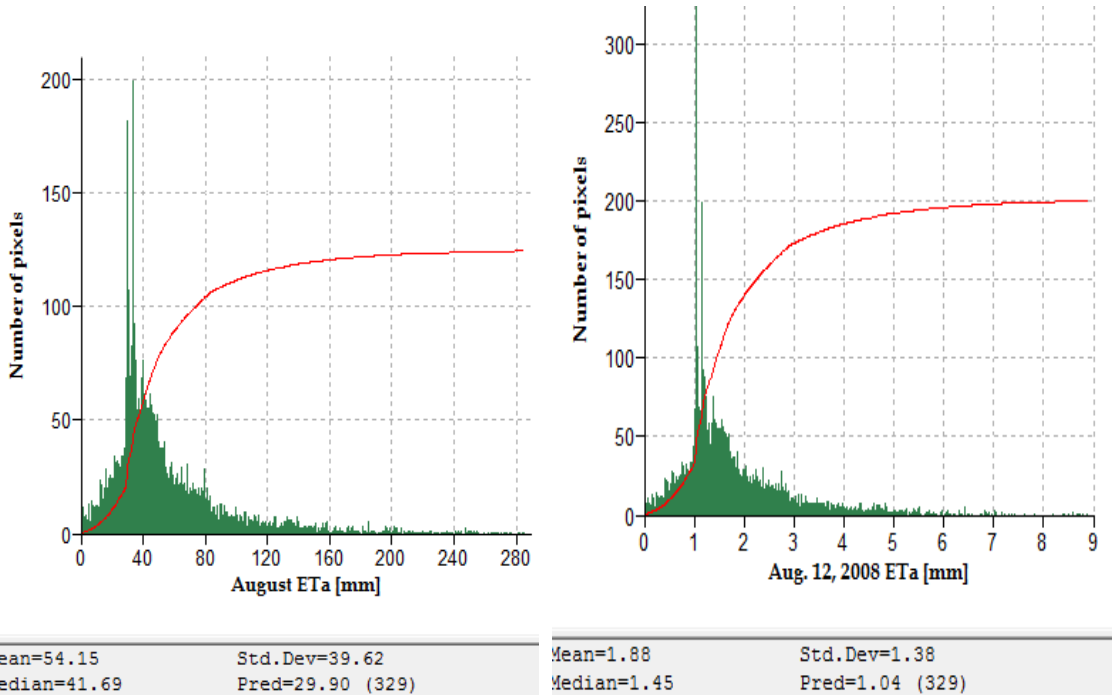

(a) Monthly evapotranspiration *(b) Daily evapotranspiration*

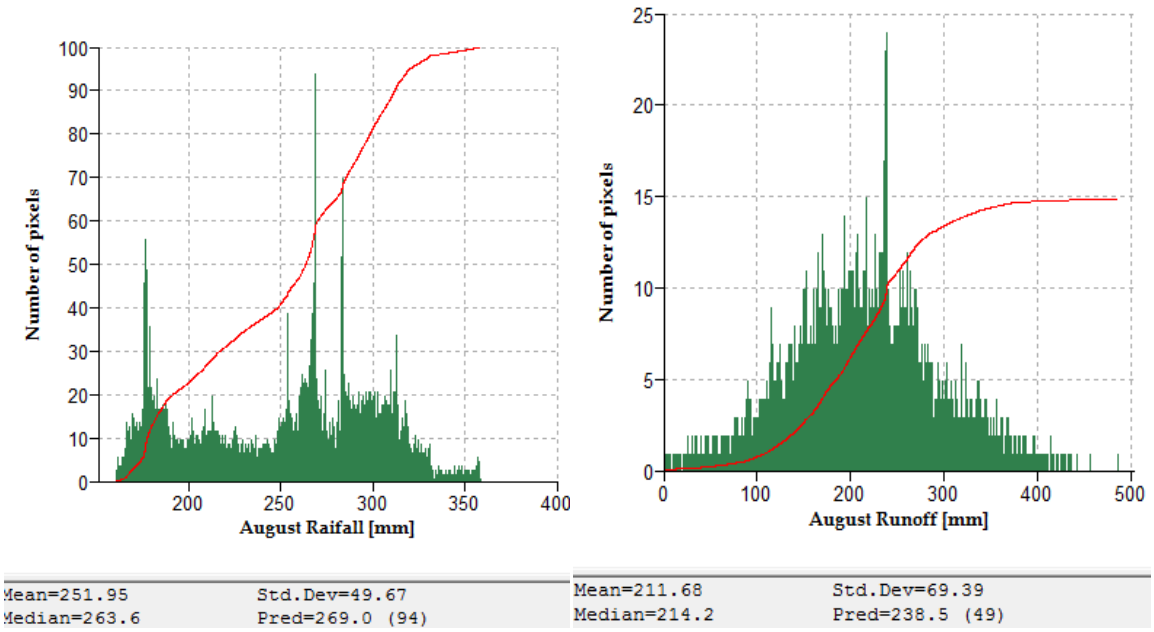

(c) Monthly rainfall *(d) Monthly runoff*

Figure 5-13 *Histograms of water balance components in August over the study area*

Table 5-6 *Water balance components of August per land use/cover units*

LULC	Area [Km²]	Rainfall [mm]	Rainfall [Mm³]	ET_a [mm]	ET_a [Mm³]	Runoff [mm]	Runoff [Mm³]	Runoff per unit area[Mm³/Km²]
0	38	288.06	10.95	38.84	1.48	249.21	9.47	0.249
1	4447	266.24	1183.95	54.27	241.33	211.97	942.62	0.212
2	3323	257.83	856.76	52.00	172.81	205.82	683.95	0.206
3	2174	259.32	563.77	52.14	113.36	207.18	450.41	0.207
4	383	285.02	109.16	62.03	23.76	222.99	85.40	0.223
5	71	307.27	21.82	68.87	4.89	238.40	16.93	0.238
6	80	337.39	26.99	77.61	6.21	259.79	20.78	0.260
7	67	333.58	22.35	77.06	5.16	256.51	17.19	0.257
8	109	425.83	46.42	91.66	9.99	334.17	36.42	0.334
Total	10692	265.82	2842.16	54.15	578.98	211.67	2263.18	

Taking the total volume of runoff, the major amount of runoff in august is runoff from the grasses/cereal crops land and the minimum is from water bodies. This is because of the land use/cover size as shown *in table 5-6*. The volume of runoff per unit area estimated shows that the maximum runoff per unit area is runoff from urban areas with a rate of 0.334 Mm^3/Km^2; this is may be attributed to low water supply through capillary action underneath the surface to meet

evapotranspiration demand and the imperviousness characteristics of surfaces in urban area. On the contrary, shrubs land and broadleaf crops land have low rate of runoff, 0.206Mm^3/Km^2 and 0.207Mm^3/Km^2, respectively. This is may be shrubs land resist the surface runoff permitting infiltration of rainfall into soil; cultivation of broadleaf crops land permits deep percolation but is release high evapotranspiration. Runoff per unit area of non-vegetated land is almost the same as to that of needle leaf forest land, under normal conditions it should be less.

5.6 Comparison of SEBS Result with Different Approaches

SEBS derived ET_a result at the weather station pixel with different ET_o approaches, namely Penman-Monteith, Hargreaves and Tornthwaite, based on point measurements at Addis Ababa station had been compared. The results are shown in *figure 5-14* below.

Even though, ground truth ET_a measured by lysimeter were required to evaluate which method fits best, it can be explained by combining the climatic condition for that period over the study area and pixel based remote sensing. Both Hargreaves and Tornthwaite approaches showed slight temporal variation, ranging from 111mm to 157mm, and 52mm to 80mm, respectively, showing similar pattern. It was recognized that Hargreaves over estimated ET_o by 63mm on average when compared to Tornthwaite method.

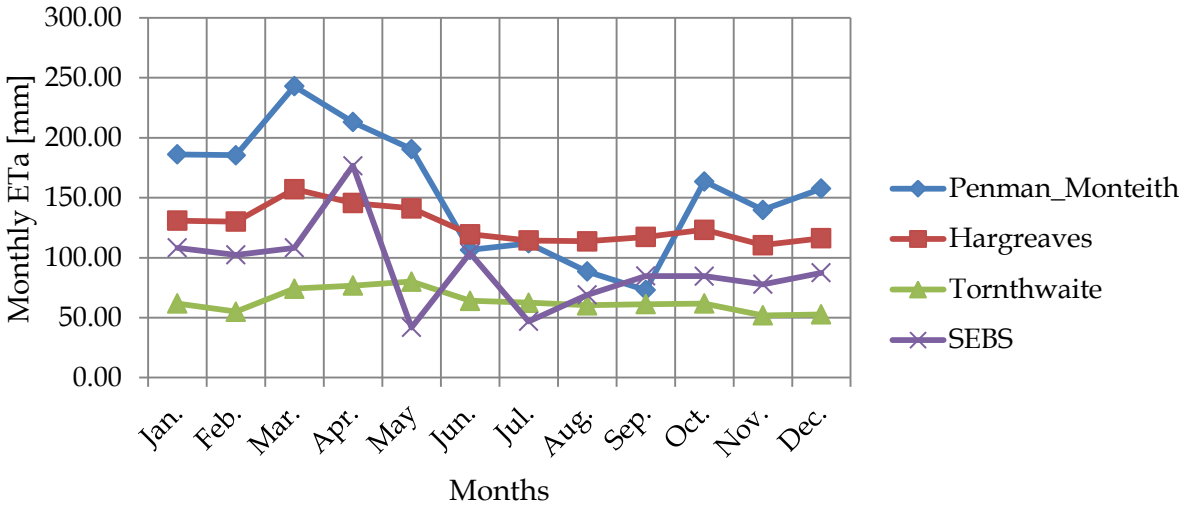

Figure 5-14 *Comparison of SEBS result of ET_a with different ET_o approaches*

Whereas, SEBS and Penman-Monteith methods showed relatively high temporal variations ranging from 42mm to 177mm, and 73mm to 186mm, respectively with different ups and downs. Images and point measurements that were changed to rater maps were all resampled to 1Km resolution. Due to the high distribution of green areas and built up areas within the pixel ($1Km^2$), lower ET_a values that weighing land covers in one pixel is reasonable to occur than measured by Penman-Monteith approach.

6. Conclusion and Recommendation

6.1 Conclusion

The estimates of major/ water balance components of the Upper Awash Basin were obtained for year 2008. Satellite rainfall data and SEBS model output were used to assess the temporal and spatial distribution of major water balance components on a pixel-by-pixel basis.

The average annual rainfall over the study area was identified to be 1049.6mm; the spatial pattern of rainfall follows the elevation of Upper Awash Basin. The wet season (June to September) made a contribution of 71% of the annual rainfall. The average monthly rainfall depth and runoff/reduced storage depth had the same pattern, despite the consequences of the evapotranspiration, providing same time to peak (July) with values of 270mm and 223.11mm, respectively.

The average annual ET_a estimate was 905.76mm. Annual ET_a, perceived from SEBS model, shows that relatively high values (above 850mm) were occured on some areas of North-East and South-West parts of the Upper Awash Basin. On the contrary, major areas of the North-West parts of the basin release 560-800mm of water through evapotranspiration.

On the annual basis, the total volume of runoff estimated using the catchment water balance method, with actual evapotranspiration derived from satellite images, amounts to 1545.99Mm^3. It is in agreement with that of the estimate from ground based flow record at Hombole station (=1575.02Mm^3), within only 2% error; the difference can be attributed to the likely uncertainties involved in the process while deriving the water balance components. This confirm that remote sensing can be considered as better alternative method, if there is a need to evaluate on pixel by pixel basis and in condition where data are not found or scarce.

Major lower parts of the study area and areas on the reach of both Modjo and Awash rivers had been cultivated and irrigated throughout the year; it was subjected to relatively high

evapotranspiration even in dry season. This made the availability of water below zero in months between October and April, even if SEBS overestimates evapotranspiration in dry season.

Areas where more than 80% of the rainfall is partitioned to ET_a are shown to be in semi-arid regions, most agricultural lands of the Upper Awash Basin. On the other hand, the highlands of the basin fall below 80% of ET_a as percent of annual rainfall.

6.2 Recommendation

The study could re-establish the fact that the application of remote sensing brings a significant contribution to estimate the spatial evapotranspiration in large areas for all land use/cover types. However, the ground based methods are always very important, especially in verifying the results of different remote sensing based approaches.

Although the results of this study have not been validated using field-collected data such as stream discharge measurements, the volumetric estimate of the Upper Awash Basin corresponds closely to the the ground based flow record at its outlet. More research is recommended to validate and integrate these results with ecohydrologic models.

The availability of continuous record of hydrological and meteorological data makes it possible to carry out a complete water balance and modeling in the near future offering the possibility of validation of the remote sensing result.

A good understanding of the spatial and temporal variation of the upper Awash Basin hydrology will help design appropriate management scenarios for (i) soil and water conservation especially South-East of the study area; (ii) Koka reservoir management; and (iii) agricultural development like expansion of Wonji and Metehara Sugar Plantation, Welinchiti Irrigation Project and Fentale Irrigation Project.

References

Adler, R. F., A. J. Negri, P. R. Keehn, and I. M. Hakkarinen, 1993. Estimation of rainfall over Japan and surrounding waters from a combination of low-orbit microwave and geosynchronous IR data. *Journal of Applied Meteorology*. 32, 335-356.

Adler, R. F., 2000. Tropical rainfall distribution using TRMM combined with other satellite and rain gauge information. *Journal of Applied Meteorology*. 39, 2007-2023.

Ahmed, M. D., T. Biggs, H. Turral and C.A. Scott, 2006. Application of SEBAL approach and MODIS time-series to map vegetation water use patterns in the data scarce Krishna river basin of India. International Water Management Institute. Global Research Division, Colombo, Sri Lanka.

Allen, R.G., L.S. Pereira, D. Raes and M. Smith, 1998. Crop evapotranspiration-Guidelines for computing crop water requirements-FAO Irrigation and Drainage Paper 56. *FAO-Food and Agriculture Organization*. Rome, Italy.

Anderson, M. C., J. M. Norman, G. R. Diak, W. P. Kustas and J. R. Mecikalski, 1997. A two-source time-integrated model for estimating surface fluxes using thermal infrared remote sensing. *Remote Sensing of Environment*. 60, 195-216.

Bastiaanssen, W. G. M. and N. R. Harshadeep, 2005. Managing scarce water resources in Asia: The nature of the problem and can remote sensing help?. *Irrigation and Drainage Systems.* 19: 269 – 284.

Bastiaanssen, W. G. M. and G. M. Mekonnen, 2000. A new simple method to determine crop coefficients for water allocation planning from satellites: Results from Kenya. *Irrigation and Drainage Systems.* 14(3): 237-256.

Bastiaanssen, W. G .M., 1995. Regionalization of surface flux densities and moisture indicators in composite terrain: A remote sensing approach under clear skies in Mediterranean climate. PhD Thesis, Wagenningen Agricultural University, The Netherlands, 273 pp.

Brutsaert, W., 1982. Evaporation into the atmosphere. Reidal, Dordrecht: 299pp.

Choudhury, B. J., N. U. Ahmed, S. B. Idso, R. J. Reginato and C. S. T. Daughtry, 1994. Relations between evaporation coefficients and vegetation indices studied by model simulations. *Remote Sensing of Environment.* 50(1): 1-17.

Choudhury, B. J., and J. L. Monteith, 1988. A four layer model for the heat budget of homogeneous land surfaces. Quarterly Journal Roy. Meteorology Society. 114, 373-398.

Chow, V. T., D. R. Maidment, and L. W. Mays, 1988. *Applied hydrology.* McGraw Hill, Newyork.

Cleugh, H. A., R. Leuning, Q. Mu and S. W. Running, 2007. Regional evaporation estimates from flux tower and MODIS satellite data. Remote Sensing of Environment. 106(3): 285-304.

Dingman, S. L., 2002. Physical hydrology. Prentice Hall, New Jersey. 84(8): 1013-1023.

FAO, 1986. In yield esponse to water. FAO *Plant Production and Protection Paper*. Rome, 33.

Gash, J. H. C., and J. Shuttleworth, 2007. Evaporation. Benchmark Papers in Hydrology. *International Association of Hydrological Sciences (IAHS).* Wallingford, 131pp.

GES DISC, 2006. Gaddard Earth Sciences, Data and Information Services Center. Last access, June 2010.

TRMM, Tropical Rainfall Measuring Mission.
http://trmm.gsfs.nasa.gov/data_dir/data.html

Gieske, A. S. M., 2003. Operational solutions of actual evapotranspiration. In I. Simmers (Editor), Understanding water in a dry environment: Hydrological processes in arid and semi arid zones. Rotterdam. 65-114.

Goode, P. R., J. Qiu, V. Yurchshyn, J. Hickey, M. C. Chu, E. Kolbe, C. T. Brown and S.E. Koonin (2001). Earthshine observations of the Earth's reflectance. *Geophysical Research Letters.* 28(9): 1671-1674.

Gomez, M. S., 2007.Spatial and temporal rainfall gauge data analysis and validation with TRMM Microwave Radiometer Surface Rainfall Retrievals. M.Sc. Thesis, ITC, Enschede, The Netherlands, 95 pp.

Halcrow, 1989. Master plan for the development of surface water resources in the Awash Basin. Final report. *Climate and Hydrology*, 4, 32.

Halcrow, 2006. Awash River Basin flood control and watershed management study project. Working Paper 2. Review and assessment of community development, settlement patterns and gender in the Awash River Basin, 46pp.

Halcrow, 2006. Awash River Basin flood control and watershed management study project. Working Paper 3. Review of physical, environmental and its impact on flooding in the Awash River Basin, 125pp.

Harrison, L. P., 1963. Fundamentals concepts and definitions relating to humidity. In FAO, Irrigation and Drainage Paper, 56. *FAO-Food and Agriculture Organization*. Rome, Italy.

Hatfield, J. L., 1989. Aerodynamic properties of partial canopies. *Agricultural and Forestry* Meteorology. 46, 15-22.

Huete, A., C. Justice and W. V. Leeuwen, 1999. MODIS vegetation index (MOD13) algorithm theoretical basis documents, version 3. University of Virginia, Department of Environmental Sciences. Clark Hall Charlottesville. VA 22903.

Huffman, G. J., R. F. Adler, M. M. Morrissey, D. T. Bolvin, S. Curtis and R. Joyce, 2004. Global precipitation at one-degree daily resolution from multi satellite observations. *Journal of Hydrology.* 2, 36-50.

Iqbal, M., 1983. Introduction to solar radiation. Academic Press, Canada, 416pp.

Irena, Y., 2007. Rainfall estimation by Remote Sensing for conceptual rainfall-runoff modeling in the Upper Blue Nile Basin. . M.Sc. Thesis, ITC, Enschede, The Netherlands, 64 pp.

Jensen, M. E., 1990. Evapotranspiration and irrigation water requirements. ASCE Manuals and reports on Engineering Practices. New York, *American Society of Civil Engineers*. 332pp.

Kidd, C., D. R. Kniveton, M. C. Todd and T. J. Bellerby, 2003. Satellite rainfall estimation using combined passive microwave and infrared algorithms. *Journal of Hydrometeorology.* 4(6)1088-1104.

Kite, G. W. and P. Droogers, 2000. Comparing evapotranspiration estimation from satellites, hydrological models and field data. *Journal of Hydrology.* 229(1-2): 3-18.

Langensiepen, M., 2008. Evaporation and Energy Balance. Department of Modeling Plant Systems, Institute of Crop Science. Humboldt University of Berlin, Berlin, Germany.

Liang, S., 2000. Narrowband to broadband conversions of land surface albedo: II. *Validation. Remote Sensing of Environment*. 84(1): 25-41.

Massman, W. J., 1999b. Molecular diffusivities of Hg vapor in air, O2 and N2 near STP and the kinematic

viscosity and the thermal diffusivity of air near STP. *Atmospheric Environment.* 33, 453-457.

Minacapilli, M., C. Agnese., F. Blanda, C. Cammalleri, G. Ciraolo, G. D'Urso, M. Iovino, D. Pumo, G. Provenzano and G. Rallo, 2009. Estimation of actual evapotranspiration of Mediterranean perennial crops by means of remote sensing based surface energy balance models. *Hydrology of Earth System Sciences*. 13, 1061-1074.

Mu, Q., F. A. Heinsch, M. Zhao and S. W. Running, 2007. Development of a global evapotranspiration algorithm based on MODIS and global meteorology data. *Remote sensing of Environment.* 111(2007): 519-536.

NASA/GSFC, 2007. National Aeronautics and Space Administration, Gaddard Space Flight Center. Last access, June 2010.

http://www.gsfc.nasa.gov/

Norman, J. M., M. C. Anderson, W. P. Kustas, A. N French, J. Mecikalski, R. Torn, G. R. Diak, T. J. Schmugge and B. C. Tanner, 2003. Remote sensing of surface energy fluxes at 101-m pixel resolutions. Water Resources Research. 39pp.

Paulos, S., 1998. Establishing water release rules for Koka Reservoir for wet seasons. M.Sc. Thesis, Addis Ababa University, Ethiopia.

Pan, M., E. F. Wood, R. Wojcik and M. F. McCabe, 2008. Estimation of regional terrestrial water cycle using multi-sensor remote sensing observations and data assimilation. *Remote sensing of Environment*. 112(2008): 1282-1294.

Peixoto, J. P. and M. A. Kettani, 1973. The control of the water cycle. *Scientific American*. 228:46-61.

Penman, H. L., 1956. Estimating evaporation. Transactions of the Ameircan Geophysical Union. 37(1): 43-50.

Peters, S. W. M., 1995. Energy- and water-balance modeling of a semi arid area using remote sensing. PhD Thesis, Vrije Universiteit, Amsterdam, 256pp.

Raupach, M. R., 1994. Simplified expressions for vegetation roughness length and zero plane displacementas functions of canopy height and area index. *Boundary Layer Meteorology.* 71: 211-216.

Richard, G. A. and S.P. Luis, 1998. Crop evapotranspiration—guidelines for computing crop water requirements. FAO Irrigation and Drainage Paper, 56. *FAO-Food and Agriculture Organization*. Rome, Italy.

Savenije, G., and G. Hubert, 1995. New definitions of moisture recycling and the relationship with land–use changes in the Sahel. *Journal of Hydrology.* 167(1): 57-58.

Schmegge, T. J., W. P. Kustas, J. C. Ritchie, T. J. Jackson and A. Rango, 2002. Remote sensing in hydrology. *Advances in Water Resources.* 25(8): 1367-1385.

Senay, G. B., K. Asante and G. Artan, 2009. Water balance dynamics in the Nile Basin. *Hydrological Processes.* Published online in Wiley Interscience, DOI:10.1002/hyp.7364.

Seth, S. M., Jain, S. K. and M. K. Jain, M. K. , 1996. Remote sensing and GIS application studies at national institute of hydrology. *National Institute of Hydrology.* Roorkee 247667 (U.P).

Shimelis, B., 2004. Stream flow simulation for the upper awash basin. M.Sc. Thesis, Addis Ababa University, Ethiopia. 83pp.

Shuttleworth, W. J., R. J. Gurney, A. Y. Hsu and J. P. Ormsby, 1989. FIFE: The variation in energy partition at surface flux sites. *IAHS Publication.* 186: 67-74.

Sobrino, J. A., J. Kharraz, and L. Z. Li (2003). Surface temperature and water vapour retrieval from

MODIS data. *International Journal of Remote Sensing*. 24(24): 5161-5182.

Sobrino, J. A., N. Raissoni, and L. Z. Li (2001). A comparative study of land surface emissivity retrieval from NOAA data. *Remote Sensing of Environment.* 75(2): 256-266.

Solomon, C. M., Z. B. Su, W. Wolters, M. G. Bos and M. Gieske, 2005. Assessment of catchment water balance using GIS and remote sensing; Roxo, Portugal. M.Sc. Thesis, ITC, Enschede, The Netherlands, 109 pp.

Su, Z. B., 2002, The Surface Energy Balance System (SEBS) for estimation of turbulent heat fluxes. *Hydrology and Earth System Sciences*. 6(1):85-99.

Su, Z. B. and C. Jacobs, 2001. Advanced earth observation: Land surface climate final report. BCRS Report 2001: USP-2 Report 2001 01-02. Delft, *Beleidscommissie Remote Sensing (BCRS):* 183pp.

Tang, Q., 2007. Estimation of evapotranspiration using remote sensing data. Land Surface Research group, Department of Civil and Environmental Engineering, University of Washington. Last access, April 2010.

http://www.geog.umd.edu/eos/

Tadesse, A. M., 2010. Estimation of actual evapotranspiration and water balance using combined geostationary and polar orbiting satellite products: A case study in Spain. M.Sc. Thesis, ITC, Enschede, The Netherlands, 75pp.

Tasumi, M., R. G. Allen and W. G. M. Bastiaanssen (2000). Application of SEBAL methodology for estimating consumptive use of water and stream flow depletion in the bear River Basin of Idaho through remote sensing, Appendix A: The theoretical basis of SEBAL. The Raytheor System Company, EOSDISP, 107 pp.

Valor, E. and V. Caselles, 1996. Mapping land surface emissivity from NDVI: Application to European, African, and South American Areas. *Remote Sensing of Environment*. 57(3): 167-184.

Van de Griend, A. A. and M. Owe, 1993. On the relationship between thermal emissivity and the Normalized Difference Vegetation Index for natural surfaces. *International Journal of Remote Sensing*. 14(6): 1119-1131.

Verhoef, A. and G. McNaughton, 1997. A parameterization of momentum roughness length and displacement height for a wide range of canopy densities. *Hydrology and Earth System Sciences.* 1(1): 81-91.

Wendimagegn, S. H., 2006. Remote sensing analysis of summar time evapotranspiration using SEBS algorithm. A case study in Regge and Dinkel. M.Sc. Thesis, ITC, Enschede, The Netherlands, 130pp.

Wenjing, L., R. Velde and Z. B. Su, 2006. Satellite based regional-scale evapotranspiration in the Hebei Plain, Northern China. Proc. Dragon 1 Programme Final results 2004-2007. Beijing, P. R. China, 21-25 April 2008 (ESA SP_655, April 2008).

Appendices

Appendix A: Weather Data and Reference Evapotranspiration

A1: Addis Ababa_Bole Station (latitude: $9^0$00' N, longitude: $38^0$45' E, altitude: 2354m)

Date	Tmax [^{0}C]	Tmin [^{0}C]	Tmean [^{0}C]	RH mean [%]	U_2 [m/s]	n [hr]	R_S [w/m^2]	P [mm]	ET_0 [mm/day]	
									Pen-Mon	Harg.
1/1/2008	25.0	8.0	16.50	37.2	4.6	10.9	265.39	0.0	6.04	4.21
1/2/2008	25.0	7.6	16.30	34	4.8	10.5	259.25	0.0	6.22	4.24
1/3/2008	26.0	7.8	16.90	32.2	3.6	10.7	262.70	0.0	5.91	4.42
1/4/2008	26.5	8.0	17.25	24.6	5.8	11.1	269.38	0.0	7.59	4.50
1/5/2008	26.5	8.0	17.25	35.4	4.6	10.9	266.48	0.0	6.39	4.51
1/6/2008	24.7	6.5	15.60	38.4	4.4	11.0	268.40	0.0	5.82	4.27
1/7/2008	26.5	6.2	16.35	32	4.2	11.0	268.73	0.0	6.33	4.62
1/8/2008	24.8	9.0	16.90	40.2	4.8	10.5	261.05	0.0	5.96	4.14
1/9/2008	24.5	8.5	16.50	40	5.4	10.6	263.02	0.0	6.14	4.13
1/10/2008	25.5	10.0	17.75	43.8	5	10.9	268.22	0.0	6.03	4.22
1/11/2008	25.3	10.0	17.65	40.8	4.6	10.5	262.16	0.0	5.98	4.19
1/12/2008	25.2	8.9	17.05	44.4	6.4	10.3	259.34	0.0	6.29	4.25
1/13/2008	24.5	11.7	18.10	42.2	6.4	10.0	254.89	0.0	6.46	3.89
1/14/2008	24.8	11.0	17.90	44	4.8	10.2	258.55	0.0	5.84	4.02
1/15/2008	24.5	10.2	17.35	53.8	5.8	6.5	198.96	0.0	5.07	4.04
1/16/2008	22.0	10.0	16.00	54.8	4	4.0	158.69	0.0	3.97	3.57
1/17/2008	22.2	11.0	16.60	55.6	4.6	9.0	240.36	0.0	4.74	3.51
1/18/2008	22.2	11.0	16.60	59.6	6.6	5.2	178.85	0.0	4.49	3.52
1/19/2008	22.9	10.2	16.55	59.6	7	8.9	239.61	0.0	4.98	3.75
1/20/2008	22.5	10.5	16.50	53	8	10.1	259.70	0.0	5.70	3.65
1/21/2008	24.2	7.8	16.00	43.4	5.2	10.5	266.76	0.0	5.86	4.21
1/22/2008	26.0	7.7	16.85	40	2.4	11.2	278.77	0.0	5.14	4.57
1/23/2008	25.5	8.5	17.00	34.6	6.6	10.7	271.10	0.0	7.18	4.44
1/24/2008	25.3	6.5	15.90	39.6	5.2	10.3	265.06	0.0	6.20	4.53
1/25/2008	25.5	6.0	15.75	29.6	6	10.6	270.55	0.0	7.18	4.60
1/26/2008	26.5	8.0	17.25	28.8	3.4	11.2	281.04	0.0	6.21	4.70
1/27/2008	24.7	8.8	16.75	29.6	6.2	10.9	276.66	0.0	7.27	4.30
1/28/2008	25.0	9.3	17.15	40.6	7.8	10.9	277.24	0.0	7.10	4.33
1/29/2008	25.5	8.5	17.00	38	4.8	11.0	279.50	0.0	6.36	4.50
1/30/2008	26.2	8.5	17.35	40.6	4.8	10.4	270.10	0.0	6.27	4.65
1/31/2008	25.0	9.0	17.00	48.2	3.8	10.7	275.70	0.0	5.41	4.39
January	**26.5**	**6.0**	**16.83**	**41.25**	**5.21**	**311.2**	**7976.2**	**0.0**	**186.1**	**130.9**

Where,

Tmax = maximum daily temperature

Tmin = minimum daily temperature

Tmean = mean daily temperature

n = actual sunshine hours

U_2 = wind speed at 2m height

RH mean = mean daily relative humidity

R_S = instantaneous downward solar radiation

P = precipitation

ET_0 Pen-Mon = Penman-Monteith reference evapotranspiration

ET_0 Harg. = Hargreaves reference evapotranspiration

Date	Tmax [^{0}C]	Tmin [^{0}C]	Tmean [^{0}C]	RH mean [%]	U_2 [m/s]	n [hr]	R_S [w/m^2]	P [mm]	ET_0 [mm/day]	
									Pen-Mon	Harg.
2/1/2008	24.5	11.0	17.75	52.6	6.4	10.3	269.61	0.0	5.86	4.13
2/2/2008	24.5	10.0	17.25	53.6	5.6	10.5	273.56	0.0	5.60	4.23
2/3/2008	25.0	9.5	17.25	46	5.8	10.9	280.88	0.0	6.23	4.39
2/4/2008	26.5	9.0	17.75	45.4	5	8.5	241.09	0.0	5.94	4.74
2/5/2008	25.5	9.5	17.50	41.2	3.4	9.1	251.76	0.0	5.47	4.51
2/6/2008	25.0	10.8	17.90	47	3.6	6.4	206.68	7.7	4.94	4.31
2/7/2008	24.0	11.5	17.75	50.6	2.4	7.0	217.32	5.3	4.33	4.04
2/8/2008	24.4	9.5	16.95	42.6	6	9.0	251.76	0.0	6.24	4.32
2/9/2008	24.8	10.3	17.55	35.6	6.2	10.9	284.64	0.0	7.08	4.34
2/10/2008	23.0	7.0	15.00	36.2	6.4	10.8	283.57	0.0	6.60	4.25
2/11/2008	24.8	7.7	16.25	28	4.4	10.5	279.07	0.0	6.61	4.57
2/12/2008	24.5	7.0	15.75	28.2	4.6	10.5	279.68	0.0	6.63	4.57
2/13/2008	24.0	5.5	14.75	33	4.6	10.8	285.44	0.0	6.28	4.57
2/14/2008	25.0	7.0	16.00	30.2	3	10.2	275.75	0.0	5.74	4.69
2/15/2008	25.0	8.1	16.55	36.8	4	10.7	284.95	0.0	6.11	4.63
2/16/2008	24.5	6.8	15.65	33	5.6	10.9	289.01	0.0	6.85	4.63
2/17/2008	25.0	7.5	16.25	36.6	7.8	10.7	286.17	0.0	7.43	4.69
2/18/2008	26.0	8.9	17.45	40.2	6.8	10.0	274.65	0.0	7.08	4.81
2/19/2008	26.0	13.0	19.50	42.4	6.8	10.6	285.63	0.0	7.23	4.45
2/20/2008	25.0	10.0	17.50	47.6	5.4	10.0	275.79	0.0	6.07	4.54
2/21/2008	24.5	7.8	16.15	43	7.4	10.7	288.54	0.0	6.78	4.62
2/22/2008	24.5	7.0	15.75	37.2	8.4	11.0	294.34	0.0	7.46	4.68
2/23/2008	23.8	5.8	14.80	28.8	5.8	10.4	284.44	0.0	7.00	4.63
2/24/2008	26.5	7.5	17.00	30.2	5.4	10.6	288.49	0.0	7.38	5.08
2/25/2008	0.0	8.5	4.25	25.6	3.6	10.5	287.29	0.0	3.96	2.16
2/26/2008	26.5	0.0	13.25	28	4.8	10.2	282.57	0.0	7.00	5.38
2/27/2008	25.5	9.5	17.50	35.4	6.6	10.0	279.57	0.0	7.36	4.77
2/28/2008	25.0	9.0	17.00	39.6	6.6	10.0	280.08	0.0	6.95	4.71
2/29/2008	24.5	7.0	15.75	36	7.2	10.8	294.68	0.0	7.26	4.76
February	**26.5**	**0.0**	**16.20**	**38.30**	**5.50**	**292.5**	**7957.0**	**13.0**	**185.5**	**130.2**

Where,

Tmax = maximum daily temperature

Tmin = minimum daily temperature

Tmean = mean daily temperature

n = actual sunshine hours

U_2 = wind speed at 2m height

RH mean = mean daily relative humidity

R_S = instantaneous downward solar radiation

P = precipitation

ET_0 Pen-Mon = Penman-Monteith reference evapotranspiration

ET_0 Harg. = Hargreaves reference evapotranspiration

Date	Tmax [^{0}C]	Tmin [^{0}C]	Tmean [^{0}C]	RH mean [%]	U_2 [m/s]	n [hr]	R_S [w/m^2]	P [mm]	ET_0 [mm/day]	
									Pen-Mon	Harg.
3/1/2008	24.5	6.5	15.50	26.8	5.6	10.8	295.19	0.0	7.30	4.80
3/2/2008	25.5	6.5	16.00	24.6	3.8	10.6	292.15	0.0	6.69	5.02
3/3/2008	26.5	8.0	17.25	22.2	5.4	10.7	294.40	0.0	7.95	5.14
3/4/2008	26.5	8.8	17.65	21	3.8	10.1	284.23	0.0	7.03	5.10
3/5/2008	26.5	9.0	17.75	20.2	4.2	10.7	295.33	0.0	7.41	5.09
3/6/2008	25.0	9.2	17.10	30.5	5.8	10.4	290.44	0.0	7.38	4.76
3/7/2008	24.5	11.2	17.85	41.6	7.8	10.6	294.43	0.0	7.29	4.47
3/8/2008	25.5	12.0	18.75	42.4	7.8	10.7	296.63	0.0	7.48	4.63
3/9/2008	25.5	9.5	17.50	38.4	6.4	10.6	295.25	0.0	7.22	4.87
3/10/2008	26.0	8.5	17.25	25.6	7	10.7	297.43	0.0	8.41	5.07
3/11/2008	26.5	9.0	17.75	22.8	5.6	10.5	294.23	0.0	8.09	5.15
3/12/2008	27.0	9.5	18.25	20	5	10.6	296.38	0.0	8.06	5.23
3/13/2008	28.5	9.9	19.20	19.8	4.8	9.5	277.03	0.0	8.13	5.55
3/14/2008	27.0	10.5	18.75	19.8	5	10.6	297.07	0.0	8.13	5.17
3/15/2008	26.4	9.2	17.80	22.2	5.8	10.8	300.97	0.0	8.27	5.15
3/16/2008	26.5	10.5	18.50	25.4	5.2	10.5	295.90	0.0	7.82	5.07
3/17/2008	27.5	11.3	19.40	27.6	4.8	10.5	296.18	0.0	7.71	5.23
3/18/2008	27.5	10.0	18.75	23.2	5	10.1	289.26	0.0	7.97	5.35
3/19/2008	28.0	12.0	20.00	22.4	3.8	10.6	298.51	0.0	7.48	5.30
3/20/2008	27.0	11.5	19.25	21.8	6.2	10.6	298.75	0.0	8.74	5.12
3/21/2008	27.0	10.2	18.60	23.8	5	10.7	300.78	0.0	7.94	5.24
3/22/2008	27.0	11.4	19.20	22.8	8.6	10.8	302.80	0.0	9.74	5.14
3/23/2008	26.0	11.5	18.75	18.6	6.2	10.7	301.19	0.0	8.76	4.90
3/24/2008	26.5	9.5	18.00	20.4	6	10.6	299.57	0.0	8.53	5.20
3/25/2008	27.0	10.2	18.60	19	4.8	10.7	301.54	0.0	8.09	5.27
3/26/2008	22.5	11.0	16.75	19.6	5.4	10.7	301.69	0.0	7.61	4.14
3/27/2008	27.5	10.8	19.15	19.8	4.2	10.4	296.41	0.0	7.75	5.34
3/28/2008	28.5	11.7	20.10	30	6.4	8.9	269.45	0.0	8.40	5.50
3/29/2008	27.0	12.8	19.90	26.2	5.6	10.0	289.40	0.0	8.18	5.03
3/30/2008	28.3	10.5	19.40	29.2	5.2	8.5	262.42	0.0	7.72	5.56
3/31/2008	26.0	14.4	20.20	40.4	4.2	4.2	184.88	0.0	5.75	4.59
March	**28.5**	**6.5**	**18.35**	**25.42**	**5.50**	**316.4**	**8989.9**	**0.0**	**243.0**	**157.2**

Where,

Tmax = maximum daily temperature

Tmin = minimum daily temperature

Tmean = mean daily temperature

n = actual sunshine hours

U_2 = wind speed at 2m height

RH mean = mean daily relative humidity

R_S = instantaneous downward solar radiation

P = precipitation

ET_0 Pen-Mon = Penman-Monteith reference evapotranspiration

ET_0 Harg. = Hargreaves reference evapotranspiration

Date	Tmax [^{0}C]	Tmin [^{0}C]	Tmean [^{0}C]	RH mean [%]	U_2 [m/s]	n [hr]	R_S [w/m^2]	P [mm]	ET_0 [mm/day]	
									Pen-Mon	Harg.
4/1/2008	26.0	11.0	18.50	52	4.6	3.8	177.72	2.1	5.05	4.99
4/2/2008	25.5	11.2	18.35	47.2	6.8	6.5	226.50	0.0	6.36	4.85
4/3/2008	25.5	13.5	19.50	45	7	7.8	249.99	0.0	6.89	4.59
4/4/2008	27.6	13.5	20.55	40	5.6	10.0	289.70	0.0	7.43	5.12
4/5/2008	27.0	15.0	21.00	46.6	6.2	8.8	268.05	0.0	7.01	4.78
4/6/2008	28.0	14.0	21.00	40.8	7.8	10.2	293.28	0.0	8.27	5.16
4/7/2008	27.5	12.7	20.10	34.4	7	10.5	298.66	0.0	8.38	5.19
4/8/2008	25.7	13.5	19.60	46.8	5.2	7.7	248.17	10.0	6.23	4.65
4/9/2008	26.5	12.5	19.50	53.6	3.2	6.6	228.33	29.1	5.04	4.97
4/10/2008	21.0	10.5	15.75	68.2	4.6	5.6	210.30	0.0	3.90	3.87
4/11/2008	21.8	11.7	16.75	66	6.4	4.5	190.47	0.0	4.22	3.91
4/12/2008	22.0	10.8	16.40	58.8	6.8	7.4	242.56	0.0	5.11	4.08
4/13/2008	24.3	12.0	18.15	50.4	7.2	8.6	264.04	0.0	6.34	4.49
4/14/2008	25.0	11.0	18.00	37	6	10.3	294.46	0.0	7.23	4.77
4/15/2008	25.5	9.5	17.50	28.2	5	11.6	317.65	0.0	7.52	5.03
4/16/2008	26.5	10.0	18.25	28.8	8.4	11.4	313.90	0.0	9.02	5.22
4/17/2008	25.7	10.2	17.95	27.6	8.2	11.0	306.57	0.0	8.83	5.01
4/18/2008	27.0	10.5	18.75	27.4	8.4	11.0	306.39	0.0	9.25	5.29
4/19/2008	26.5	12.0	19.25	25.2	7.6	10.8	302.62	0.0	9.09	5.02
4/20/2008	27.0	12.0	19.50	26.8	7.2	8.0	252.40	0.0	8.60	5.14
4/21/2008	27.0	11.5	19.25	29.4	5.2	10.8	302.22	0.0	7.81	5.19
4/22/2008	25.5	12.7	19.10	39.8	5.8	5.0	198.56	0.0	6.45	4.70
4/23/2008	26.0	12.5	19.25	34.6	8.6	10.0	287.53	0.0	8.49	4.84
4/24/2008	25.8	11.5	18.65	38.6	6.6	10.1	289.09	0.0	7.45	4.90
4/25/2008	24.0	11.6	17.80	49.2	8.8	9.8	283.53	0.0	6.78	4.45
4/26/2008	25.0	12.0	18.50	41	6.6	11.2	308.17	0.0	7.30	4.65
4/27/2008	26.6	12.2	19.40	40.2	6.4	10.8	300.81	0.0	7.54	5.01
4/28/2008	28.2	11.7	19.95	35	7	10.9	302.32	0.0	8.44	5.44
4/29/2008	28.0	12.5	20.25	30.2	5.4	9.5	277.26	0.0	7.90	5.31
4/30/2008	26.4	12.0	19.20	58.2	5.2	5.6	208.04	8.2	5.17	4.98
April	**28.2**	**9.5**	**18.86**	**41.57**	**6.49**	**265.8**	**8039.3**	**49.4**	**213.1**	**145.6**

Where,

Tmax = maximum daily temperature

Tmin = minimum daily temperature

Tmean = mean daily temperature

n = actual sunshine hours

U_2 = wind speed at 2m height

RH mean = mean daily relative humidity

R_S = instantaneous downward solar radiation

P = precipitation

ET_0 Pen-Mon = Penman-Monteith reference evapotranspiration

ET_0 Harg. = Hargreaves reference evapotranspiration

Date	Tmax [^{0}C]	Tmin [^{0}C]	Tmean [^{0}C]	RH mean [%]	U_2 [m/s]	n [hr]	R_S [w/m^2]	P [mm]	ET_0 [mm/day]	
									Pen-Mon	Harg.
5/1/2008	25.5	13.3	19.40	49.2	5.8	8.2	253.79	0.8	6.26	4.60
5/2/2008	26.0	13.4	19.70	45.6	5.6	7.5	241.21	0.0	6.42	4.71
5/3/2008	24.8	13.0	18.90	49.2	4.6	3.7	174.01	8.6	5.13	4.46
5/4/2008	21.5	13.3	17.40	73.8	3.4	0.4	115.77	30.4	2.77	3.56
5/5/2008	21.5	12.0	16.75	69.4	3.4	1.8	140.31	1.3	3.15	3.76
5/6/2008	23.9	12.0	17.95	62	3.8	7.5	240.31	5.6	4.66	4.35
5/7/2008	20.5	12.2	16.35	72.4	2.6	4.7	190.96	25.5	3.34	3.47
5/8/2008	24.0	11.0	17.50	57	6	9.2	269.63	0.0	5.56	4.49
5/9/2008	25.5	11.5	18.50	38.8	7.2	10.7	295.61	0.0	7.59	4.79
5/10/2008	25.5	13.2	19.35	36.4	5.8	8.2	251.61	0.0	7.09	4.59
5/11/2008	25.0	12.0	18.50	49.6	6.6	7.3	235.64	0.0	6.15	4.60
5/12/2008	27.2	12.0	19.60	43.8	6.4	9.2	268.54	0.8	7.12	5.13
5/13/2008	24.5	13.5	19.00	53.8	6.2	4.6	188.16	2.2	5.40	4.29
5/14/2008	25.5	12.4	18.95	48.4	5.6	9.0	264.52	1.2	6.28	4.67
5/15/2008	25.5	11.5	18.50	43.6	6.6	10.3	286.83	0.0	7.00	4.76
5/16/2008	26.0	13.2	19.60	40.6	7.4	10.8	295.22	0.5	7.72	4.69
5/17/2008	26.0	12.0	19.00	40.2	7	11.4	305.31	0.0	7.61	4.82
5/18/2008	27.5	12.0	19.75	36.6	4.2	9.3	268.65	0.0	6.73	5.17
5/19/2008	26.0	12.5	19.25	43.4	4.2	7.0	228.61	6.7	5.86	4.76
5/20/2008	25.0	13.2	19.10	47	7.6	7.4	235.30	0.0	6.67	4.43
5/21/2008	26.5	12.5	19.50	31.2	6.8	11.1	298.92	0.0	8.30	4.87
5/22/2008	25.0	13.0	19.00	29.2	8.4	9.8	276.22	0.0	8.61	4.45
5/23/2008	25.0	13.5	19.25	39	6.8	6.2	213.99	0.0	6.93	4.38
5/24/2008	27.0	12.5	19.75	43.8	5.8	8.3	249.91	0.0	6.76	4.98
5/25/2008	25.5	12.0	18.75	43.4	5.8	9.8	275.46	0.0	6.71	4.68
5/26/2008	27.5	13.0	20.25	40.4	5.4	11.0	295.80	0.0	7.30	5.04
5/27/2008	27.8	12.0	19.90	42.2	6.4	10.2	281.83	0.0	7.43	5.21
5/28/2008	27.5	12.4	19.95	42.4	6	9.5	269.60	0.0	7.15	5.10
5/29/2008	25.5	12.5	19.00	54.6	4.2	7.1	228.31	0.0	5.19	4.61
5/30/2008	23.0	11.8	17.40	62.8	5.4	3.7	170.00	2.1	4.22	4.09
5/31/2008	21.0	11.2	16.10	63.8	3	3.4	164.76	9.8	3.45	3.68
May	**27.8**	**11.0**	**18.77**	**48.18**	**5.61**	**238.3**	**7474.8**	**95.5**	**190.6**	**141.2**

Where,

Tmax = maximum daily temperature

Tmin = minimum daily temperature

Tmean = mean daily temperature

n = actual sunshine hours

U_2 = wind speed at 2m height

RH mean = mean daily relative humidity

R_S = instantaneous downward solar radiation

P = precipitation

ET_0 Pen-Mon = Penman-Monteith reference evapotranspiration

ET_0 Harg. = Hargreaves reference evapotranspiration

Date	Tmax [^{0}C]	Tmin [^{0}C]	Tmean [^{0}C]	RH mean [%]	U_2 [m/s]	n [hr]	R_S [w/m^2]	P [mm]	ET_0 [mm/day]	
									Pen-Mon	Harg.
6/1/2008	20.5	11.0	15.75	76.6	2.2	1.0	123.69	13.6	2.45	3.59
6/2/2008	22.0	10.5	16.25	71.6	4	6.7	220.81	1.0	3.81	4.00
6/3/2008	20.5	11.6	16.05	74.8	3.8	3.3	162.73	21.5	3.08	3.50
6/4/2008	19.5	12.0	15.75	70.2	3.6	1.8	137.09	2.1	2.99	3.18
6/5/2008	21.7	11.0	16.35	69.2	2.6	5.7	203.36	6.8	3.57	3.86
6/6/2008	24.5	11.2	17.85	52.8	4	9.8	272.95	0.0	5.43	4.50
6/7/2008	0.0	12.0	6.00	65.4	5.2	4.8	187.84	0.0	2.71	2.85
6/8/2008	24.0	10.7	17.35	67.7	3.4	7.7	236.98	6.6	4.23	4.43
6/9/2008	22.5	12.5	17.50	65	3.8	7.1	226.68	0.9	4.27	3.85
6/10/2008	23.5	11.0	17.25	63.4	3.8	6.4	214.70	0.0	4.26	4.28
6/11/2008	24.0	11.5	17.75	70.6	3.6	3.6	167.14	5.1	3.51	4.34
6/12/2008	21.5	10.2	15.85	60.2	3	3.1	158.61	8.4	3.53	3.90
6/13/2008	24.8	12.0	18.40	57.75	5	9.1	260.17	0.0	5.37	4.47
6/14/2008	23.5	11.8	17.65	64	3.2	4.3	178.82	2.4	3.81	4.18
6/15/2008	24.0	12.5	18.25	52.4	3.6	4.8	187.23	2.9	4.59	4.21
6/16/2008	21.0	12.8	16.90	65.6	3.2	3.7	168.57	1.7	3.51	3.42
6/17/2008	22.0	12.0	17.00	70	3.2	3.0	156.69	1.7	3.25	3.79
6/18/2008	22.2	11.5	16.85	69.4	3.6	3.0	156.66	1.2	3.34	3.90
6/19/2008	21.0	12.3	16.65	67.4	3	1.1	124.51	1.7	2.98	3.50
6/20/2008	20.5	12.0	16.25	78.6	3.2	2.8	153.23	1.5	2.78	3.42
6/21/2008	21.8	11.5	16.65	71.4	3	6.4	214.08	4.3	3.67	3.81
6/22/2008	22.5	10.8	16.65	66	1.6	6.1	209.00	0.7	3.56	4.06
6/23/2008	19.6	11.0	15.29	59	4.8	10.0	274.92	0.0	4.75	3.34
6/24/2008	24.8	11.0	17.90	56.6	2.8	8.0	241.12	0.0	4.64	4.57
6/25/2008	23.5	11.5	17.50	63.4	4.4	5.8	203.94	0.5	4.30	4.21
6/26/2008	23.5	11.5	17.50	64.6	3.8	6.8	220.86	3.7	4.28	4.21
6/27/2008	24.0	11.4	17.70	56.4	4.2	10.5	283.47	0.0	5.34	4.34
6/28/2008	24.0	10.7	17.35	56.6	4.8	9.0	258.14	0.6	5.22	4.41
6/29/2008	26.5	12.0	19.25	50.2	4.6	8.6	251.43	0.0	5.84	4.86
6/30/2008	24.5	10.5	17.50	52.4	5.6	8.1	243.02	0.0	5.59	4.55
June	**26.5**	**10.2**	**16.70**	**64.31**	**3.69**	**172.1**	**6098.4**	**88.9**	**120.7**	**119.5**

Where,

Tmax = maximum daily temperature

Tmin = minimum daily temperature

Tmean = mean daily temperature

n = actual sunshine hours

U_2 = wind speed at 2m height

RH mean = mean daily relative humidity

R_S = instantaneous downward solar radiation

P = precipitation

ET_0 Pen-Mon = Penman-Monteith reference evapotranspiration

ET_0 Harg. = Hargreaves reference evapotranspiration

Date	Tmax [^{0}C]	Tmin [^{0}C]	Tmean [^{0}C]	RH mean [%]	U_2 [m/s]	n [hr]	R_S [w/m^2]	P [mm]	ET_0 [mm/day]	
									Pen-Mon	Harg.
7/1/2008	25.7	11.9	18.80	54.4	2.6	8.3	246.47	21.1	4.82	4.68
7/2/2008	24.0	11.0	17.50	57.2	4.4	8.6	251.63	13.1	5.06	4.39
7/3/2008	23.0	11.5	17.25	64.4	3.2	7.6	234.77	8.6	4.26	4.10
7/4/2008	21.0	12.2	16.60	65.4	3	4.4	180.61	2.7	3.57	3.52
7/5/2008	21.5	11.5	16.50	62.6	4.4	4.7	185.77	23.1	4.02	3.74
7/6/2008	22.0	11.8	16.90	63.4	2.8	4.7	185.84	5.2	3.70	3.82
7/7/2008	21.5	12.2	16.85	75.4	3.6	4.5	182.53	23.8	3.29	3.65
7/8/2008	21.0	10.5	15.75	66.6	5.4	4.5	182.61	0.0	3.84	3.75
7/9/2008	23.5	11.2	17.35	61.8	3	3.0	157.20	0.0	3.63	4.26
7/10/2008	24.0	12.3	18.15	65.2	5	5.2	194.70	19.4	4.31	4.25
7/11/2008	20.0	11.0	15.50	74.8	4	2.7	152.25	1.6	2.95	3.45
7/12/2008	15.0	11.0	13.00	82.4	4.6	0.0	106.34	12.2	2.02	2.13
7/13/2008	21.0	9.3	15.15	71	3.2	4.5	183.10	2.1	3.30	3.90
7/14/2008	23.0	10.8	16.90	62.8	4.4	6.5	217.33	9.7	4.37	4.19
7/15/2008	21.5	11.0	16.25	69.4	4.2	7.3	231.13	0.0	4.00	3.82
7/16/2008	21.6	12.2	16.90	70.2	2.8	5.5	200.52	0.6	3.58	3.69
7/17/2008	21.6	13.0	17.30	72.6	4	2.5	149.35	4.6	3.21	3.57
7/18/2008	21.0	10.5	15.75	68.8	3.4	2.0	140.89	0.3	3.09	3.77
7/19/2008	21.0	11.8	16.40	77.6	4.4	2.5	149.54	19.7	2.91	3.60
7/20/2008	20.2	10.5	15.35	79.2	3.8	6.3	214.81	8.5	3.27	3.58
7/21/2008	19.0	10.6	14.80	75.4	3.8	3.2	161.75	5.6	2.92	3.28
7/22/2008	20.0	9.7	14.85	76.6	3.4	3.7	170.46	2.6	2.94	3.64
7/23/2008	21.0	12.0	16.50	75.2	2.2	3.5	167.14	1.4	2.98	3.58
7/24/2008	20.5	11.0	15.75	68	3.6	4.1	177.59	4.1	3.47	3.60
7/25/2008	21.5	11.5	16.50	72.2	4.6	3.3	163.94	11.4	3.37	3.78
7/26/2008	19.8	11.0	15.40	77	4	3.1	160.61	7.7	2.91	3.43
7/27/2008	22.0	11.5	16.75	79.4	2.2	3.6	169.36	17.4	2.91	3.90
7/28/2008	20.5	11.9	16.20	77	3.4	2.6	152.20	14.2	2.86	3.48
7/29/2008	21.0	11.5	16.25	75.4	3.6	4.3	181.72	17.5	3.23	3.66
7/30/2008	18.0	10.0	14.00	86.4	3.2	0.8	121.23	18.7	2.02	3.14
7/31/2008	18.2	11.3	14.75	78	3	5.6	204.54	0.0	3.13	2.99
July	**25.7**	**9.3**	**16.19**	**71.15**	**3.65**	**133.1**	**5577.9**	**276.9**	**105.9**	**114.3**

Where,

Tmax = maximum daily temperature

Tmin = minimum daily temperature

Tmean = mean daily temperature

n = actual sunshine hours

U_2 = wind speed at 2m height

RH mean = mean daily relative humidity

R_S = instantaneous downward solar radiation

P = precipitation

ET_0 Pen-Mon = Penman-Monteith reference evapotranspiration

ET_0 Harg. = Hargreaves reference evapotranspiration

Date	Tmax [^{0}C]	Tmin [^{0}C]	Tmean [^{0}C]	RH mean [%]	U_2 [m/s]	n [hr]	R_S [w/m^2]	P [mm]	ET_0 [mm/day]	
									Pen-Mon	Harg.
8/1/2008	22.0	10.5	16.25	73.8	3.2	5.6	204.71	0.0	3.50	4.04
8/2/2008	20.5	11.4	15.95	74	2.8	4.6	187.49	8.3	3.24	3.56
8/3/2008	21.8	11.3	16.55	75.8	3.6	5.4	201.55	30.2	3.44	3.90
8/4/2008	20.2	11.3	15.75	75	3.4	4.7	189.52	7.4	3.25	3.50
8/5/2008	18.7	11.0	14.85	85	1.6	3.7	172.23	9.8	2.63	3.17
8/6/2008	20.5	11.4	15.95	77	3.4	0.0	107.78	1.0	2.45	3.57
8/7/2008	19.0	11.5	15.25	81.8	2	1.7	137.53	5.3	2.38	3.17
8/8/2008	21.5	10.5	16.00	78.6	3.4	0.6	118.38	17.0	2.49	3.93
8/9/2008	18.0	11.8	14.90	78	4	2.7	155.20	7.0	2.76	2.86
8/10/2008	17.5	11.0	14.25	84.6	3	2.0	143.03	4.0	2.30	2.87
8/11/2008	20.2	10.5	15.35	74	2.2	0.0	108.03	24.7	2.36	3.63
8/12/2008	19.5	10.5	15.00	76	4	1.9	141.43	5.5	2.77	3.46
8/13/2008	20.0	12.0	16.00	83	3.4	2.7	155.56	26.2	2.62	3.36
8/14/2008	22.2	11.0	16.60	81.2	3	7.2	234.80	3.9	3.53	4.05
8/15/2008	22.5	11.7	17.10	71	3.2	5.1	197.98	24.5	3.64	4.03
8/16/2008	21.0	11.0	16.00	73.6	3.6	2.0	143.46	14.7	2.96	3.76
8/17/2008	20.5	10.0	15.25	72.8	3.8	6.4	221.13	2.6	3.62	3.77
8/18/2008	22.4	10.2	16.30	70.4	4.6	6.2	217.72	12.4	3.94	4.19
8/19/2008	20.0	11.0	15.50	75	3.4	2.6	154.23	13.9	2.92	3.52
8/20/2008	21.7	10.5	16.10	69.8	4.2	9.2	270.99	0.4	4.33	4.00
8/21/2008	22.0	12.2	17.10	73.6	3.6	8.6	260.51	6.4	4.14	3.85
8/22/2008	22.5	12.6	17.55	73.2	2.4	4.2	182.72	4.5	3.33	3.92
8/23/2008	22.5	11.0	16.75	70.6	3.8	5.7	209.36	5.9	3.81	4.13
8/24/2008	22.0	14.3	18.15	67.6	3.4	3.7	173.97	12.7	3.66	3.51
8/25/2008	21.5	11.5	16.50	81.6	5.4	4.7	191.76	46.2	3.11	3.82
8/26/2008	19.5	10.0	14.75	80.6	3.2	3.8	175.82	6.5	2.81	3.54
8/27/2008	19.5	10.8	15.15	78	3.6	3.5	170.52	6.2	2.91	3.42
8/28/2008	22.0	11.0	16.50	71.2	4.2	7.2	236.32	29.2	4.02	4.01
8/29/2008	20.8	11.5	16.15	79.4	2.2	4.0	179.45	7.2	2.96	3.65
8/30/2008	21.0	10.3	15.65	68	3.8	6.4	222.17	17.4	3.89	3.85
8/31/2008	21.0	12.0	16.50	76.6	3.2	4.0	179.47	12.6	3.16	3.62
August	**22.5**	**10.0**	**15.99**	**75.83**	**3.37**	**130.1**	**5644.8**	**373.6**	**98.9**	**113.7**

Where,

Tmax = maximum daily temperature

Tmin = minimum daily temperature

Tmean = mean daily temperature

n = actual sunshine hours

U_2 = wind speed at 2m height

RH mean = mean daily relative humidity

R_S = instantaneous downward solar radiation

P = precipitation

ET_0 Pen-Mon = Penman-Monteith reference evapotranspiration

ET_0 Harg. = Hargreaves reference evapotranspiration

Date	Tmax [^{0}C]	Tmin [^{0}C]	Tmean [^{0}C]	RH mean [%]	U_2 [m/s]	n [hr]	R_S [w/m^2]	P [mm]	ET_0 [mm/day]	
									Pen-Mon	Harg.
9/1/2008	23.0	11.0	17.00	67.2	3.6	7.9	248.92	9.9	4.337	4.24
9/2/2008	22.5	12.0	17.25	69.2	2.8	7.8	247.15	9.4	4.142	4.00
9/3/2008	23.0	12.5	17.75	75.8	4.8	4.4	186.57	2.0	3.530	4.05
9/4/2008	23.0	10.6	16.80	68.8	4.2	8.3	256.06	5.5	4.375	4.28
9/5/2008	23.4	12.0	17.70	70.4	4.8	4.2	182.94	3.6	3.823	4.21
9/6/2008	20.0	10.5	15.25	69.6	2.6	4.2	182.90	19.6	3.261	3.58
9/7/2008	19.0	11.0	15.00	77.2	2.8	3.4	168.58	3.3	2.856	3.26
9/8/2008	21.0	10.9	15.95	78	3	2.6	154.25	3.4	2.804	3.76
9/9/2008	19.5	12.5	16.00	73.4	2.8	2.2	147.05	2.0	2.867	3.14
9/10/2008	22.5	10.2	16.35	58.8	3.8	8.5	259.34	0.0	4.743	4.20
9/11/2008	22.0	12.0	17.00	69.2	2.4	5.2	200.39	33.8	3.583	3.85
9/12/2008	20.0	11.0	15.50	82.6	3.8	1.8	139.66	4.6	2.471	3.49
9/13/2008	21.2	11.5	16.35	77.8	3.4	6.0	214.46	37.1	3.429	3.72
9/14/2008	21.0	10.5	15.75	71.6	3.2	5.6	207.21	39.1	3.544	3.80
9/15/2008	22.0	11.0	16.50	68.6	1.8	3.0	160.74	3.4	3.044	3.97
9/16/2008	23.0	10.7	16.85	65.2	3.4	6.0	214.07	0.8	4.052	4.23
9/17/2008	21.7	11.0	16.35	69.2	5.4	8.5	258.45	6.5	4.365	3.89
9/18/2008	20.0	12.8	16.40	79	3	1.6	135.41	16.8	2.593	3.19
9/19/2008	23.2	11.0	17.10	65.4	5.4	9.9	283.00	0.0	4.936	4.23
9/20/2008	23.0	12.0	17.50	58.2	6.6	10.6	295.23	0.0	5.674	4.06
9/21/2008	23.2	12.0	17.60	63.2	4.6	8.4	255.88	0.0	4.788	4.10
9/22/2008	23.0	12.5	17.75	72.6	1.4	3.0	159.70	2.8	2.938	3.99
9/23/2008	20.7	12.0	16.35	73.2	2.6	3.8	173.73	3.2	3.133	3.48
9/24/2008	22.5	11.2	16.85	70.4	2.8	4.1	178.86	7.2	3.385	4.02
9/25/2008	18.6	12.0	15.30	75.6	3.8	0.7	118.36	37.7	2.567	2.93
9/26/2008	22.0	11.3	16.65	62.8	3.8	4.9	192.61	0.0	3.979	3.88
9/27/2008	23.5	10.5	17.00	56.4	6.2	10.6	293.28	0.0	5.678	4.31
9/28/2008	24.5	10.5	17.50	50.8	7.4	10.8	296.48	0.0	6.453	4.53
9/29/2008	24.5	10.0	17.25	48.4	5.2	10.6	292.59	0.0	6.066	4.57
9/30/2008	23.5	10.0	16.75	61.6	4	5.9	209.26	5.0	4.288	4.34
September	**24.5**	**10.0**	**16.65**	**68.34**	**3.85**	**174.5**	**6313.1**	**256.7**	**117.7**	**117.3**

Where,

Tmax = maximum daily temperature

Tmin = minimum daily temperature

Tmean = mean daily temperature

n = actual sunshine hours

U_2 = wind speed at 2m height

RH mean = mean daily relative humidity

R_S = instantaneous downward solar radiation

P = precipitation

ET_0 Pen-Mon = Penman-Monteith reference evapotranspiration

ET_0 Harg. = Hargreaves reference evapotranspiration

Date	Tmax [^{0}C]	Tmin [^{0}C]	Tmean [^{0}C]	RH mean [%]	U_2 [m/s]	n [hr]	R_S [w/m^2]	P [mm]	ET_0 [mm/day]	
									Pen-Mon	Harg.
10/1/2008	20.5	10.5	15.50	55	4.4	4.2	179.00	0.0	4.21	3.59
10/2/2008	22.5	10.5	16.50	40	6.2	10.8	295.00	0.0	6.58	4.05
10/3/2008	23.5	12.0	17.75	40.6	4.6	9.1	264.68	0.0	6.06	4.10
10/4/2008	20.5	12.5	16.50	46	7.2	0.7	116.66	0.0	5.16	3.29
10/5/2008	23.2	8.8	16.00	34.2	7.6	10.7	292.00	0.0	7.33	4.34
10/6/2008	24.5	10.0	17.25	40	6.2	10.8	293.32	0.0	6.86	4.51
10/7/2008	23.5	9.8	16.65	42.8	7	10.2	282.36	0.0	6.62	4.30
10/8/2008	23.6	11.0	17.30	47.8	4.6	6.8	222.46	0.0	5.31	4.19
10/9/2008	23.0	10.2	16.60	53.2	6.6	10.0	277.97	0.0	5.73	4.14
10/10/2008	22.7	12.3	17.50	59.4	6.2	5.5	199.03	0.0	4.77	3.82
10/11/2008	23.5	9.5	16.50	50.6	6.2	9.0	259.62	0.0	5.73	4.29
10/12/2008	23.0	10.5	16.75	46.6	5.2	9.8	273.08	0.0	5.81	4.08
10/13/2008	23.5	9.0	16.25	38	6.6	10.7	288.22	0.0	6.82	4.32
10/14/2008	22.5	12.0	17.25	46.8	6.8	5.5	197.56	0.0	5.72	3.78
10/15/2008	23.0	9.5	16.25	44.4	6.2	10.7	287.19	0.0	6.23	4.15
10/16/2008	23.5	9.5	16.50	44.4	4.6	10.8	288.39	0.0	5.86	4.25
10/17/2008	23.0	9.0	16.00	41.8	5.6	10.8	287.85	0.0	6.19	4.18
10/18/2008	23.5	10.5	17.00	36	5.2	10.5	282.14	0.0	6.51	4.13
10/19/2008	22.5	10.0	16.25	40	4.4	7.9	236.89	0.0	5.53	3.96
10/20/2008	22.5	9.5	16.00	44.2	3.2	7.5	229.55	0.0	4.80	4.00
10/21/2008	22.5	9.8	16.15	45	2.6	8.4	244.51	0.0	4.65	3.96
10/22/2008	23.0	12.0	17.50	53.6	3.6	8.8	250.85	0.0	4.88	3.82
10/23/2008	24.0	11.0	17.50	54.4	3.8	10.5	279.37	0.0	5.19	4.14
10/24/2008	22.5	10.5	16.50	44.6	4	10.4	277.10	0.0	5.47	3.86
10/25/2008	24.5	10.5	17.50	46.6	4	9.5	261.23	0.0	5.49	4.28
10/26/2008	21.5	11.0	16.25	71	3.2	3.1	152.00	33.4	3.05	3.56
10/27/2008	22.5	10.0	16.25	71.2	5.6	4.9	182.17	0.0	3.63	3.88
10/28/2008	23.0	12.5	17.75	61.8	4.4	9.0	251.15	1.5	4.69	3.70
10/29/2008	21.5	11.0	16.25	72.8	2	2.4	139.15	53.3	2.66	3.54
10/30/2008	22.0	9.0	15.50	72.8	3.8	5.2	186.03	0.0	3.30	3.84
10/31/2008	20.5	11.5	16.00	73.4	3.4	1.6	125.06	0.0	2.70	3.24
October	**24.5**	**8.8**	**16.63**	**50.29**	**5.00**	**245.8**	**7401.6**	**88.2**	**163.6**	**123.3**

Where,

Tmax = maximum daily temperature

Tmin = minimum daily temperature

Tmean = mean daily temperature

n = actual sunshine hours

U_2 = wind speed at 2m height

RH mean = mean daily relative humidity

R_S = instantaneous downward solar radiation

P = precipitation

ET_0 Pen-Mon = Penman-Monteith reference evapotranspiration

ET_0 Harg. = Hargreaves reference evapotranspiration

Date	Tmax [^{0}C]	Tmin [^{0}C]	Tmean [^{0}C]	RH mean [%]	U_2 [m/s]	n [hr]	R_S [w/m^2]	P [mm]	ET_0 [mm/day]	
									Pen-Mon	Harg.
11/1/2008	21.0	11.5	16.25	71.8	4	5.3	186.90	1.5	3.40	3.34
11/2/2008	23.5	11.5	17.50	73.4	3.8	4.7	176.44	14.6	3.37	3.88
11/3/2008	20.5	11.5	16.00	74	3.4	2.5	139.24	32.3	2.79	3.21
11/4/2008	18.5	12.0	15.25	77	1.6	3.0	147.28	27.9	2.47	2.66
11/5/2008	20.7	13.0	16.85	75.2	2.2	3.0	146.95	2.5	2.71	3.03
11/6/2008	21.0	11.3	16.15	71.4	4	5.0	179.89	0.0	3.34	3.33
11/7/2008	21.5	10.5	16.00	70.8	5.4	5.2	182.83	0.6	3.55	3.52
11/8/2008	20.7	10.5	15.60	63.6	6	5.4	185.76	0.0	4.01	3.34
11/9/2008	21.0	8.2	14.60	55.8	6	10.6	271.41	0.0	4.94	3.62
11/10/2008	20.5	7.0	13.75	52.4	5.4	11.0	277.47	0.0	4.94	3.61
11/11/2008	22.8	7.5	15.15	47.8	4.6	11.2	280.22	0.0	5.34	4.01
11/12/2008	22.5	8.0	15.25	49.4	4.6	10.9	274.74	0.0	5.20	3.90
11/13/2008	22.5	7.5	15.00	42.8	4.4	10.9	274.20	0.0	5.43	3.93
11/14/2008	22.7	8.8	15.75	48.6	4	8.8	239.24	0.0	4.88	3.86
11/15/2008	23.5	8.7	16.10	50	3.6	10.9	273.17	0.0	5.02	4.02
11/16/2008	22.5	8.0	15.25	49.2	4.8	11.0	274.30	0.0	5.24	3.87
11/17/2008	21.7	8.5	15.10	52.6	5.8	7.0	208.54	0.0	4.79	3.67
11/18/2008	21.5	7.5	14.50	53.2	5.6	10.7	268.43	0.0	5.01	3.70
11/19/2008	21.0	6.0	13.50	50	6.2	10.3	261.45	0.0	5.12	3.70
11/20/2008	20.8	6.0	13.40	41	7	10.8	269.12	0.0	5.84	3.66
11/21/2008	22.0	6.0	14.00	42.2	5.8	10.9	270.30	0.0	5.68	3.87
11/22/2008	23.0	7.0	15.00	47	4.6	10.2	258.52	0.0	5.20	3.99
11/23/2008	23.0	8.7	15.85	47.6	5.4	10.8	267.81	0.0	5.53	3.86
11/24/2008	22.5	8.5	15.50	52.2	5	10.7	265.79	0.0	5.08	3.77
11/25/2008	23.5	9.0	16.25	47.8	5.6	10.8	267.00	0.0	5.64	3.92
11/26/2008	23.5	8.5	16.00	54.4	5	10.8	266.62	0.0	5.09	3.95
11/27/2008	24.0	8.7	16.35	51.2	2.8	10.0	253.38	0.0	4.56	4.02
11/28/2008	23.0	9.0	16.00	48.8	4.6	9.2	240.20	0.0	5.06	3.80
11/29/2008	23.3	9.5	16.40	49.6	5	10.2	255.92	0.0	5.29	3.81
11/30/2008	22.5	8.7	15.60	52.8	6.6	10.7	263.62	0.0	5.36	3.72
November	**24.0**	**6.0**	**15.46**	**55.45**	**4.76**	**262.5**	**7126.7**	**79.4**	**139.9**	**110.6**

Where,

Tmax = maximum daily temperature

Tmin = minimum daily temperature

Tmean = mean daily temperature

n = actual sunshine hours

U_2 = wind speed at 2m height

RH mean = mean daily relative humidity

R_S = instantaneous downward solar radiation

P = precipitation

ET_0 Pen-Mon = Penman-Monteith reference evapotranspiration

ET_0 Harg. = Hargreaves reference evapotranspiration

Date	Tmax [^{0}C]	Tmin [^{0}C]	Tmean [^{0}C]	RH mean [%]	U_2 [m/s]	n [hr]	R_S [w/m^2]	P [mm]	ET_0 [mm/day]	
									Pen-Mon	Harg.
12/1/2008	22.5	9.0	15.75	50.6	5	10.7	263.31	0.0	5.16	3.69
12/2/2008	23.0	9.0	16.00	51.6	5	8.2	223.04	0.0	4.90	3.78
12/3/2008	22.5	10.5	16.50	53	4	7.2	206.83	0.0	4.45	3.55
12/4/2008	21.5	10.0	15.75	57.2	5.6	8.2	222.58	0.0	4.58	3.39
12/5/2008	21.7	9.5	15.60	56.2	7.2	10.7	262.23	0.0	5.15	3.48
12/6/2008	21.5	8.7	15.10	57.2	5.4	10.7	262.01	0.0	4.73	3.50
12/7/2008	22.5	8.0	15.25	57.8	4.6	9.8	247.47	22.5	4.53	3.74
12/8/2008	22.2	8.5	15.35	54.8	4.8	9.6	244.10	0.4	4.69	3.65
12/9/2008	22.5	8.8	15.65	57.8	4.4	9.5	242.35	0.0	4.49	3.68
12/10/2008	22.0	9.0	15.50	48.4	5.6	10.7	261.27	0.0	5.34	3.56
12/11/2008	22.7	6.5	14.60	43.8	4.4	10.8	262.72	0.0	5.22	3.87
12/12/2008	22.5	7.0	14.75	42.8	3	10.6	259.42	0.0	4.72	3.80
12/13/2008	22.5	7.5	15.00	41.4	4.8	10.7	260.90	0.0	5.48	3.76
12/14/2008	23.3	7.7	15.50	45	2	10.7	260.82	0.0	4.32	3.89
12/15/2008	22.5	8.0	15.25	41.8	5.6	10.5	257.58	0.0	5.71	3.73
12/16/2008	22.0	6.8	14.40	44.2	3	10.6	259.11	0.0	4.61	3.72
12/17/2008	23.5	6.5	15.00	43.4	4.2	10.8	262.26	0.0	5.28	4.00
12/18/2008	22.0	7.0	14.50	45.8	4.6	10.7	260.66	0.0	5.10	3.70
12/19/2008	21.5	7.0	14.25	50.8	5.6	10.4	255.91	0.0	4.99	3.61
12/20/2008	21.8	7.5	14.65	46.6	5.8	10.3	254.35	0.0	5.34	3.63
12/21/2008	22.5	6.8	14.65	49.4	3.4	10.0	249.63	0.0	4.55	3.81
12/22/2008	23.0	7.2	15.10	46.6	5	10.4	256.04	0.0	5.29	3.87
12/23/2008	24.0	8.0	16.00	37.4	4.6	10.8	262.47	0.0	5.85	4.00
12/24/2008	23.5	9.2	16.35	41.8	5.6	10.4	256.22	0.0	5.91	3.83
12/25/2008	22.5	7.0	14.75	43.6	4.8	9.9	248.39	0.0	5.27	3.80
12/26/2008	23.0	8.5	15.75	46.4	5.2	9.8	246.94	0.0	5.37	3.79
12/27/2008	22.5	7.0	14.75	45.4	5	10.6	259.80	0.0	5.30	3.80
12/28/2008	23.5	7.0	15.25	44.6	4.6	10.4	256.79	0.0	5.34	3.99
12/29/2008	24.8	9.5	17.15	50.8	4.8	10.6	260.17	0.0	5.38	4.06
12/30/2008	24.0	9.3	16.65	55.2	5.2	10.3	255.60	0.0	5.09	3.93
12/31/2008	22.5	9.0	15.75	51.6	6.6	10.4	257.41	0.0	5.41	3.67
December	**24.8**	**6.5**	**15.37**	**48.48**	**4.82**	**315.0**	**7838.4**	**22.9**	**157.6**	**116.3**

Where,

Tmax = maximum daily temperature

Tmin = minimum daily temperature

Tmean = mean daily temperature

n = actual sunshine hours

U_2 = wind speed at 2m height

RH mean = mean daily relative humidity

R_S = instantaneous downward solar radiation

P = precipitation

ET_0 Pen-Mon = Penman-Monteith reference evapotranspiration

ET_0 Harg. = Hargreaves reference evapotranspiration

A2: Nazareth Station (atitude: $8^0$35' N, longitude: $39^0$17' E, altitude: 1622m)

Date	Tmax [^{0}C]	Tmin [^{0}C]	Tmean [^{0}C]	RH mean [%]	U_2 [m/s]	n [hr]	R_S [w/m^2]	ET_0 [mm/day]	
								Pen-Mon	Harg.
1/1/2008	27.4	12	19.7	49.4	2.99	10.8	265.23	5.24	4.41
1/2/2008	26.7	12.8	19.75	43.6	2.99	11	268.68	5.45	4.20
1/3/2008	25.2	13	19.1	42.8	3.59	10	252.89	5.51	3.87
1/4/2008	25	10	17.5	41.2	1.94	10.9	267.62	4.64	4.11
1/5/2008	26	12.5	19.25	38.4	3.89	10.7	264.69	6.02	4.10
1/6/2008	26.2	13.2	19.7	37.8	4.49	10.9	268.22	6.45	4.08
1/7/2008	26.2	12.2	19.2	41.2	1.35	10.9	268.55	4.42	4.18
1/8/2008	26.2	14	20.1	58.6	3.89	10.3	259.21	5.09	4.00
1/9/2008	25.2	14.4	19.8	59.6	3.29	8.8	235.32	4.58	3.74
1/10/2008	25.7	14.2	19.95	54.4	1.94	10.6	264.77	4.55	3.88
1/11/2008	27.5	14.5	21	51.2	2.39	10	255.44	4.94	4.25
1/12/2008	26	14.6	20.3	59.6	4.34	9.6	249.33	5.10	3.91
1/13/2008	26.5	16	21.25	54.8	2.99	10.2	259.46	5.09	3.86
1/14/2008	26	16	21	57.8	2.54	9.8	253.37	4.72	3.75
1/15/2008	25.3	16.4	20.85	63.8	4.19	4.7	170.69	4.19	3.53
1/16/2008	24.1	16.5	20.3	69	4.79	9	241.16	4.50	3.22
1/17/2008	25	15.5	20.25	70.8	2.54	8.7	236.68	4.03	3.60
1/18/2008	29.5	15.2	22.35	79.2	4.19	5	176.53	3.59	4.67
1/19/2008	28.5	15.5	22	78.6	2.09	6.1	194.90	3.49	4.43
1/20/2008	26	14.4	20.2	70.4	4.49	8.6	236.34	4.41	4.00
1/21/2008	24.1	12	18.05	56	3.29	11.1	277.92	4.90	3.86
1/22/2008	24.6	9.5	17.05	47.2	1.65	11	276.81	4.44	4.20
1/23/2008	24.8	11	17.9	49.6	4.19	10.7	272.39	5.48	4.13
1/24/2008	28	14.6	21.3	48.8	4.19	9.3	249.77	5.93	4.46
1/25/2008	25.2	14	19.6	41.6	1.80	10.9	276.79	4.86	3.91
1/26/2008	24	12	18	39.4	1.05	10.7	274.03	4.19	3.89
1/27/2008	21.8	14.8	18.3	42.4	3.59	10	262.94	5.40	3.00
1/28/2008	23.5	15	19.25	52.6	4.79	10.4	270.16	5.58	3.40
1/29/2008	25.5	15	20.25	52.8	3.59	10.4	270.72	5.41	3.89
1/30/2008	25.4	15.7	20.55	53.8	3.14	10.6	274.64	5.27	3.78
1/31/2008	27.5	15	21.25	56.6	2.09	xxx	xxx	xxx	4.38
January	**29.5**	**9.5**	**19.84**	**53.65**	**3.17**	**291.7**	**7595.3**	**147.5**	**123**

Where,

Tmax = maximum daily temperature

Tmin = minimum daily temperature

Tmean = mean daily temperature

n = actual sunshine hours

U_2 = wind speed at 2m height

RH mean = mean daily relative humidity

R_S = instantaneous downward solar radiation

xxx = missed data/no output

ET_0 Pen-Mon = Penman-Monteith ref. evapotranspiration

$ET_{0\ Harg.}$ = Hargreaves reference evapotranspiration

Date	Tmax [^{0}C]	Tmin [^{0}C]	Tmean [^{0}C]	RH mean [%]	U_2 [m/s]	n [hr]	R_S [w/m^2]	ET_0 [mm/day]	
								Pen-Mon	Harg.
2/1/2008	25.8	15.6	20.7	67.2	5.68	10.7	277.49	5.21	3.91
2/2/2008	25.4	15.6	20.5	66.8	4.19	10.5	274.72	4.94	3.82
2/3/2008	26	15	20.5	61.6	2.54	10.2	270.25	4.78	4.06
2/4/2008	25.5	14.5	20	54	1.68	10.3	272.53	4.62	4.01
2/5/2008	26.7	12.9	19.8	57.4	3.74	8.9	249.42	5.12	4.48
2/6/2008	29.4	13.8	21.6	50.6	1.87	8.2	238.09	4.75	5.01
2/7/2008	27.8	15.6	21.7	53.4	2.80	7.1	219.91	4.90	4.45
2/8/2008	25.5	14	19.75	48	5.24	9.4	259.57	6.15	4.12
2/9/2008	26.5	13.5	20	49.8	3.29	10.3	275.50	5.55	4.42
2/10/2008	28.9	12.5	20.7	42.4	4.79	10.7	282.93	6.94	5.07
2/11/2008	30	12.4	21.2	33.6	4.49	9.3	259.56	7.34	5.33
2/12/2008	27.7	10.8	19.25	36.6	3.37	10.7	284.15	6.28	4.98
2/13/2008	28	10.5	19.25	30.8	4.30	10.8	286.47	7.17	5.08
2/14/2008	27.7	11.7	19.7	40	3.37	10.9	288.80	6.21	4.93
2/15/2008	28.8	11.2	20	37.8	3.74	10.9	289.40	6.67	5.22
2/16/2008	27.7	14.5	21.1	41.6	2.69	10.8	288.27	5.89	4.66
2/17/2008	26.7	13.6	20.15	48	3.59	10.8	288.86	5.93	4.54
2/18/2008	25.3	15	20.15	49.6	3.89	10.3	280.77	5.82	4.04
2/19/2008	26.4	14	20.2	63.8	5.39	7.4	230.91	5.05	4.45
2/20/2008	27.8	16.5	22.15	65.6	6.36	8.9	257.51	5.63	4.47
2/21/2008	30	16	23	58.8	4.94	10.8	291.18	6.38	5.10
2/22/2008	29.4	13	21.2	44.8	4.79	9.5	269.02	6.83	5.29
2/23/2008	30.2	11	20.6	44.6	5.98	9.8	274.79	7.45	5.65
2/24/2008	29.5	12.5	21	33.6	2.69	10.1	280.57	6.27	5.38
2/25/2008	29.5	14	21.75	34.2	1.94	10	279.33	5.69	5.25
2/26/2008	29.5	14.4	21.95	39.4	2.24	9.6	272.80	5.76	5.22
2/27/2008	30.5	14	22.25	44.4	5.09	9.8	276.81	7.30	5.51
2/28/2008	31	15	23	46.6	4.94	8.7	257.89	7.05	5.54
2/29/2008	xxx	15.2	xxx	31.6	4.94	10.1	283.07	xxx	5.58
February	**31.0**	**10.5**	**20.83**	**47.47**	**3.95**	**285.5**	**7860.6**	**167.7**	**140**

Where,

Tmax = maximum daily temperature

Tmin = minimum daily temperature

Tmean = mean daily temperature

n = actual sunshine hours

U_2 = wind speed at 2m height

RH mean = mean daily relative humidity

R_S = instantaneous downward solar radiation

xxx = missed data/no output

ET_0 Pen-Mon = Penman-Monteith ref. evapotranspiration

$ET_{0\ Harg.}$ = Hargreaves reference evapotranspiration

Date	Tmax [^{0}C]	Tmin [^{0}C]	Tmean [^{0}C]	RH mean [%]	U_2 [m/s]	n [hr]	R_S [w/m^2]	ET_0 [mm/day]	
								Pen-Mon	Harg.
3/1/2008	30.5	12	21.25	25.6	2.69	10.8	295.93	6.81	5.72
3/2/2008	28.9	12.5	20.7	30.6	2.69	9.7	276.92	6.30	5.32
3/3/2008	29	10.5	19.75	28.8	2.09	10.8	296.88	5.98	5.53
3/4/2008	29.7	10.5	20.1	24.8	1.94	10.9	299.11	6.03	5.69
3/5/2008	30.2	15	22.6	21.2	2.69	10.9	299.56	7.03	5.41
3/6/2008	29.5	16	22.75	35.8	2.99	10.3	289.30	6.66	5.13
3/7/2008	28.5	15	21.75	40.2	4.49	9.6	277.22	7.05	5.01
3/8/2008	29	15.6	22.3	57.6	3.59	10.4	291.89	5.95	5.07
3/9/2008	30.5	14.5	22.5	35.8	4.34	9.5	276.18	7.52	5.58
3/10/2008	30.7	14	22.35	28.6	3.89	10.5	294.43	7.78	5.68
3/11/2008	29	13.6	21.3	29	3.89	10.4	292.99	7.46	5.32
3/12/2008	28.6	11.5	20.05	31.2	2.09	10.6	296.92	5.94	5.44
3/13/2008	28.3	10.6	19.45	30	1.94	10.4	293.66	5.76	5.46
3/14/2008	29.6	12.5	21.05	27.8	0.60	10.5	295.77	4.62	5.60
3/15/2008	30.5	14	22.25	32.8	1.50	10.5	296.06	5.65	5.68
3/16/2008	30.5	15	22.75	30.2	2.69	9.4	276.57	6.64	5.58
3/17/2008	30.5	14.9	22.7	34.8	2.69	10.6	298.42	6.68	5.60
3/18/2008	30.7	13.2	21.95	32.2	1.31	10.5	296.87	5.49	5.83
3/19/2008	30.6	12	21.3	27.4	2.43	10.7	300.71	6.64	5.92
3/20/2008	30.3	13	21.65	30.2	2.39	11	306.34	6.57	5.77
3/21/2008	32	14.5	23.25	30.4	1.50	0	108.21	4.00	6.04
3/22/2008	32.8	17	24.9	28	3.29	10.8	303.14	7.87	5.98
3/23/2008	32.9	13.2	23.05	20.6	3.59	11	306.93	8.41	6.39
3/24/2008	32.9	16	24.45	21.8	2.39	10.7	301.67	7.17	6.13
3/25/2008	31	13	22	24.8	1.05	10.9	305.43	5.37	5.96
3/26/2008	31.2	16	23.6	21	2.69	10.8	303.76	7.31	5.70
3/27/2008	31.7	13.5	22.6	22.4	0.30	10.3	294.84	4.33	6.10
3/28/2008	30.9	13	21.95	29.6	2.24	9.9	287.71	6.38	5.95
3/29/2008	31	16.2	23.6	35.6	2.09	10.5	298.63	6.31	5.64
3/30/2008	27.6	16	21.8	36.2	2.24	9.3	277.02	5.85	4.78
3/31/2008	28.6	19	23.8	41.4	1.94	xxx	xxx	xxx	4.57
March	**32.9**	**10.5**	**22.11**	**30.53**	**2.46**	**302.2**	**8639.1**	**191.6**	**174**

Where,

Tmax = maximum daily temperature

Tmin = minimum daily temperature

Tmean = mean daily temperature

n = actual sunshine hours

U_2 = wind speed at 2m height

RH mean = mean daily relative humidity

R_S = instantaneous downward solar radiation

xxx = missed data/no output

ET_0 Pen-Mon = Penman-Monteith ref. evapotranspiration

$ET_{0\ Harg.}$ = Hargreaves reference evapotranspiration

Date	Tmax [^{0}C]	Tmin [^{0}C]	Tmean [^{0}C]	RH mean [%]	U_2 [m/s]	n [hr]	R_S [w/m^2]	ET_0 [mm/day]	
								Pen-Mon	Harg.
4/1/2008	26	17.2	21.6	44.2	2.39	xxx	xxx	xxx	4.15
4/2/2008	30	19	24.5	46.2	3.44	xxx	xxx	xxx	4.98
4/3/2008	29.9	18	23.95	50.2	2.69	xxx	xxx	xxx	5.12
4/4/2008	29	16.2	22.6	41.4	3.29	xxx	xxx	xxx	5.14
4/5/2008	26.3	18	22.15	47	2.09	xxx	xxx	xxx	4.09
4/6/2008	25.7	17.5	21.6	34.2	2.99	xxx	xxx	xxx	4.01
4/7/2008	26.6	18	22.3	37	2.99	xxx	xxx	xxx	4.18
4/8/2008	28.8	19	23.9	40.8	1.50	xxx	xxx	xxx	4.64
4/9/2008	30	17	23.5	55.8	1.50	xxx	xxx	xxx	5.30
4/10/2008	30.4	14	22.2	74.4	2.24	xxx	xxx	xxx	5.76
4/11/2008	28.9	14.5	21.7	72.6	1.94	xxx	xxx	xxx	5.33
4/12/2008	29	15.7	22.35	71.8	4.64	xxx	xxx	xxx	5.21
4/13/2008	29	15.2	22.1	61.6	3.29	xxx	xxx	xxx	5.27
4/14/2008	30.9	13.8	22.35	45.6	3.29	xxx	xxx	xxx	5.91
4/15/2008	31.5	12.5	22	27.6	2.84	xxx	xxx	xxx	6.17
4/16/2008	33	17	25	34.2	4.79	xxx	xxx	xxx	6.09
4/17/2008	31	17.2	24.1	36.6	3.14	xxx	xxx	xxx	5.54
4/18/2008	30	13.7	21.85	33	3.29	xxx	xxx	xxx	5.69
4/19/2008	31	17.8	24.4	28.2	3.89	xxx	xxx	xxx	5.45
4/20/2008	30.8	17.5	24.15	34.8	3.89	xxx	xxx	xxx	5.44
4/21/2008	31	17	24	36.2	3.89	xxx	xxx	xxx	5.56
4/22/2008	31.4	18.4	24.9	43.6	2.99	xxx	xxx	xxx	5.47
4/23/2008	30.8	19	24.9	42	2.69	xxx	xxx	xxx	5.21
4/24/2008	30.4	19	24.7	39.6	4.19	xxx	xxx	xxx	5.09
4/25/2008	30	17.5	23.75	48.2	4.49	xxx	xxx	xxx	5.21
4/26/2008	28.4	18.5	23.45	38.2	2.69	xxx	xxx	xxx	4.60
4/27/2008	30.5	16	23.25	41.2	2.69	xxx	xxx	xxx	5.54
4/28/2008	31.4	17	24.2	36.5	4.04	xxx	xxx	xxx	5.64
4/29/2008	31.3	16	23.65	37.8	3.89	xxx	xxx	xxx	5.74
4/30/2008	31.8	15.5	23.65	37.75	3.29	xxx	xxx	xxx	5.92
April	**33.0**	**12.5**	**23.29**	**43.94**	**3.17**	**0.0**	**0.0**	**0.0**	**157**

Where,

Tmax = maximum daily temperature

Tmin = minimum daily temperature

Tmean = mean daily temperature

n = actual sunshine hours

U_2 = wind speed at 2m height

RH mean = mean daily relative humidity

R_S = instantaneous downward solar radiation

xxx = missed data/no output

ET_0 Pen-Mon = Penman-Monteith ref. evapotranspiration

$ET_{0\ Harg.}$ = Hargreaves reference evapotranspiration

Date	Tmax [^{0}C]	Tmin [^{0}C]	Tmean [^{0}C]	RH mean [%]	U_2 [m/s]	n [hr]	R_S [w/m^2]	ET_0 [mm/day]	
								Pen-Mon	Harg.
5/1/2008	31.6	18	24.8	58.4	3.89	8.1	251.69	6.05	5.55
5/2/2008	31.2	19	25.1	52.8	1.50	6.7	226.77	4.80	5.29
5/3/2008	30	16.5	23.25	57.8	0.90	8	249.44	4.49	5.32
5/4/2008	30.5	19.5	25	71.8	3.29	1.7	138.38	3.76	5.01
5/5/2008	30.2	18	24.1	68.6	2.69	6.6	224.35	4.69	5.16
5/6/2008	31	18	24.5	62.4	2.99	8.1	250.45	5.43	5.37
5/7/2008	30.6	14.6	22.6	77.4	1.20	6.1	215.15	3.87	5.69
5/8/2008	31.7	17.5	24.6	55.4	2.54	9.3	270.94	5.81	5.62
5/9/2008	31.5	16	23.75	51.6	2.09	10	282.89	5.75	5.75
5/10/2008	31.4	16.5	23.95	41.2	2.09	10.4	289.58	6.11	5.66
5/11/2008	31	18.6	24.8	57.6	2.69	8.6	257.88	5.62	5.26
5/12/2008	31	19.5	25.25	52	1.80	11.1	301.15	5.88	5.12
5/13/2008	31.5	16	23.75	54.6	2.69	6.7	224.29	5.32	5.73
5/14/2008	31.2	17	24.1	49.6	2.99	7.2	232.74	5.79	5.53
5/15/2008	29.5	14	21.75	51	2.99	11.1	300.18	6.10	5.45
5/16/2008	28	16.5	22.25	48.2	2.99	9.9	279.06	5.96	4.75
5/17/2008	30.7	15.5	23.1	44.2	2.69	11.2	301.27	6.42	5.57
5/18/2008	28.2	18	23.1	43.8	2.69	11	297.50	6.23	4.56
5/19/2008	28.5	18	23.25	40.2	1.50	10.1	281.64	5.38	4.64
5/20/2008	31.2	18	24.6	47.6	0.90	9.1	264.11	4.84	5.37
5/21/2008	31	15.5	23.25	39	2.99	10.8	293.13	6.76	5.62
5/22/2008	31.5	18	24.75	36.6	4.79	8.2	248.10	7.84	5.44
5/23/2008	31.8	15.5	23.65	46.6	2.69	9.5	270.20	6.13	5.82
5/24/2008	31.4	19.5	25.45	53	2.99	6.4	216.72	5.57	5.18
5/25/2008	31.2	19.5	25.35	46.8	3.59	9.8	274.84	6.79	5.12
5/26/2008	31.8	19.5	25.65	44.8	3.29	10	278.01	6.82	5.28
5/27/2008	31.8	18	24.9	47	3.29	10.3	282.90	6.70	5.50
5/28/2008	32.2	18.6	25.4	44.8	5.83	10.8	291.20	8.31	5.52
5/29/2008	31.5	19	25.25	65.2	2.39	8.6	253.36	5.21	5.27
5/30/2008	31.6	15	23.3	73.2	1.80	4.2	178.05	3.69	5.79
5/31/2008	32.5	15	23.75	76.8	3.59	xxx	xxx	xxx	6.01
May	**32.5**	**14.0**	**24.14**	**53.55**	**2.72**	**259.6**	**7726.0**	**172.1**	**167**

Where,

Tmax = maximum daily temperature

Tmin = minimum daily temperature

Tmean = mean daily temperature

n = actual sunshine hours

U_2 = wind speed at 2m height

RH mean = mean daily relative humidity

R_S = instantaneous downward solar radiation

xxx = missed data/no output

ET_0 Pen-Mon = Penman-Monteith ref. evapotranspiration

$ET_{0\ Harg.}$ = Hargreaves reference evapotranspiration

Date	Tmax [^{0}C]	Tmin [^{0}C]	Tmean [^{0}C]	RH mean [%]	U_2 [m/s]	n [hr]	R_S [w/m^2]	ET_0 [mm/day]	
								Pen-Mon	Harg.
6/1/2008	33	16.4	24.7	67	2.39	6.4	215.27	4.70	5.98
6/2/2008	33.4	14.4	23.9	64.8	2.39	6.9	223.63	4.86	6.27
6/3/2008	32.6	17.4	25	64.4	5.09	7.4	231.98	5.89	5.76
6/4/2008	31.7	17.5	24.6	63.2	1.80	5.6	201.23	4.35	5.51
6/5/2008	32.6	15	23.8	61.2	2.09	6.6	218.08	4.75	6.01
6/6/2008	33	16	24.5	55.6	1.50	9.7	270.56	5.28	6.01
6/7/2008	33.1	18.6	25.85	52.8	4.04	8.5	250.05	6.61	5.72
6/8/2008	31.8	17.2	24.5	45.8	4.49	10.6	285.50	7.38	5.56
6/9/2008	32.5	18.8	25.65	55.8	3.74	8.6	251.47	6.24	5.53
6/10/2008	32.3	16.5	24.4	57.8	4.19	9	258.12	6.25	5.77
6/11/2008	32.5	17.4	24.95	56.2	4.49	7.9	239.39	6.35	5.71
6/12/2008	33	16.6	24.8	55.8	2.99	6	207.15	5.37	5.93
6/13/2008	34	17.6	25.8	46.4	3.59	10.4	281.46	7.14	6.06
6/14/2008	33.6	17.5	25.55	54.6	3.59	9.4	264.46	6.46	5.97
6/15/2008	31.5	17.8	24.65	50.2	2.69	11	291.41	6.26	5.39
6/16/2008	28.9	16.5	22.7	51.8	5.09	7.5	232.22	6.31	4.89
6/17/2008	30.4	15	22.7	75.4	2.69	0	105.52	2.89	5.45
6/18/2008	29.5	15.5	22.5	62	3.29	0	105.51	3.76	5.17
6/19/2008	31.1	16.5	23.8	66	3.74	0.2	108.87	3.86	5.45
6/20/2008	30.1	16.4	23.25	70	3.44	5.8	203.36	4.48	5.21
6/21/2008	30.6	15.3	22.95	60.2	5.39	8.7	252.28	6.13	5.46
6/22/2008	32.5	17.7	25.1	57.2	4.04	10.1	275.89	6.49	5.66
6/23/2008	32.3	18.5	25.4	51.4	4.04	10	274.20	6.83	5.50
6/24/2008	31.4	18	24.7	49.6	4.04	10.4	280.96	6.86	5.33
6/25/2008	31	18	24.5	54.2	5.09	9.6	267.48	6.82	5.23
6/26/2008	30.5	15.4	22.95	62	2.69	10	274.26	5.41	5.43
6/27/2008	31.3	14	22.65	63.8	3.89	9.7	269.23	5.67	5.77
6/28/2008	28.9	17	22.95	56.6	3.74	10.8	287.85	6.06	4.82
6/29/2008	28.9	16.8	22.85	51	3.74	10.9	289.61	6.36	4.85
6/30/2008	28	19.5	23.75	46	2.54	9.9	272.78	5.85	4.16
June	**34.0**	**14.0**	**24.18**	**57.63**	**3.55**	**237.6**	**7189.8**	**171.7**	**166**

Where,

Tmax = maximum daily temperature

Tmin = minimum daily temperature

Tmean = mean daily temperature

n = actual sunshine hours

U_2 = wind speed at 2m height

RH mean = mean daily relative humidity

R_S = instantaneous downward solar radiation

xxx = missed data/no output

ET_0 Pen-Mon = Penman-Monteith ref. evapotranspiration

$ET_{0\ Harg.}$ = Hargreaves reference evapotranspiration

Date	Tmax [^{0}C]	Tmin [^{0}C]	Tmean [^{0}C]	RH mean [%]	U_2 [m/s]	n [hr]	R_S [w/m^2]	ET_0 [mm/day]	
								Pen-Mon	Harg.
7/1/2008	23.4	18	20.7	45.2	5.53	11	291.45	6.77	3.07
7/2/2008	27.2	18.5	22.85	44.8	3.29	10.5	283.10	6.28	4.11
7/3/2008	26.8	16.8	21.8	57.6	2.54	10.22	278.46	5.28	4.30
7/4/2008	27	16.5	21.75	65.4	5.09	7.7	235.93	5.16	4.40
7/5/2008	29	14.2	21.6	62.6	2.54	10.4	281.74	5.22	5.21
7/6/2008	27.7	15.5	21.6	63.4	1.35	5.3	195.48	3.77	4.73
7/7/2008	24.2	14	19.1	75.4	4.49	7.9	239.64	4.09	4.05
7/8/2008	25.5	14.5	20	71.8	5.09	8.4	248.24	4.58	4.31
7/9/2008	27.3	15.7	21.5	69.6	2.69	7.6	234.80	4.42	4.60
7/10/2008	27.7	17	22.35	60.8	5.53	9.8	272.29	6.02	4.52
7/11/2008	25.5	14	19.75	76.2	5.24	6	207.88	3.93	4.38
7/12/2008	29.6	15.6	22.6	90.2	3.29	0	105.96	2.17	5.21
7/13/2008	28.2	14	21.1	65.6	1.35	9.2	262.60	4.49	5.05
7/14/2008	28.2	16	22.1	60.2	2.09	7.3	230.41	4.60	4.81
7/15/2008	27.3	15.4	21.35	72.4	4.64	9.8	273.19	4.96	4.66
7/16/2008	26.6	17	21.8	62	4.49	8.3	247.80	5.35	4.24
7/17/2008	26.5	16.8	21.65	60.4	5.68	8.12	244.91	5.70	4.24
7/18/2008	25	13.8	19.4	76.2	3.44	5.1	193.47	3.58	4.30
7/19/2008	24.5	14.3	19.4	75.4	3.89	8	243.23	4.12	4.11
7/20/2008	27.5	14.8	21.15	70.2	5.68	8.4	250.27	5.01	4.80
7/21/2008	26.5	17	21.75	68.6	4.94	6.6	219.62	4.75	4.22
7/22/2008	26.7	16.5	21.6	65.4	4.34	5.3	197.49	4.62	4.36
7/23/2008	27.4	15.7	21.55	74.6	3.74	6	209.67	4.11	4.67
7/24/2008	27	15.5	21.25	68.4	5.83	8.4	251.11	5.16	4.59
7/25/2008	25.8	14	19.9	79	3.59	7	227.23	3.85	4.49
7/26/2008	26.2	14	20.1	83.6	5.53	2	141.27	2.88	4.60
7/27/2008	26.9	14	20.45	64.8	3.29	6.9	225.89	4.58	4.77
7/28/2008	27.8	16.3	22.05	74	3.29	6.4	217.45	4.22	4.70
7/29/2008	26.9	15.8	21.35	75.2	4.64	6.1	212.45	4.19	4.54
7/30/2008	28	14.2	21.1	78.4	3.59	1.5	133.04	3.08	5.03
7/31/2008	28	14.3	21.15	69.2	4.34	xxx	xxx	xxx	5.02
July	**29.6**	**13.8**	**21.15**	**68.60**	**4.03**	**215.2**	**6856.0**	**137.0**	**140**

Where,

Tmax = maximum daily temperature

Tmin = minimum daily temperature

Tmean = mean daily temperature

n = actual sunshine hours

U_2 = wind speed at 2m height

RH mean = mean daily relative humidity

R_S = instantaneous downward solar radiation

xxx = missed data/no output

ET_0 Pen-Mon = Penman-Monteith ref. evapotranspiration

$ET_{0\ Harg.}$ = Hargreaves reference evapotranspiration

Date	Tmax [^{0}C]	Tmin [^{0}C]	Tmean [^{0}C]	RH mean [%]	U_2 [m/s]	n [hr]	R_S [w/m^2]	ET_0 [mm/day]	
								Pen-Mon	Harg.
8/1/2008	27.2	16.2	21.7	66.4	4.34	10.2	284.10	5.43	4.57
8/2/2008	25.3	16.8	21.05	69.2	3.44	7.8	242.69	4.57	3.95
8/3/2008	25.5	14.5	20	72.2	2.24	7.9	244.64	4.18	4.38
8/4/2008	26.7	16.7	21.7	72.2	5.09	5.9	210.06	4.45	4.36
8/5/2008	26.8	15.8	21.3	76.6	4.19	2.8	156.24	3.48	4.53
8/6/2008	26.3	14.8	20.55	73.8	3.74	1.8	138.92	3.34	4.55
8/7/2008	25	14.3	19.65	69.6	1.05	3.3	165.19	3.05	4.29
8/8/2008	26.4	15.7	21.05	82.6	4.34	3	160.07	3.13	4.45
8/9/2008	25	15.8	20.4	88.2	3.29	2.3	147.94	2.59	4.06
8/10/2008	24.5	14.7	19.6	81	1.80	0.5	116.52	2.38	4.10
8/11/2008	23.8	15.2	19.5	68.8	3.89	5.9	211.23	4.17	3.83
8/12/2008	28.2	16.4	22.3	74.4	4.49	4.8	192.09	4.16	4.83
8/13/2008	28.1	15	21.55	63	4.34	8.7	260.72	5.45	5.00
8/14/2008	27.5	16.3	21.9	61	4.34	9	266.19	5.63	4.66
8/15/2008	25.6	16.8	21.2	60.4	2.99	8.3	254.06	5.01	4.06
8/16/2008	27	13.8	20.4	75	2.54	5.9	211.97	3.86	4.87
8/17/2008	25.7	14.2	19.95	72.2	2.84	5.7	208.57	3.91	4.50
8/18/2008	23.8	16.5	20.15	68.2	2.54	10.1	286.35	4.78	3.60
8/19/2008	27.3	14.4	20.85	73.6	2.69	8.1	251.21	4.41	4.88
8/20/2008	24.2	14.5	19.35	68.8	2.39	8.7	261.96	4.41	4.07
8/21/2008	25	17.2	21.1	64	3.44	10	285.11	5.24	3.82
8/22/2008	26.2	18.5	22.35	60.8	4.64	10.4	292.36	5.95	3.92
8/23/2008	26.7	14	20.35	62	3.44	9.8	281.88	5.29	4.78
8/24/2008	27.5	14.5	21	78.4	4.49	4.7	191.59	3.76	4.92
8/25/2008	26.8	14	20.4	72.2	4.19	8.3	255.53	4.65	4.81
8/26/2008	25.5	14.2	19.85	72	3.14	4.4	186.39	3.73	4.45
8/27/2008	27	14	20.5	71.8	2.84	8.7	262.84	4.58	4.86
8/28/2008	27.6	16.9	22.25	66.4	3.74	9.2	271.82	5.29	4.61
8/29/2008	27	15.8	21.4	66.8	1.94	8	250.55	4.52	4.62
8/30/2008	26.8	14.5	20.65	64	2.24	9.7	280.87	4.94	4.74
8/31/2008	25.5	16.8	21.15	65.2	3.89	xxx	xxx	xxx	4.04
August	**28.2**	**13.8**	**20.81**	**70.35**	**3.37**	**203.9**	**6829.6**	**130.4**	**137**

Where,

Tmax = maximum daily temperature

Tmin = minimum daily temperature

Tmean = mean daily temperature

n = actual sunshine hours

U_2 = wind speed at 2m height

RH mean = mean daily relative humidity

R_S = instantaneous downward solar radiation

xxx = missed data/no output

ET_0 Pen-Mon = Penman-Monteith ref. evapotranspiration

$ET_{0\ Harg.}$ = Hargreaves reference evapotranspiration

Date	Tmax [^{0}C]	Tmin [^{0}C]	Tmean [^{0}C]	RH mean [%]	U_2 [m/s]	n [hr]	R_S [w/m^2]	ET_0 [mm/day]	
								Pen-Mon	Harg.
9/1/2008	28	16	22	65.6	3.14	8.6	261.39	5.08	4.85
9/2/2008	27.2	17	22.1	62.2	3.44	8.6	261.43	5.29	4.48
9/3/2008	26.5	16.5	21.5	67	2.84	0	108.13	3.22	4.37
9/4/2008	25.5	15.5	20.5	64.2	4.49	0	108.10	3.79	4.26
9/5/2008	27.2	17	22.1	64.4	1.94	0	108.05	3.03	4.48
9/6/2008	26.7	14.8	20.75	64.2	2.24	0	108.01	3.09	4.67
9/7/2008	27.2	16.5	21.85	76.6	3.89	0	107.96	2.99	4.55
9/8/2008	27.2	15	21.1	70.2	3.59	0	107.90	3.27	4.77
9/9/2008	27.7	16	21.85	70.8	2.24	0	107.84	2.90	4.75
9/10/2008	26.6	16.8	21.7	62.2	1.35	0	107.77	2.78	4.33
9/11/2008	28.8	17	22.9	71.4	0.75	0	107.70	2.40	4.89
9/12/2008	30	14.5	22.25	73	1.65	0	107.62	2.69	5.52
9/13/2008	30.4	15.5	22.95	60.8	1.35	0	107.54	2.93	5.50
9/14/2008	29.9	17.2	23.55	65	2.69	10.4	293.04	5.56	5.15
9/15/2008	29	14.4	21.7	64.4	1.05	4.9	194.78	3.67	5.27
9/16/2008	29	17	23	62.6	1.65	8.7	262.44	4.85	4.93
9/17/2008	28.5	17.5	23	61.6	2.39	8.7	262.29	5.12	4.71
9/18/2008	30.4	16.8	23.6	77.6	2.39	3.9	176.56	3.63	5.31
9/19/2008	30.5	16	23.25	60.2	2.84	8.7	261.95	5.45	5.43
9/20/2008	30.4	15.2	22.8	61.6	3.59	10.8	299.17	5.98	5.50
9/21/2008	30.2	18	24.1	56	1.05	9.4	274.02	4.93	5.08
9/22/2008	30.4	15	22.7	61.2	2.24	3.5	168.83	4.08	5.51
9/23/2008	30	16	23	71	1.35	6.5	222.00	4.10	5.28
9/24/2008	27.9	14.5	21.2	67.8	1.05	7	230.67	3.99	4.93
9/25/2008	30.2	17.1	23.65	81	2.09	2.9	157.64	3.20	5.18
9/26/2008	27	16.4	21.7	61.4	1.35	9.4	272.79	4.69	4.43
9/27/2008	29	13.3	21.15	62.4	3.29	10.5	292.01	5.51	5.31
9/28/2008	29.8	14.8	22.3	54.8	3.74	10.8	297.01	6.24	5.34
9/29/2008	30.3	13.2	21.75	55.2	1.50	9.1	266.59	4.91	5.61
9/30/2008	28.5	16	22.25	56.2	3.44	7.6	239.74	5.41	4.85
September	**30.5**	**13.2**	**22.28**	**65.09**	**2.35**	**150.0**	**5881.0**	**124.8**	**149**

Where,

Tmax = maximum daily temperature

Tmin = minimum daily temperature

Tmean = mean daily temperature

n = actual sunshine hours

U_2 = wind speed at 2m height

RH mean = mean daily relative humidity

R_S = instantaneous downward solar radiation

xxx = missed data/no output

ET_0 Pen-Mon = Penman-Monteith ref. evapotranspiration

$ET_{0\ Harg.}$ = Hargreaves reference evapotranspiration

Date	Tmax [^{0}C]	Tmin [^{0}C]	Tmean [^{0}C]	RH mean [%]	U_2 [m/s]	n [hr]	R_S [w/m^2]	ET_0 [mm/day]	
								Pen-Mon	Harg.
10/1/2008	29.5	14.3	21.9	56	3.29	9.9	280.08	5.79	5.29
10/2/2008	30	11.8	20.9	45.8	2.69	11	299.14	6.07	5.64
10/3/2008	30.2	13.4	21.8	42.8	1.94	10.5	289.93	5.68	5.53
10/4/2008	30.5	16.8	23.65	38.8	5.83	4.8	189.16	7.53	5.22
10/5/2008	31.2	13.4	22.3	30.8	3.89	11.1	299.70	7.73	5.74
10/6/2008	30.9	11	20.95	39.8	2.84	11	297.51	6.45	5.86
10/7/2008	30.5	15	22.75	40.8	3.29	11	297.08	6.77	5.40
10/8/2008	28	15.2	21.6	48	3.44	9.8	275.60	6.02	4.76
10/9/2008	23.5	14.5	19	55.2	4.04	10	278.67	5.37	3.72
10/10/2008	27.5	15.4	21.45	66	2.54	6.2	211.80	4.25	4.59
10/11/2008	27	15.4	21.2	47.8	5.39	11	295.23	6.84	4.46
10/12/2008	25.4	17.5	21.45	37.2	5.39	10	277.31	7.32	3.69
10/13/2008	23.9	13.6	18.75	30.8	3.74	10.2	280.33	6.38	3.92
10/14/2008	24	18	21	51.2	4.04	3.8	168.61	4.91	3.17
10/15/2008	25	13.3	19.15	44.4	3.89	9.8	272.41	5.88	4.21
10/16/2008	25.4	12.8	19.1	38.2	3.74	11.1	294.45	6.30	4.35
10/17/2008	25.5	14.5	20	31.6	2.39	11.1	293.92	5.81	4.15
10/18/2008	26.2	13.8	20	29.4	4.19	11	291.65	7.10	4.40
10/19/2008	25.5	12	18.75	39	3.14	10.4	280.77	5.81	4.43
10/20/2008	25	13.5	19.25	36.8	2.54	10.5	281.96	5.56	4.13
10/21/2008	25.2	11.5	18.35	45.2	0.45	5.8	200.65	3.18	4.39
10/22/2008	26.5	17	21.75	51.6	1.35	8.9	253.43	4.51	3.99
10/23/2008	27.2	14.5	20.85	50.8	1.80	9.5	263.21	4.82	4.50
10/24/2008	28	12	20	44.2	1.80	10.6	281.49	5.11	4.93
10/25/2008	28	14	21	55.6	2.39	9.8	267.29	5.06	4.72
10/26/2008	27.5	18	22.75	65.4	2.69	1.1	118.54	3.39	4.05
10/27/2008	27.4	15.5	21.45	74.6	3.89	5.2	187.99	3.84	4.38
10/28/2008	26.8	16.4	21.6	66.4	3.89	7.8	231.73	4.71	4.10
10/29/2008	26.5	15.5	21	72.4	2.24	3.9	165.17	3.33	4.15
10/30/2008	26.4	15	20.7	76.4	1.94	5.7	195.26	3.44	4.18
10/31/2008	26.3	16.5	21.4	90	0.90	xxx	xxx	xxx	3.93
October	**31.2**	**11.0**	**20.83**	**49.77**	**3.08**	**262.5**	**7620.0**	**165.0**	**140**

Where,

Tmax = maximum daily temperature

Tmin = minimum daily temperature

Tmean = mean daily temperature

n = actual sunshine hours

U_2 = wind speed at 2m height

RH mean = mean daily relative humidity

R_S = instantaneous downward solar radiation

xxx = missed data/no output

ET_0 Pen-Mon = Penman-Monteith ref. evapotranspiration

$ET_{0\ Harg.}$ = Hargreaves reference evapotranspiration

Date	Tmax [^{0}C]	Tmin [^{0}C]	Tmean [^{0}C]	RH mean [%]	U_2 [m/s]	n [hr]	R_S [w/m^2]	ET_0 [mm/day]	
								Pen-Mon	Harg.
11/1/2008	27.5	16.4	21.95	80.8	1.94	xxx	xxx	xxx	4.24
11/2/2008	26.6	15	20.8	74	2.09	xxx	xxx	xxx	4.19
11/3/2008	25	15.4	20.2	78.4	2.09	xxx	xxx	xxx	3.75
11/4/2008	25.6	15.8	20.7	78.6	0.60	xxx	xxx	xxx	3.83
11/5/2008	25.2	15.9	20.55	72.6	2.54	xxx	xxx	xxx	3.71
11/6/2008	25.5	14.2	19.85	62.2	0.60	xxx	xxx	xxx	4.00
11/7/2008	24.7	15	19.85	85.4	2.39	xxx	xxx	xxx	3.70
11/8/2008	26.1	14.5	20.3	80.8	4.34	xxx	xxx	xxx	4.08
11/9/2008	27.3	13.5	20.4	56	4.64	xxx	xxx	xxx	4.45
11/10/2008	28	13	20.5	59	5.09	xxx	xxx	xxx	4.65
11/11/2008	30	9	19.5	52.2	2.39	xxx	xxx	xxx	5.34
11/12/2008	28.5	12	20.25	53.8	4.34	xxx	xxx	xxx	4.82
11/13/2008	28	10	19	48.8	3.14	xxx	xxx	xxx	4.86
11/14/2008	27.2	10	18.6	51.4	2.24	xxx	xxx	xxx	4.69
11/15/2008	27.2	11	19.1	46.2	3.59	xxx	xxx	xxx	4.60
11/16/2008	27.2	13.1	20.15	46	4.49	xxx	xxx	xxx	4.41
11/17/2008	27.5	13.5	20.5	51.6	5.09	xxx	xxx	xxx	4.42
11/18/2008	28.8	11.8	20.3	53.4	5.68	xxx	xxx	xxx	4.84
11/19/2008	27.4	11.5	19.45	41	4.34	xxx	xxx	xxx	4.56
11/20/2008	27.5	11.3	19.4	49.2	3.14	xxx	xxx	xxx	4.59
11/21/2008	27.9	10.6	19.25	48.8	3.29	xxx	xxx	xxx	4.72
11/22/2008	28.7	8	18.35	43.4	1.35	xxx	xxx	xxx	5.03
11/23/2008	28.1	9	18.55	48.2	2.24	xxx	xxx	xxx	4.85
11/24/2008	26.7	15.2	20.95	57	4.04	xxx	xxx	xxx	4.00
11/25/2008	27	15	21	57.4	5.24	xxx	xxx	xxx	4.09
11/26/2008	28.5	11.8	20.15	49	2.84	xxx	xxx	xxx	4.71
11/27/2008	29.2	11.8	20.5	51.8	2.54	xxx	xxx	xxx	4.84
11/28/2008	27.6	13.5	20.55	48.4	2.84	xxx	xxx	xxx	4.36
11/29/2008	27.8	13.5	20.65	48.2	4.04	xxx	xxx	xxx	4.39
11/30/2008	24.9	12.9	18.9	49.8	4.04	xxx	xxx	xxx	3.84
November	**30.0**	**8.0**	**20.01**	**57.45**	**3.24**	**xxx**	**xxx**	**xxx**	**133**

Where,

Tmax = maximum daily temperature

Tmin = minimum daily temperature

Tmean = mean daily temperature

n = actual sunshine hours

U_2 = wind speed at 2m height

RH mean = mean daily relative humidity

R_S = instantaneous downward solar radiation

xxx = missed data/no output

ET_0 Pen-Mon = Penman-Monteith ref. evapotranspiration

$ET_{0\ Harg.}$ = Hargreaves reference evapotranspiration

Date	Tmax [^{0}C]	Tmin [^{0}C]	Tmean [^{0}C]	RH mean [%]	U_2 [m/s]	n [hr]	R_S [w/m^2]	ET_0 [mm/day]	
								Pen-Mon	Harg.
12/1/2008	22.3	13.2	17.75	50	1.94	xxx	xxx	xxx	3.23
12/2/2008	24	13	18.5	48.2	2.54	xxx	xxx	xxx	3.62
12/3/2008	26.6	15	20.8	54.6	3.89	xxx	xxx	xxx	3.95
12/4/2008	27.5	14.2	20.85	58.8	5.68	xxx	xxx	xxx	4.23
12/5/2008	27.5	13.6	20.55	61	3.89	xxx	xxx	xxx	4.29
12/6/2008	27.5	13.5	20.5	61.6	4.64	xxx	xxx	xxx	4.29
12/7/2008	28.5	14.2	21.35	55.4	3.89	xxx	xxx	xxx	4.43
12/8/2008	28.1	13.6	20.85	54.6	3.14	xxx	xxx	xxx	4.40
12/9/2008	26.3	14	20.15	54.2	2.84	xxx	xxx	xxx	3.98
12/10/2008	26.9	12.2	19.55	43.4	4.79	xxx	xxx	xxx	4.28
12/11/2008	28.2	11.2	19.7	39.6	4.19	xxx	xxx	xxx	4.62
12/12/2008	24.8	8.8	16.8	33.2	2.69	xxx	xxx	xxx	4.13
12/13/2008	24.1	12	18.05	39.2	3.59	xxx	xxx	xxx	3.72
12/14/2008	25.1	11.5	18.3	37.2	2.69	xxx	xxx	xxx	3.97
12/15/2008	25.5	12	18.75	37.2	4.19	xxx	xxx	xxx	4.00
12/16/2008	26.7	7.5	17.1	42.2	2.39	xxx	xxx	xxx	4.56
12/17/2008	28.5	7.2	17.85	32.6	3.29	xxx	xxx	xxx	4.90
12/18/2008	27	13.5	20.25	49.4	7.63	xxx	xxx	xxx	4.16
12/19/2008	26.5	11.5	19	51.2	4.49	xxx	xxx	xxx	4.25
12/20/2008	25.5	12	18.75	48.2	5.68	xxx	xxx	xxx	4.00
12/21/2008	24.3	11.2	17.75	52.4	3.74	xxx	xxx	xxx	3.83
12/22/2008	25	7.8	16.4	45.6	1.65	xxx	xxx	xxx	4.23
12/23/2008	25.6	11	18.3	49.8	3.14	xxx	xxx	xxx	4.11
12/24/2008	25	11.1	18.05	49.2	4.04	xxx	xxx	xxx	3.99
12/25/2008	24.5	12.5	18.5	49.4	3.59	xxx	xxx	xxx	3.75
12/26/2008	26.4	12.9	19.65	51.2	4.04	xxx	xxx	xxx	4.11
12/27/2008	24.9	12.5	18.7	44.4	4.19	xxx	xxx	xxx	3.84
12/28/2008	21.5	12.5	17	43.4	2.39	xxx	xxx	xxx	3.12
12/29/2008	26.1	13.5	19.8	45.8	3.59	xxx	xxx	xxx	3.99
12/30/2008	27.6	14.9	21.25	58.2	4.34	xxx	xxx	xxx	4.17
12/31/2008	27.9	13	20.45	45.4	4.34	xxx	xxx	xxx	4.43
December	**28.5**	**7.2**	**19.07**	**47.95**	**3.78**	**xxx**	**xxx**	**xxx**	**127**

Where,

Tmax = maximum daily temperature

Tmin = minimum daily temperature

Tmean = mean daily temperature

n = actual sunshine hours

U_2 = wind speed at 2m height

RH mean = mean daily relative humidity

R_S = instantaneous downward solar radiation

xxx = missed data/no output

ET_0 Pen-Mon = Penman-Monteith ref. evapotranspiration

$ET_{0\ Harg.}$ = Hargreaves reference evapotranspiration

Appendix B: SEBS Model Interface